

4.6 Use of Field Study Data for Air Quality Model Development

The tracer and meteorological data collected during the California Delta field tests offer a very comprehensive data base describing the transport and dispersion characteristics of the region. In this report, particularly in Volume II, we have presented all of the pertinent, available data which might be necessary for development and testing of atmospheric dispersion models.

All of the tabulated tracer and meteorological data in Volume II has been compiled on computer cards and is available from the California Air Resources Board upon request. Also available are digital topography data in 200 foot increments for the region extending from 37° to 39° latitude and 121° to 123° longitude; this encompasses all of the San Francisco Bay Area and the California Delta Region as far east as Sacramento and Stockton.

In the next section we present a short analysis of the applicability of a simple air quality model. This analysis is an example of how the field study data can be used to calibrate or validate other atmospheric models.

4.7 Applicability of the Gaussian Plume Model in the California Delta Region

The commonly used Gaussian plume model provides a simple and rapid means of predicting pollutant concentrations downwind of a continuous point source. Although the Gaussian model is restricted by assumptions related to stationary and homogeneous turbulence, and by the availability of empirical dispersion parameters, it is often used by industrial planners and regulatory agency personnel as a means of estimating the impact

of industrial emissions. For this reason, we will test the Gaussian model in the California Delta Region by using it to predict the tracer data. In this manner, we can estimate the suitability of the Gaussian model as an impact analysis tool for industrial development in the California Delta Region.

The Gaussian plume model may be used in the form given by Turner (1970):

$$\begin{aligned}
 c = \frac{Q}{2\pi \sigma_y \sigma_z u} \exp \left[-\frac{1}{2} \left(\frac{y}{\sigma_y} \right)^2 \right] & \left\{ \exp \left[-\frac{1}{2} \left(\frac{z+H}{\sigma_z} \right)^2 \right] + \right. \\
 \exp \left[-\frac{1}{2} \left(\frac{z-H}{\sigma_z} \right)^2 \right] & + \sum_{n=1}^4 \left(\exp \left[-\frac{1}{2} \left(\frac{z+H-2nL}{\sigma_z} \right)^2 \right] + \right. \\
 \exp \left[-\frac{1}{2} \left(\frac{z+H+2nL}{\sigma_z} \right)^2 \right] & + \exp \left[-\frac{1}{2} \left(\frac{z-H-2nL}{\sigma_z} \right)^2 \right] + \\
 \left. \left. \exp \left[-\frac{1}{2} \left(\frac{z-H+2nL}{\sigma_z} \right)^2 \right] \right) \right\} & \quad (15)
 \end{aligned}$$

where u is the average wind speed, Q is the release rate, H is the effective stack height, and L is the height of the mixing layer. The dispersion parameters, σ_y and σ_z , can be taken from the empirical curves given by Turner as functions of the Pasquill stability classes. These empirical curves were determined from data taken over flat, open terrain.

The topography of the Delta area can be characterized as relatively flat, open country. This description suggests that the Gaussian model used with the dispersion parameters from Turner (1970) may be suitable for application in the Delta region. However, the comparison of the tracer

dispersion curves with Pasquill's curves in Section 4.5 indicate that the unique wind patterns of the region effect the dispersion to a much greater extent than might be expected. . Although the Gaussian model may be applicable, it appears that it may be best applied using the experimental dispersion parameters. To test the Gaussian model and the two available sets of dispersion parameters, the Gaussian expression was used to predict the centerline tracer concentrations from the automobile traverses for each test. In this prediction, σ_y and σ_z were taken from the best-fit lines through the tracer data for each test. If a curve for σ_z were not available, the curve from Turner was used. The effective stack height, H, was set equal to the release height, 5 m, and the release rate, Q, was assumed to be equal to the average release rate for each test as given in Table 2 . The value of u for each test was obtained by vector averaging hourly wind data from all stations downwind of the tracer release point over the time of interest. The mixing height, L, was determined by averaging the hourly heights from the available stations for the test period.

The predicted results for the automobile traverse tracer data are given in Figures 97-109 in terms of ground-level centerline concentrations as a function of downwind distance. In each figure, the experimental maximum 10-second and hourly averaged concentrations are also plotted as a function of downwind distance. Additionally, predicted concentrations using the dispersion curves from Turner are shown for each test.

The predicted results based on Turner's σ_y and σ_z fall very close to the measured concentrations in Test 1 for class C stability. The curve based on the experimental dispersion data underestimates the concentrations

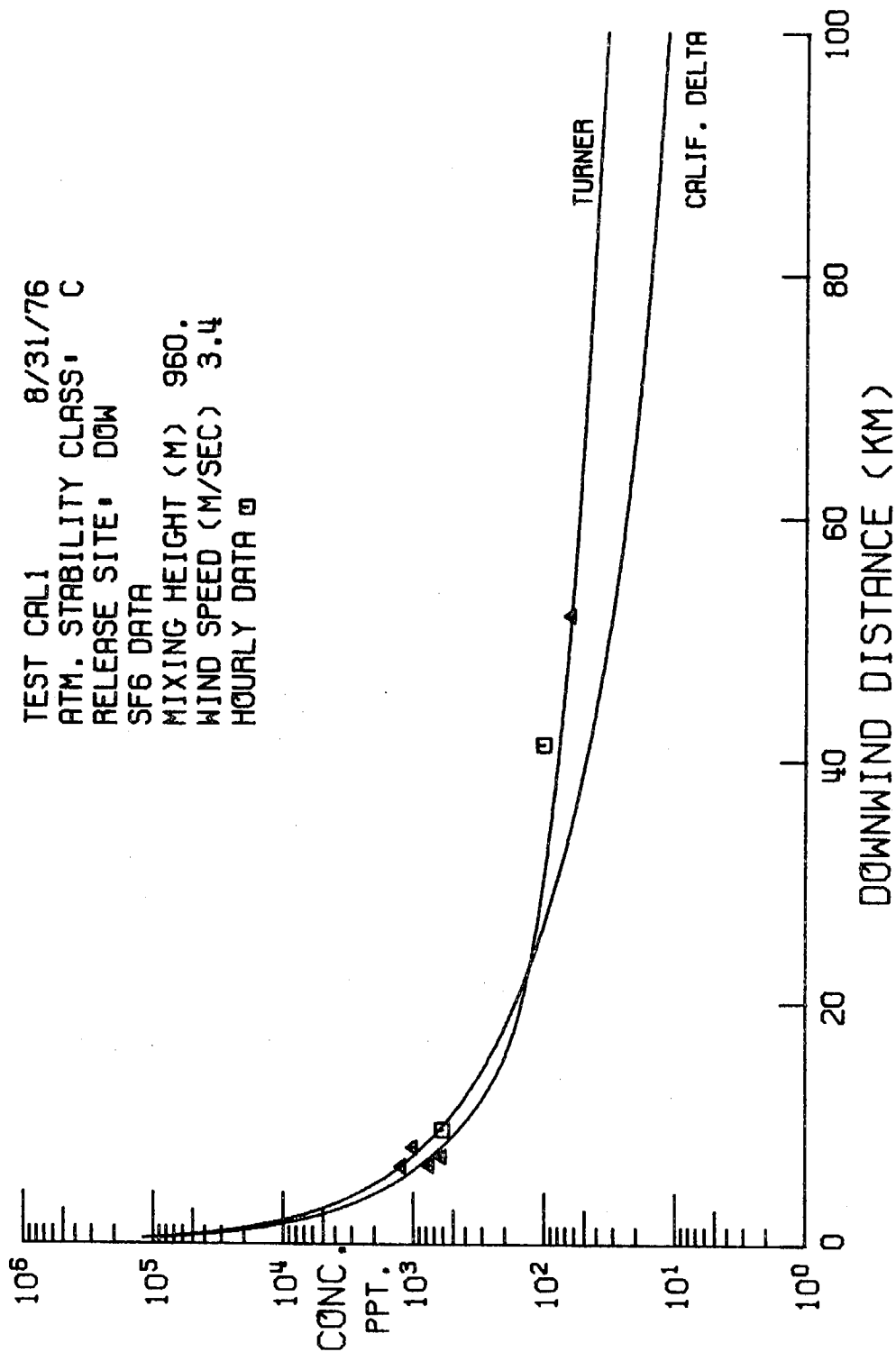


Figure 97. Centerline tracer concentrations compared with centerline concentrations predicted using the Gaussian plume model. The "Turner" curve is based upon Pasquill dispersion parameters given by Turner (1970); the "Calif. Delta" curve is based upon experimental dispersion parameters.

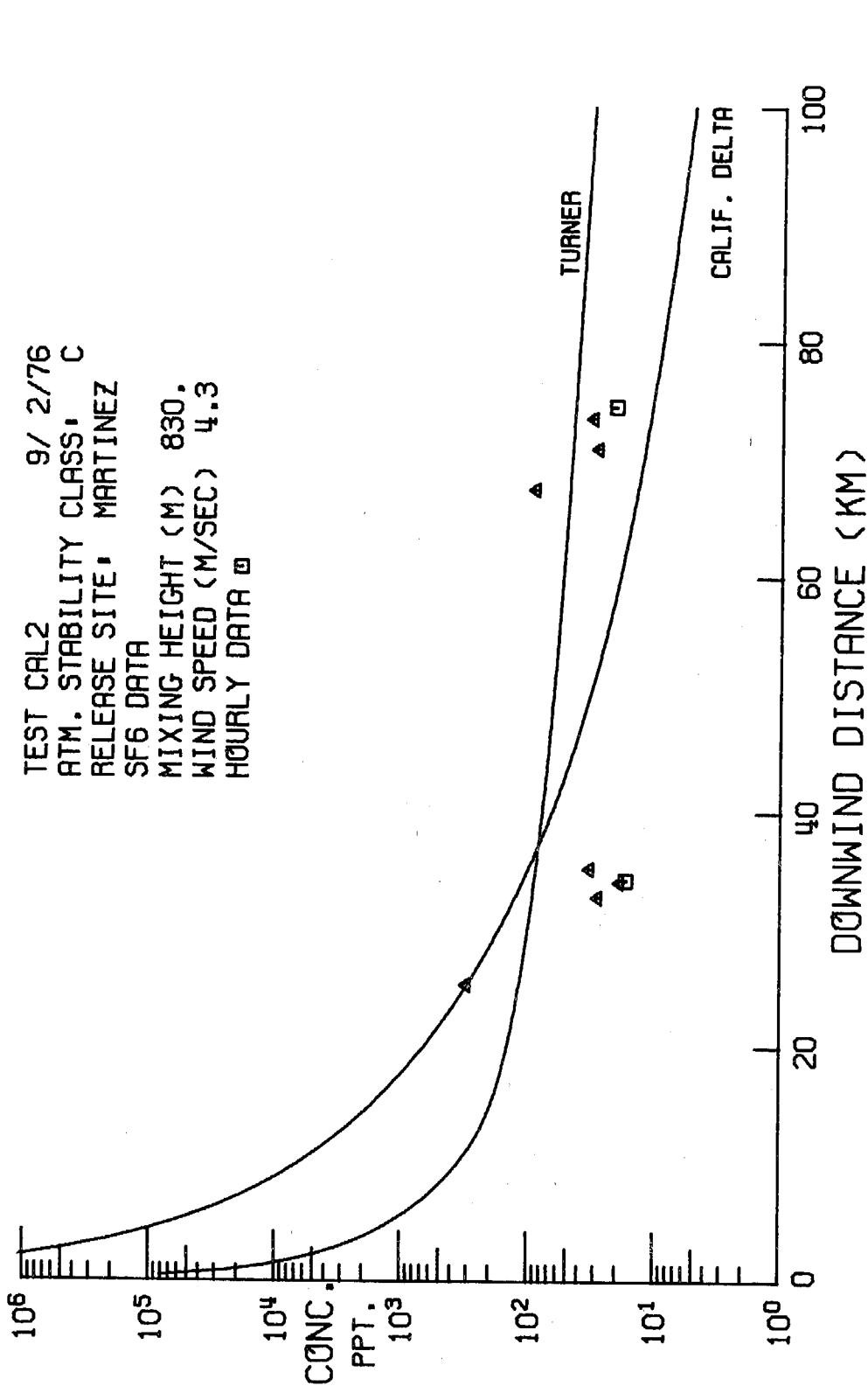


Figure 98. Centerline tracer concentrations compared with centerline concentrations predicted using the Gaussian plume model. The "Turner" curve is based upon Pasquill dispersion parameters given by Turner (1970); the "Calif. Delta" curve is based upon experimental dispersion parameters.

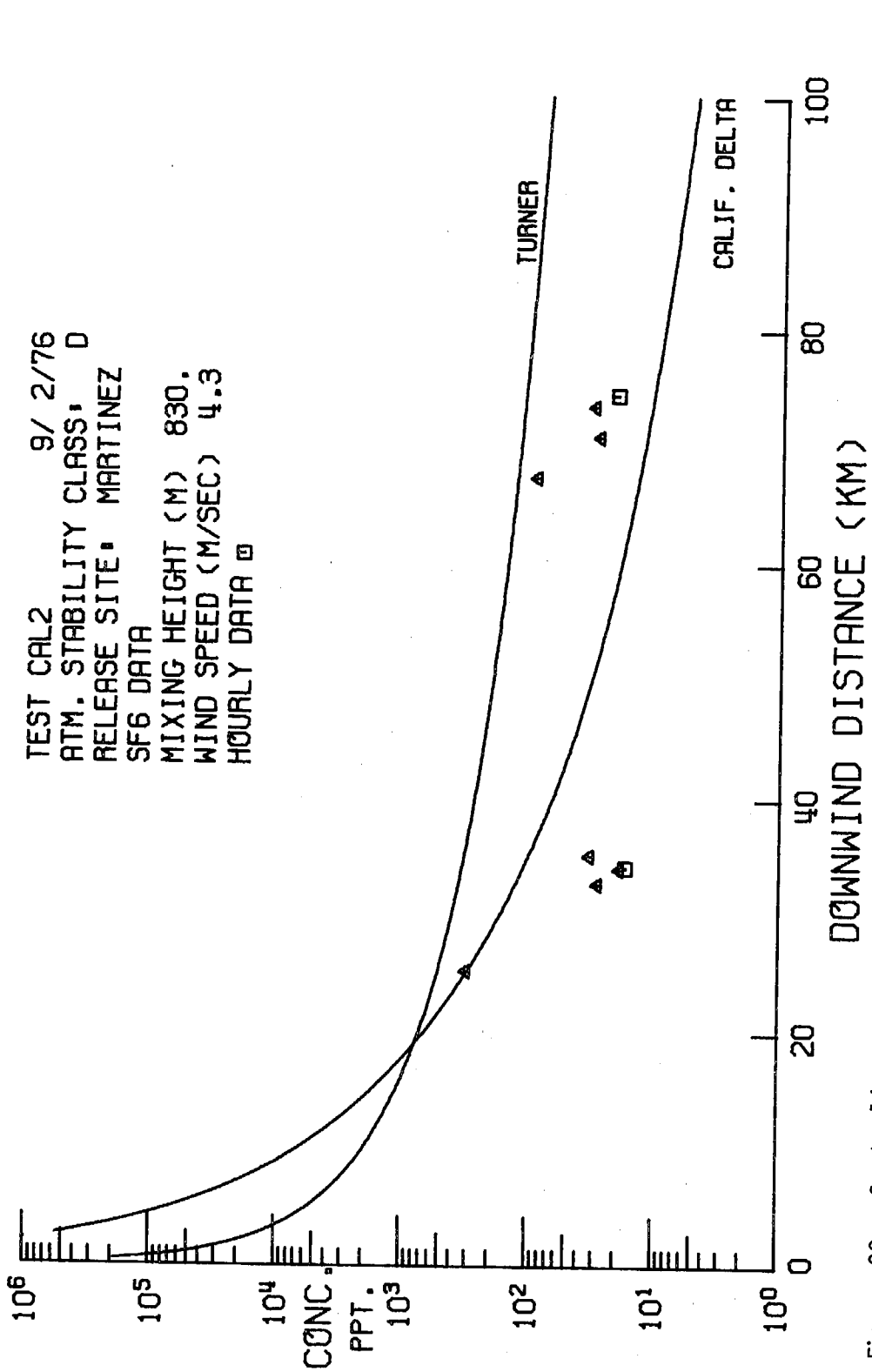


Figure 99. Centerline tracer concentrations compared with centerline concentrations predicted using the Gaussian plume model. The "Turner" curve is based upon Pasquill dispersion parameters given by Turner (1970); the "Calif. Delta" curve is based upon experimental dispersion parameters.

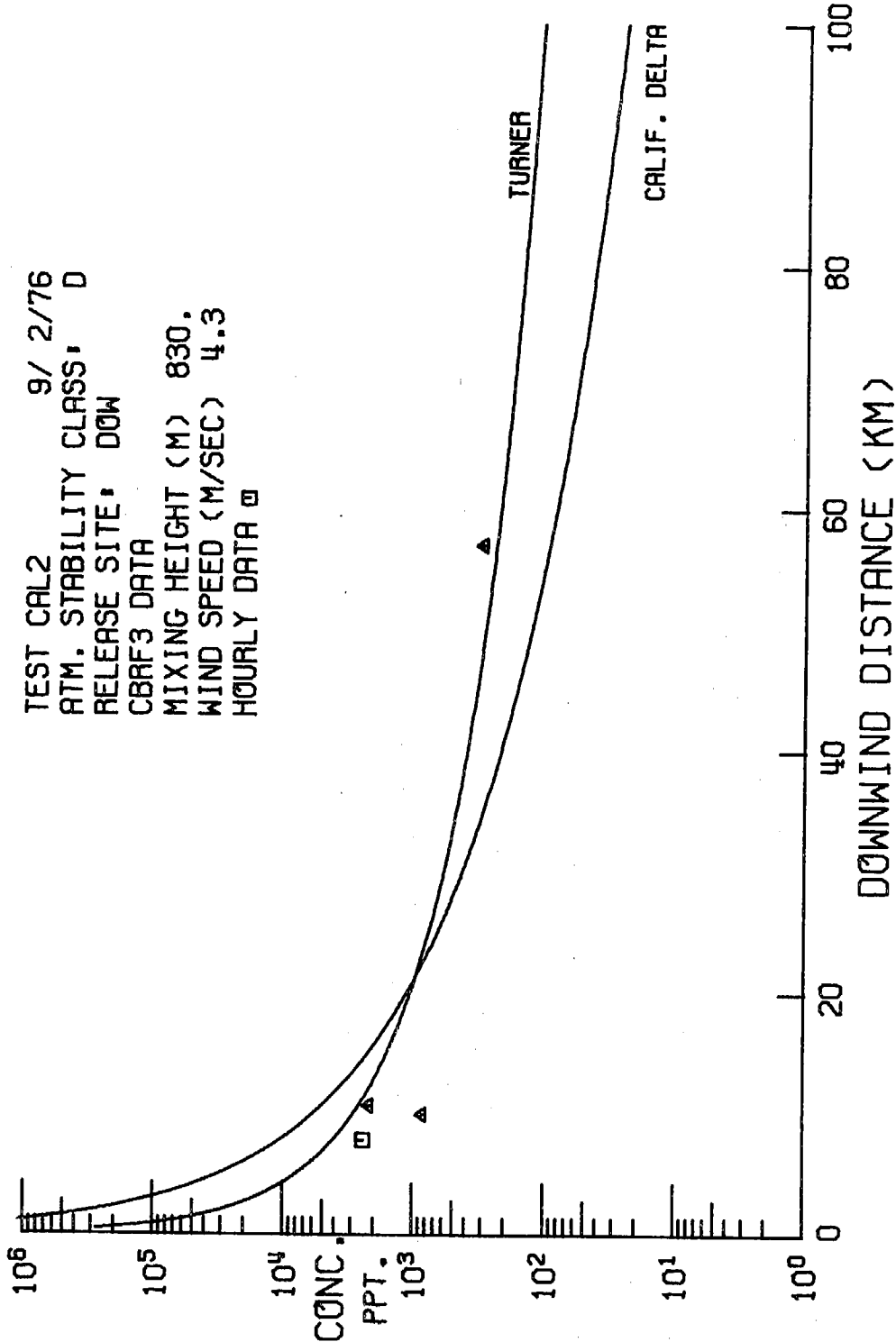


Figure 100. Centerline tracer concentrations compared with centerline concentrations predicted using the Gaussian plume model. The "Turner" curve is based upon Pasquill dispersion parameters given by Turner (1970); the "Calif. Delta" curve is based upon experimental dispersion parameters.

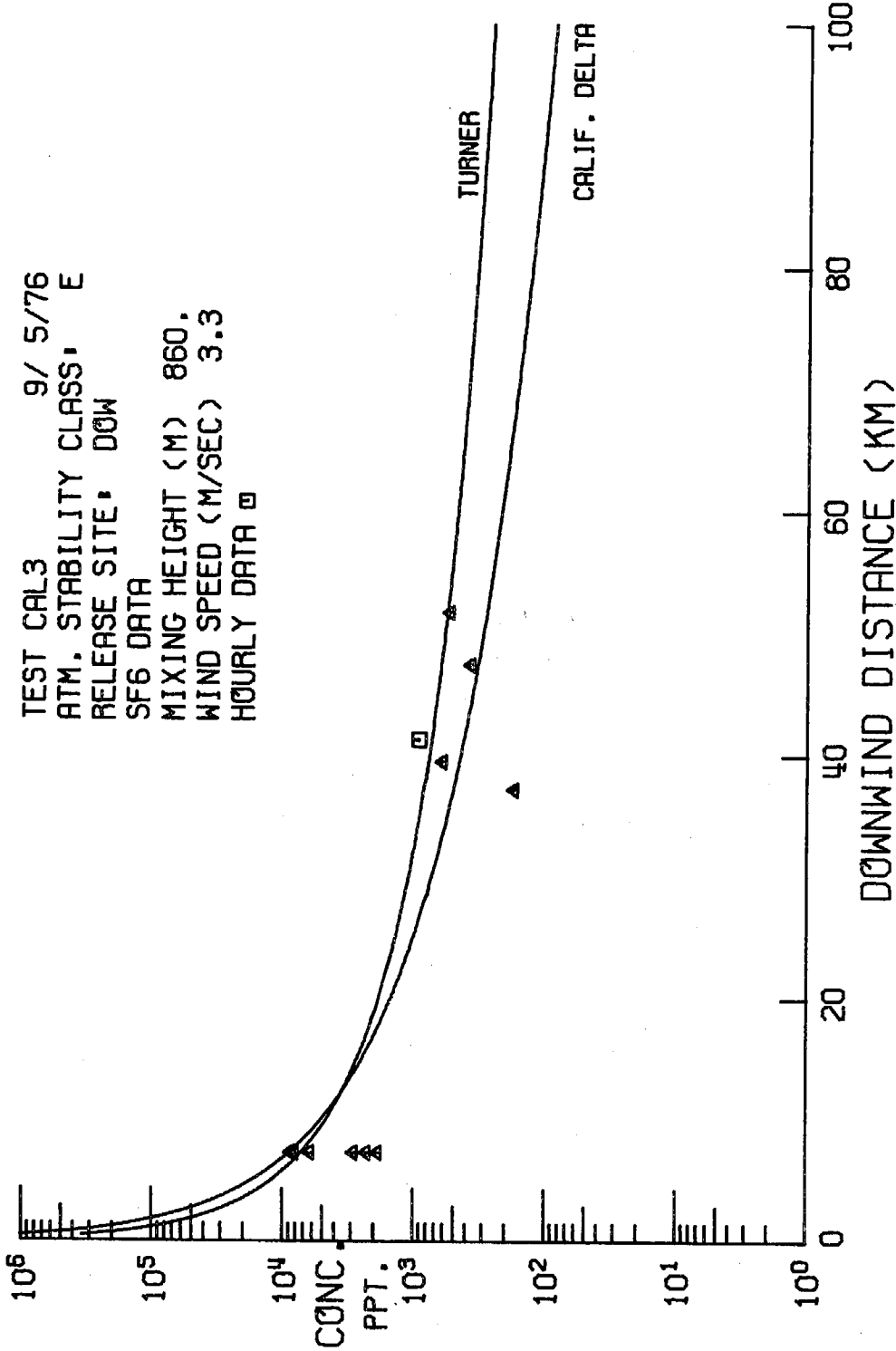


Figure 101. Centerline tracer concentrations compared with centerline concentrations predicted using the Gaussian plume model. The "Turner" curve is based upon Pasquill dispersion parameters given by Turner (1970); the "Calif. Delta" curve is based upon experimental dispersion parameters.

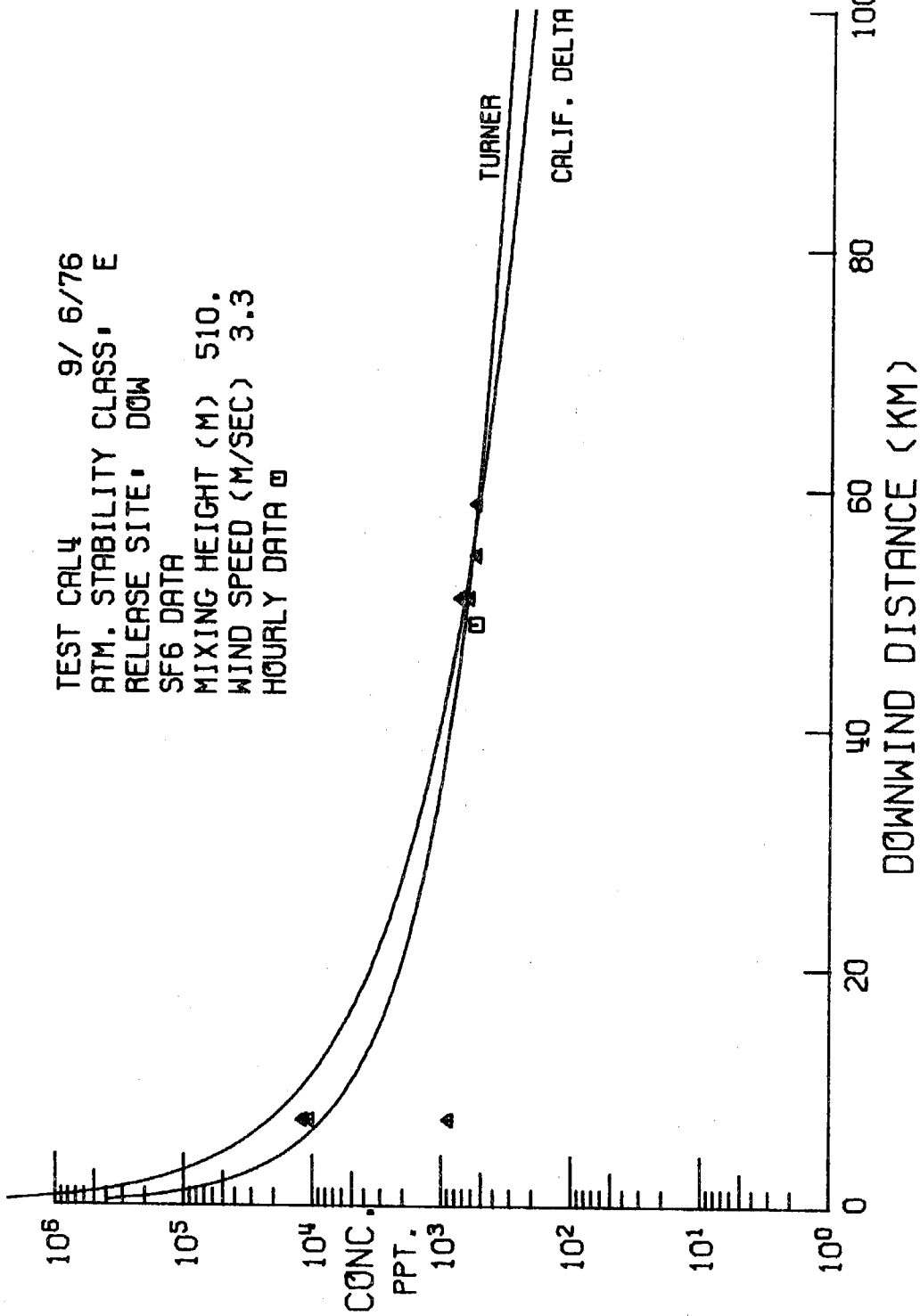


Figure 102. Centerline tracer concentrations compared with centerline concentrations predicted using the Gaussian plume model. The "Turner" curve is based upon Pasquill dispersion parameters given by Turner (1970); the "Calif. Delta" curve is based upon experimental dispersion parameters.

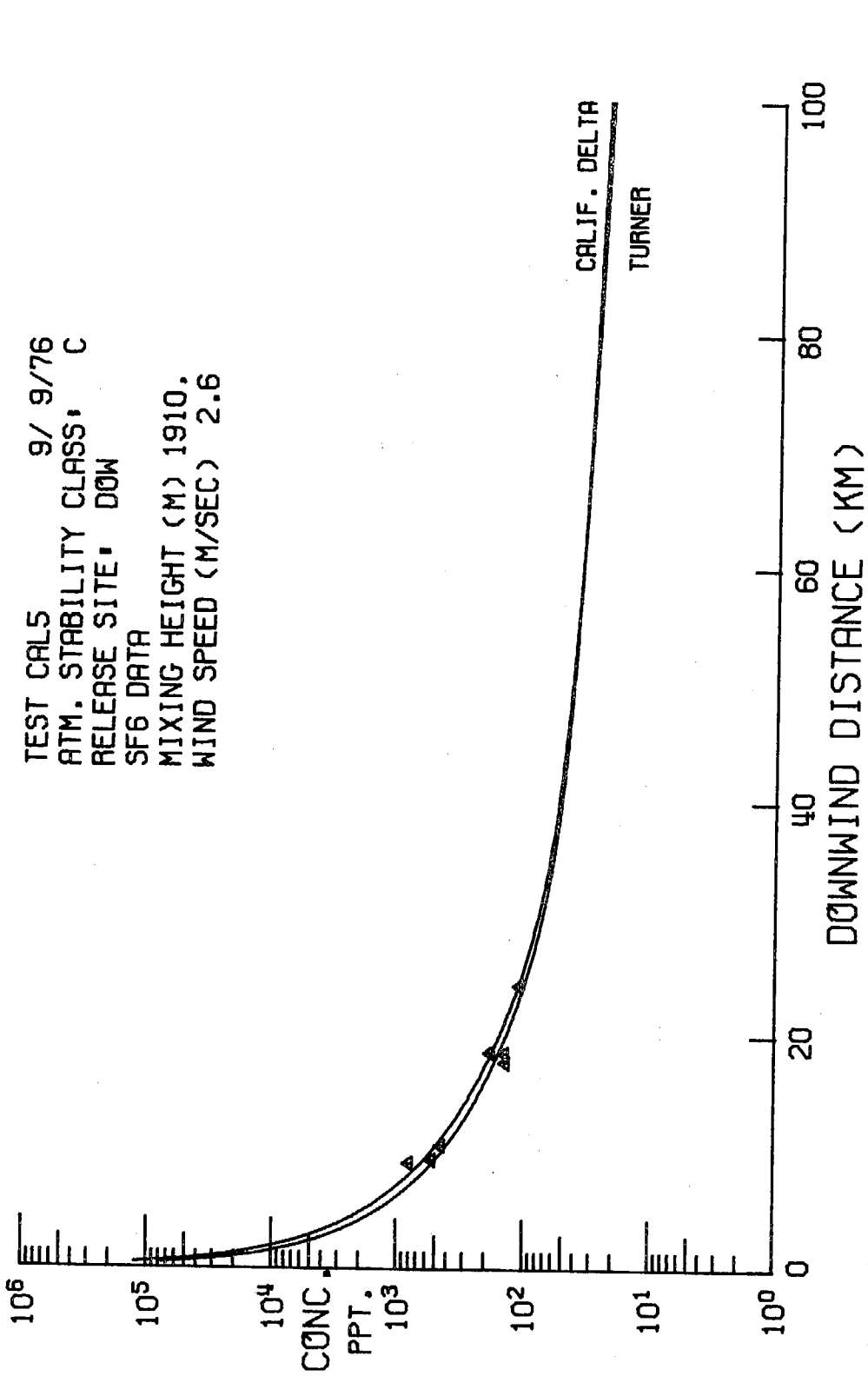


Figure 103. Centerline tracer concentrations compared with centerline concentrations predicted using the Gaussian plume model. The "Turner" curve is based upon Pasquill dispersion parameters given by Turner (1970); the "Calif. Delta" curve is based upon experimental dispersion parameters.

TEST CAL6 9/10/76
ATM. STABILITY CLASS: B
RELEASE SITE: DOW
SF6 DATA
MIXING HEIGHT (M) 1250.
WIND SPEED (M/SEC) 1.2
HOURLY DATA

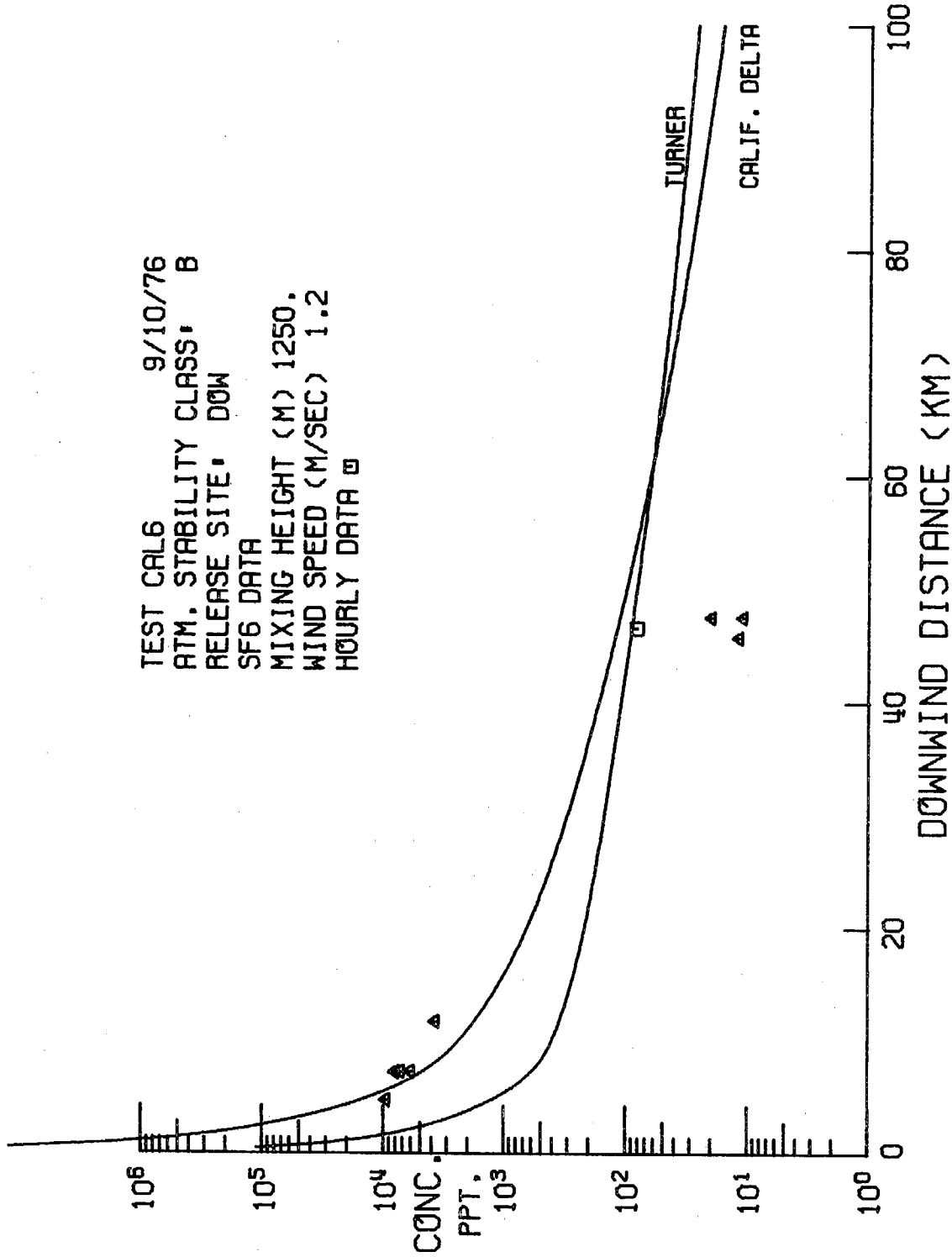


Figure 104. Centerline tracer concentrations compared with centerline concentrations predicted using the Gaussian plume model. The "Turner" curve is based upon Pasquill dispersion parameters given by Turner (1970); the "Calif. Delta" curve is based upon experimental dispersion parameters.

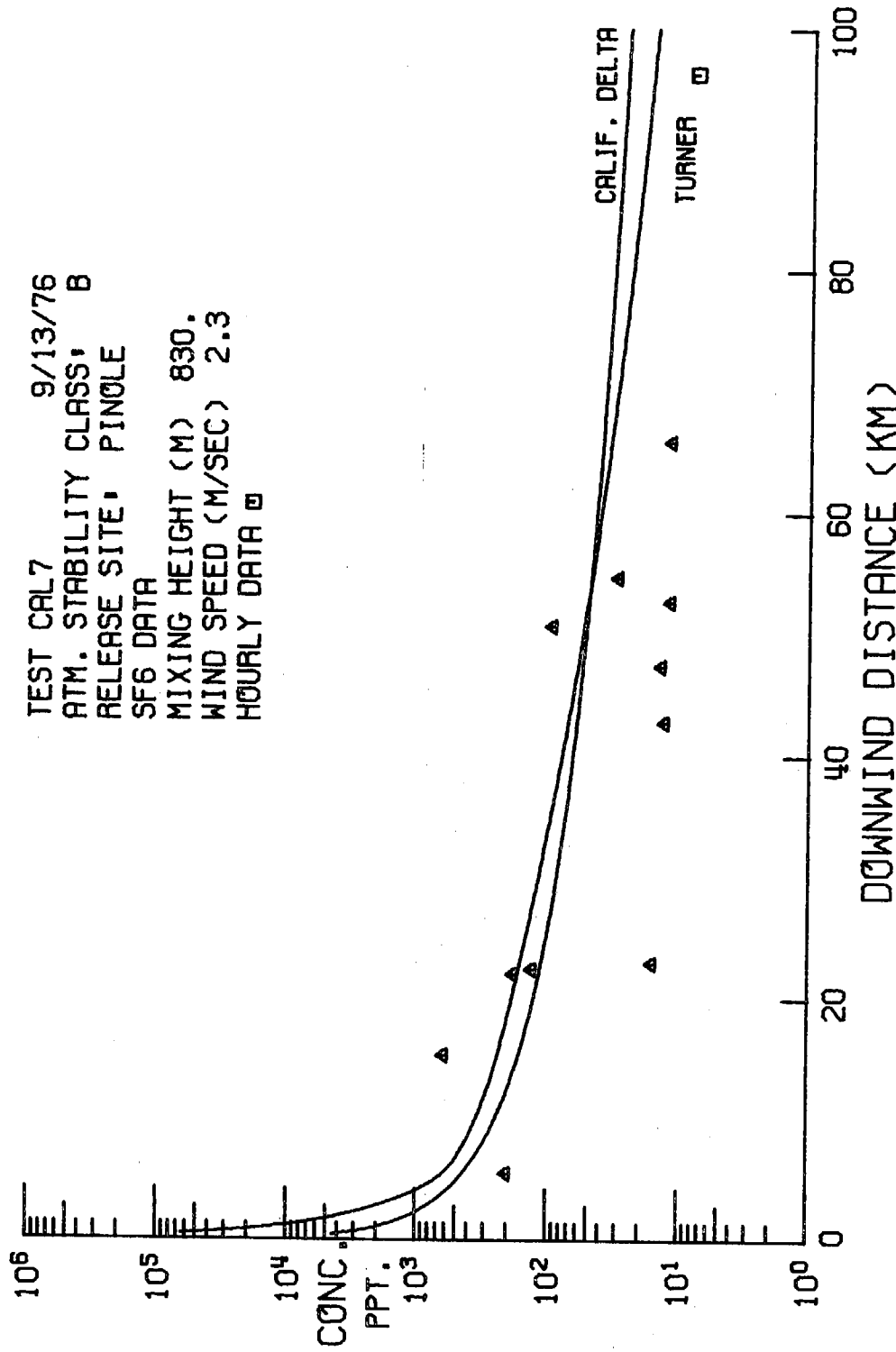


Figure 105. Centerline tracer concentrations compared with centerline concentrations predicted using the Gaussian plume model. The "Turner" curve is based upon Pasquill dispersion parameters given by Turner (1970); the "Calif. Delta" curve is based upon experimental dispersion parameters.

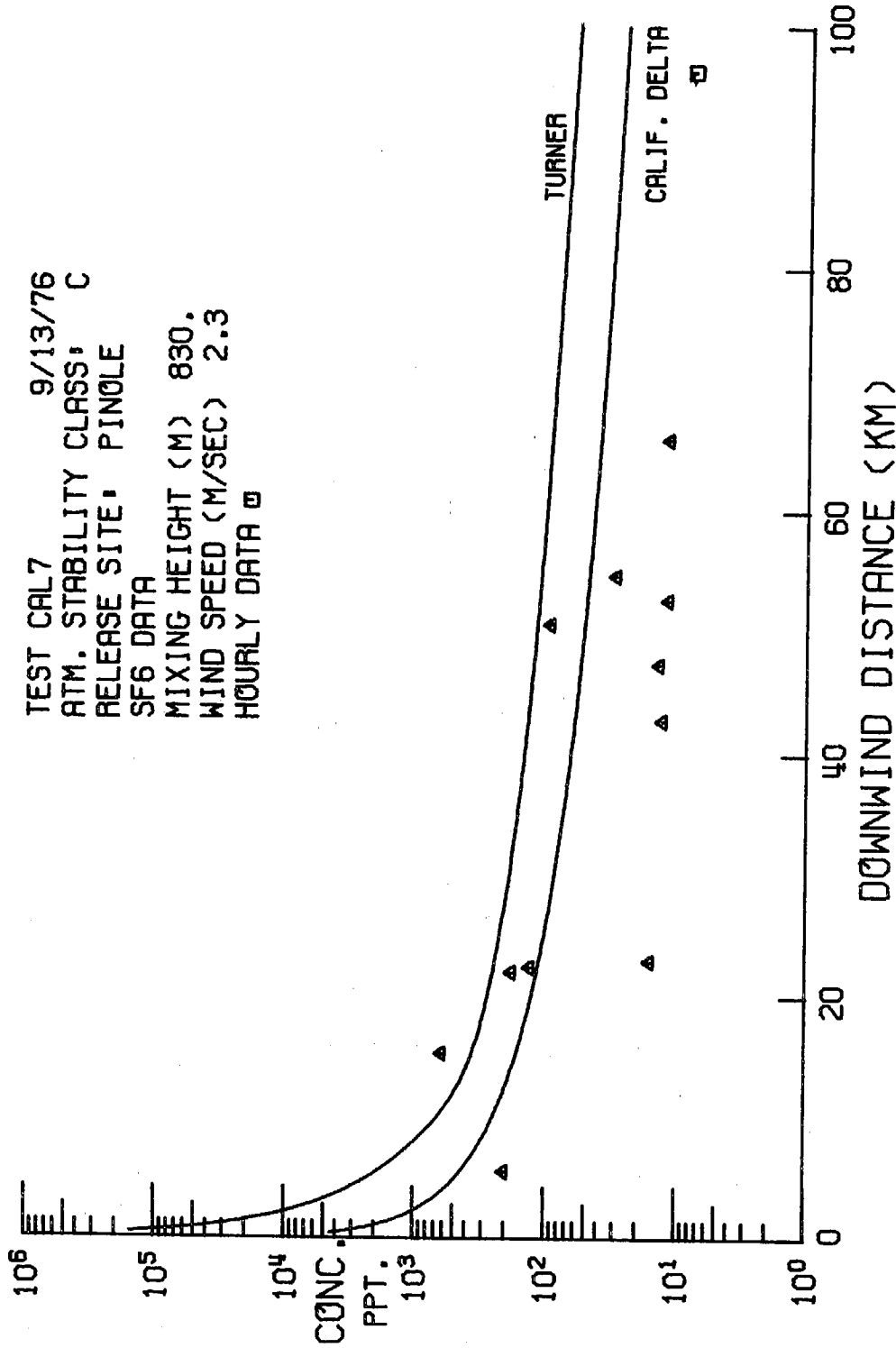


Figure 106. Centerline tracer concentrations compared with centerline concentrations predicted using the Gaussian plume model. The "Turner" curve is based upon Pasquill dispersion parameters given by Turner (1970); the "Calif. Delta" curve is based upon experimental dispersion parameters.

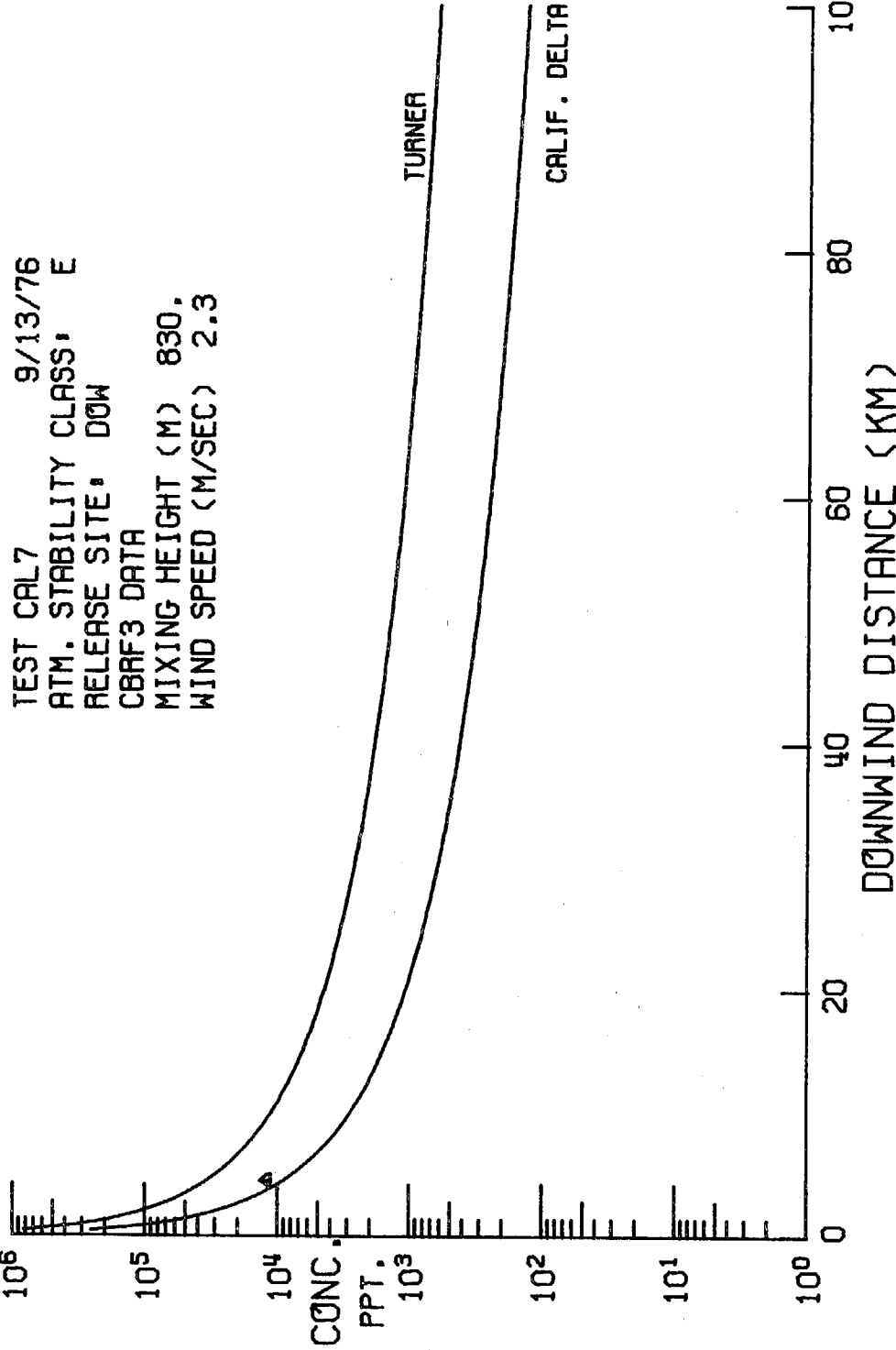


Figure 107. Centerline tracer concentrations compared with centerline concentrations predicted using the Gaussian plume model. The "Turner" curve is based upon Pasquill dispersion parameters given by Turner (1970); the "Calif. Delta" curve is based upon experimental dispersion parameters.

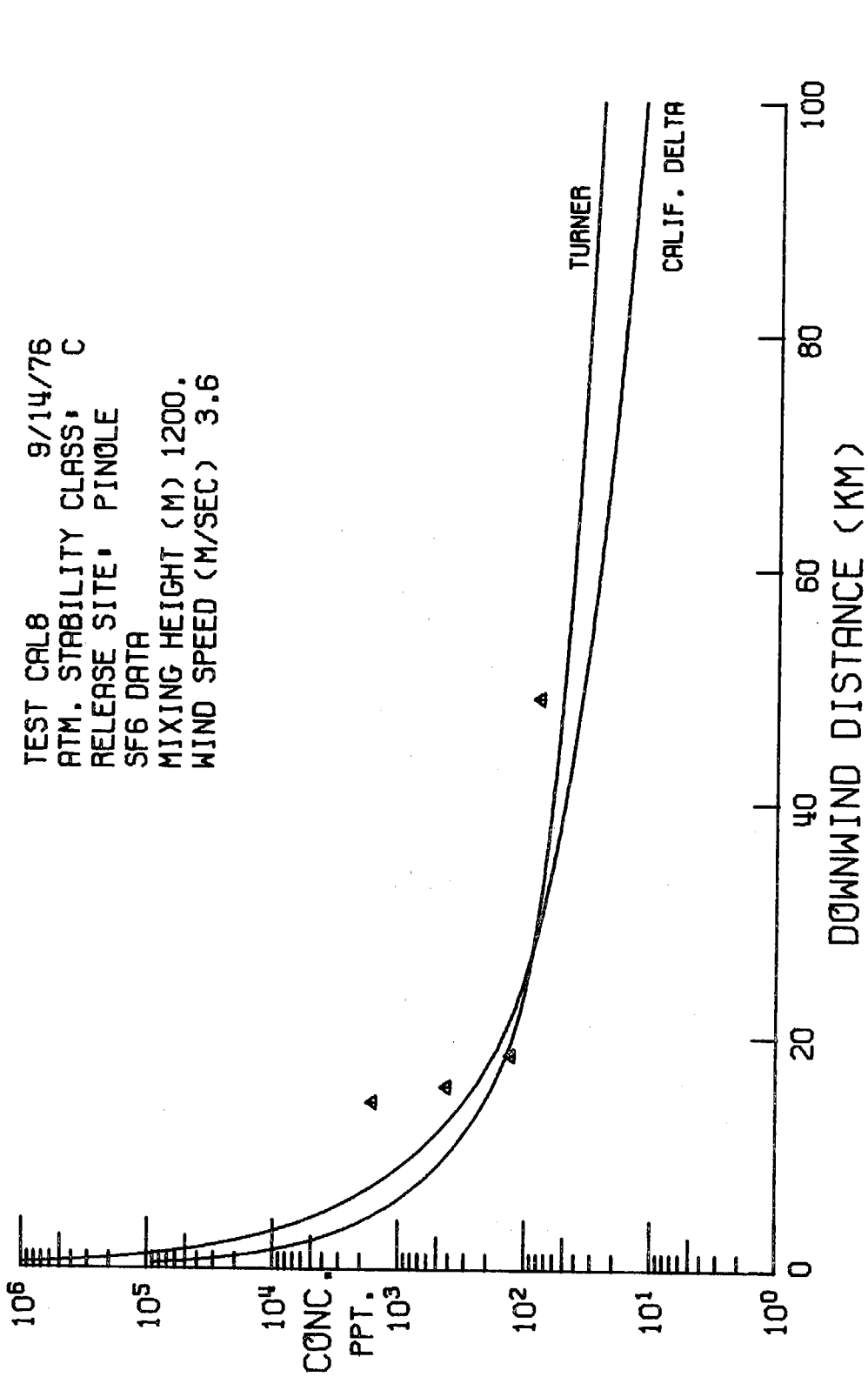


Figure 108. Centerline tracer concentrations compared with centerline concentrations predicted using the Gaussian plume model. The "Turner" curve is based upon Pasquill dispersion parameters given by Turner (1970); the "Calif. Delta" curve is based upon experimental dispersion parameters.

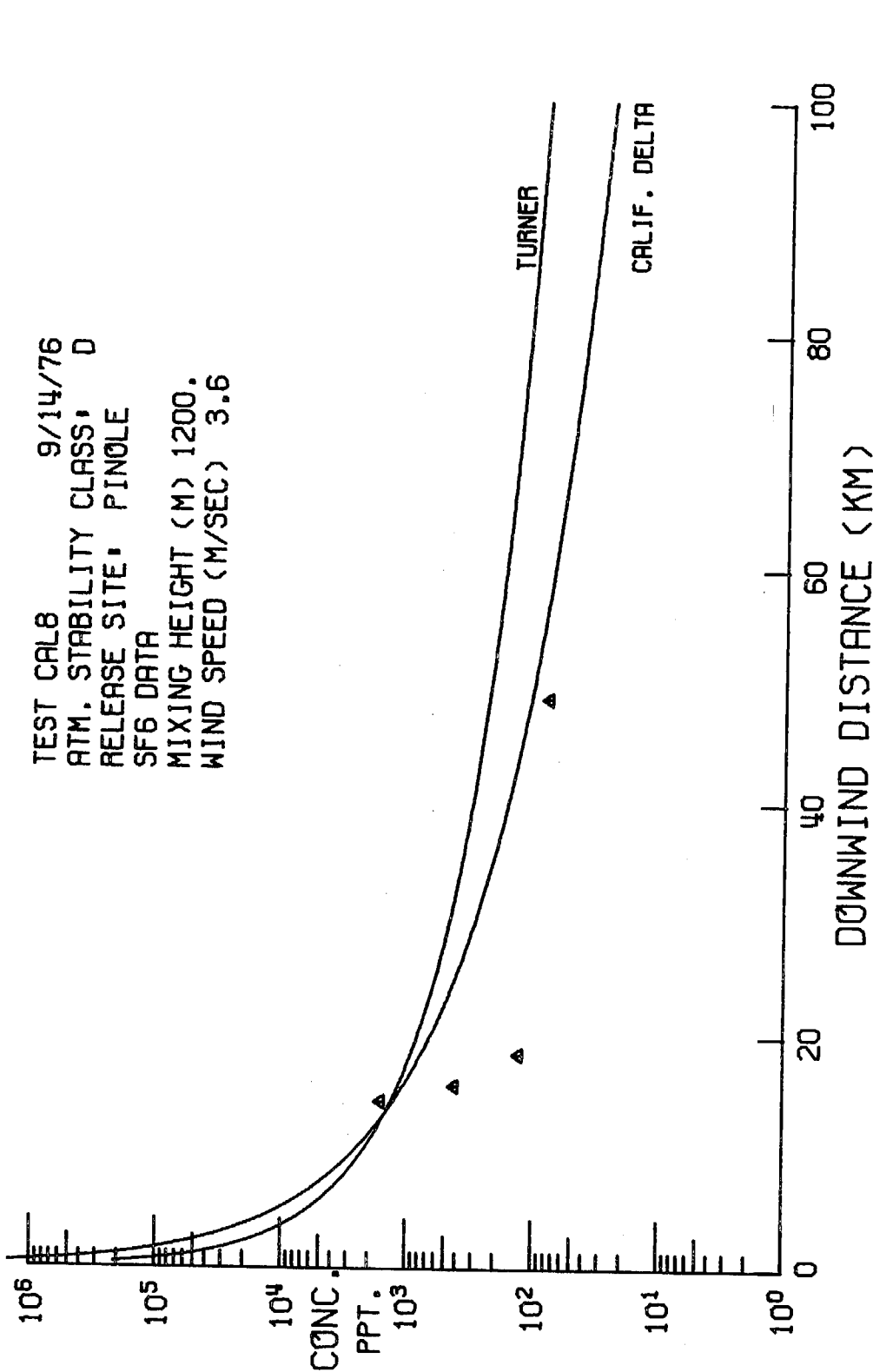


Figure 109. Centerline tracer concentrations compared with centerline concentrations predicted using the Gaussian plume model. The "Turner" curve is based upon Pasquill dispersion parameters given by Turner (1970); the "Calif. Delta" curve is based upon experimental dispersion parameters.

at 40 to 65 km but predicts the experimental concentrations very closely at 10 km. Note that there is essentially no difference between the 10-second and hourly averaged experimental concentrations. Test 1 stability conditions were determined to be close to classes B-C from the meteorology. The predicted curves for the Test 2 release from Martinez for class C conditions do not fall very near the experimental data. The Turner curve under class D conditions serves as an upper bound on the data. Conditions during Test 2 were Pasquill classes B-C. The Turner curves for the Test 2 release from Dow lies fairly close to the experimental data under class D stability. The California Delta curve overestimates concentrations less than 20 km from Dow and underestimates the data point taken 60 km from Dow. The predicted results for Test 3 using Turner's σ_y and σ_z represent the data relatively well under class E conditions. The curve obtained from the experimental dispersion data correctly predicts the tracer concentrations between 40 and 50 km downwind, but the curve overestimates the data at 10 km. The California Delta curve comes much closer to the data in Test 4. However, the Turner curve also fits the Test 4 data fairly well under class E stability. The data from Test 5 is predicted almost exactly by both calculated curves under class C stability conditions. The California Delta curve for Test 6 fits the tracer concentrations at 10 km fairly well, but the curve overestimates the data obtained at 45 km. The curve from the Turner parameters provides a very poor fit of the data under the same conditions. The tracer data from Test 7 is widely scattered and appears to be fitted best by the California Delta curve. Results for class C conditions indicate that the curve using the parameters from Turner serves as an upper bound for the data. The single data point from

the Test 7 Dow release is predicted quite closely by the California Delta curve. Note that the curve from Turner could be made to predict the data point by adjusting the stability condition and wind speed. The data from Test 8 is not represented very closely by either calculated curve for classes C or D. The Turner curve for class D conditions serves as an approximate upper bound to the data.

The results of the Gaussian prediction show that in most of the cases considered, the Gaussian plume model predicts the experimental data reasonably well. Where the model was used with the empirical dispersion curves from Turner and for the stability classes determined from the meteorology, reasonable fits of the tracer data were obtained for Tests 1, 3, 4, 5, 7 and 8. In cases where the experimental dispersion parameters were used, reasonable fits of the tracer data were obtained for Tests 1, 3, 4, 5, 6, 7 (Pinole) and 7(Dow).

It appears that both sets of dispersion parameters can be used with the Gaussian plume model with a measurable degree of success. Notably, the predictions appear to fit the tracer data best under the more stable evening and nighttime conditions; these are the periods where it appears worst-case impact can occur. During the daytime in Test 5, the data are perfectly predicted. However, weak northerly winds prevailed during the day and the strong jet of air over Montezuma Hills was not present. In the absence of the strong westerly flow, the dispersion process appeared to follow the classical Pasquill dispersion pattern. Data obtained during the Martinez and Pinole releases were more scattered than for Dow releases. In the Bay Area releases, plumes appeared to diverge widely across the Delta region; the automobile traverses in some cases did not cover the

entire width of the plume. During Test 7, the data suggest that the plume split into at least two streams upwind of the Montezuma Hills. It is very difficult to apply the Gaussian model under these conditions.

This presentation of predicted and experimental results indicate that averaging the wind field and mixing heights is a reasonable and, probably the most straightforward method of supplying the necessary input data to the model. In view of the large wind velocity gradients present in the region, the apparent usefulness of average input values is somewhat surprising.

The availability of detailed concentration profiles as obtained from the automobile traverse data is extremely rare. Also, the Gaussian model is rarely used to predict more than plume centerline concentrations. However, because the data are available and the model can be used to determine concentration profiles, we have presented the calculated and experimental traverse profiles for four evening and nighttime traverses in Figures 110-112. The input values for Figures 110 and 111 represent the overall average conditions during the test. The two smooth curves were calculated with the dispersion parameters from Turner and from the field study. In Test 3- Traverse 6, the Delta curve fits the data almost perfectly; the Turner curve underestimates the peak concentration and overestimates the plume width. Further downwind in Traverse 10, the Delta curve slightly underestimates the peak value, and gives a reasonable approximation of the plume width. The Turner curve again overestimates the maximum concentration, but predicts the plume width fairly well. The results from Test 4, 51 km downwind, are extremely impressive; using overall average input values, both curves predict the tracer data almost perfectly. In Traverse

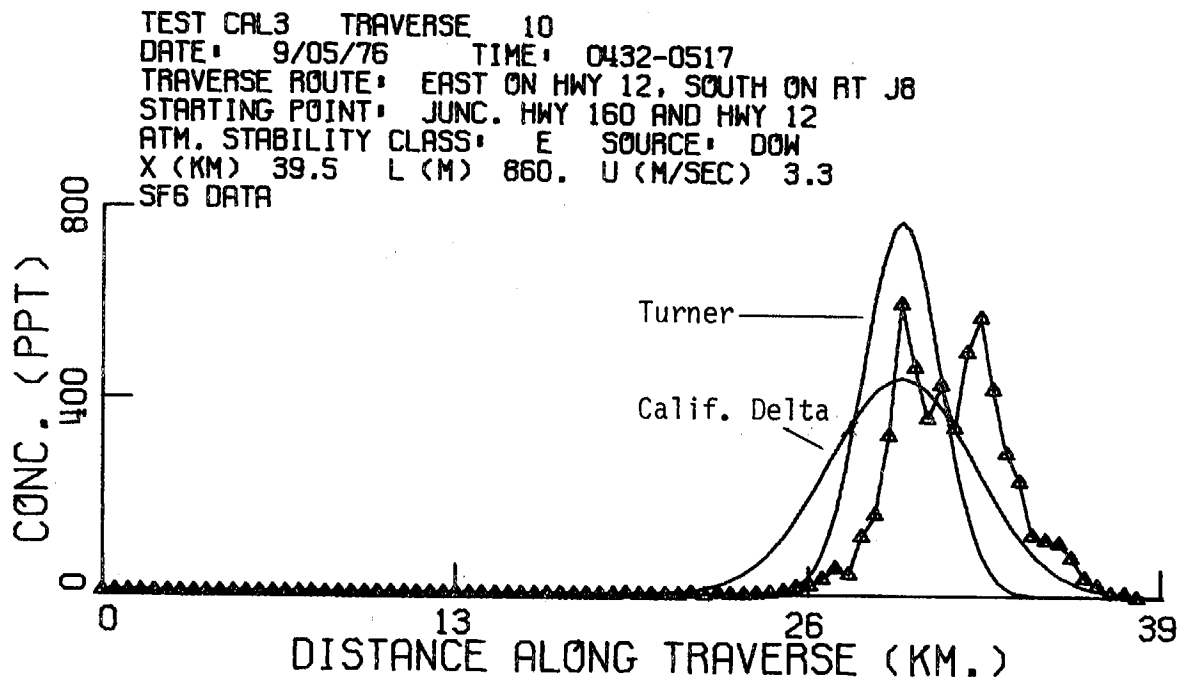
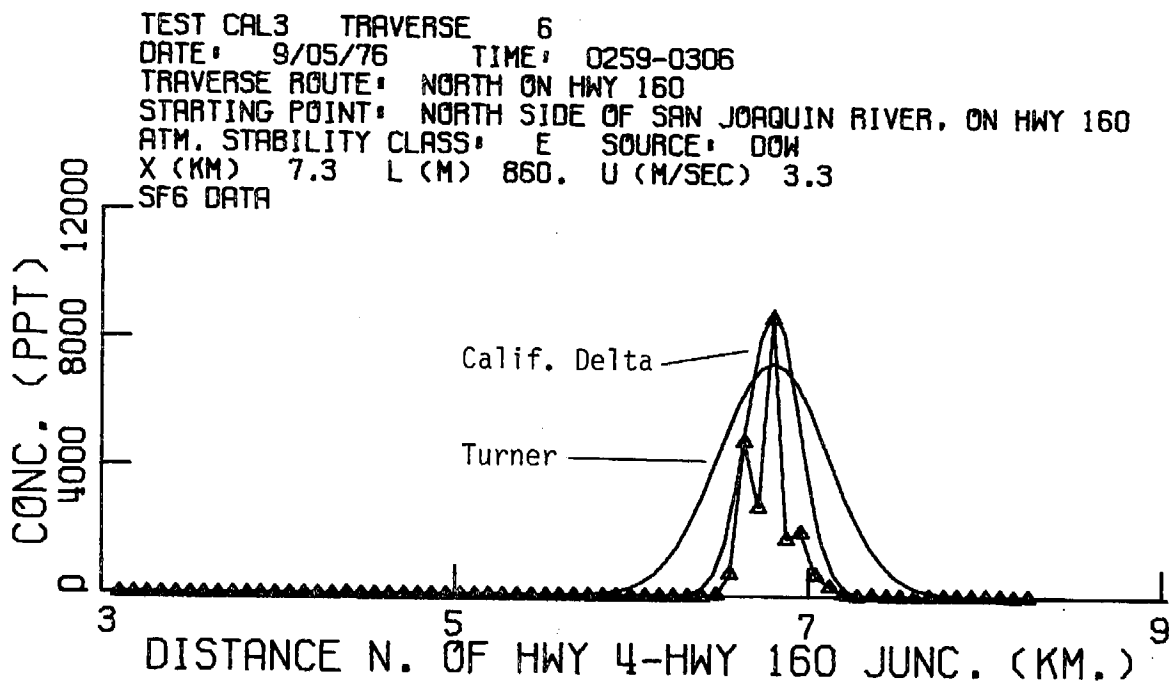


Figure 110. Crosswind tracer profiles compared with crosswind profiles predicted using the Gaussian plume model. The "Turner" curve is based upon Pasquill dispersion parameters given by Turner (1970); the "Calif. Delta" curve is based upon experimental dispersion parameters. Meteorological data represent the average values for the region during the test.

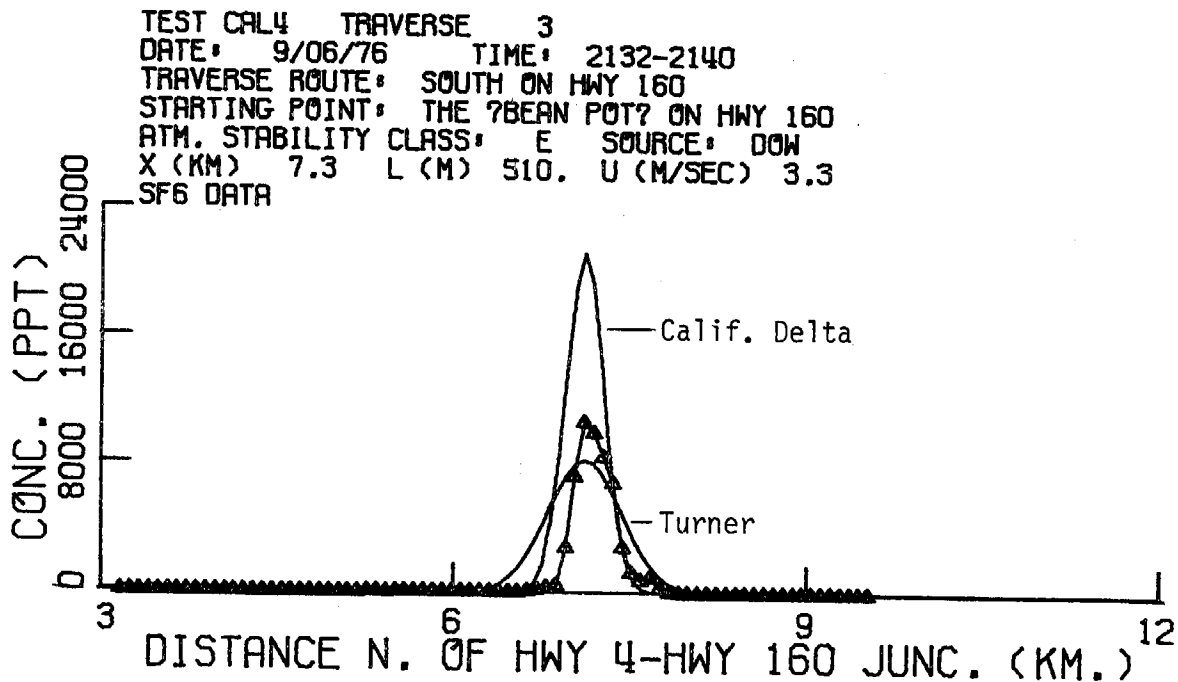
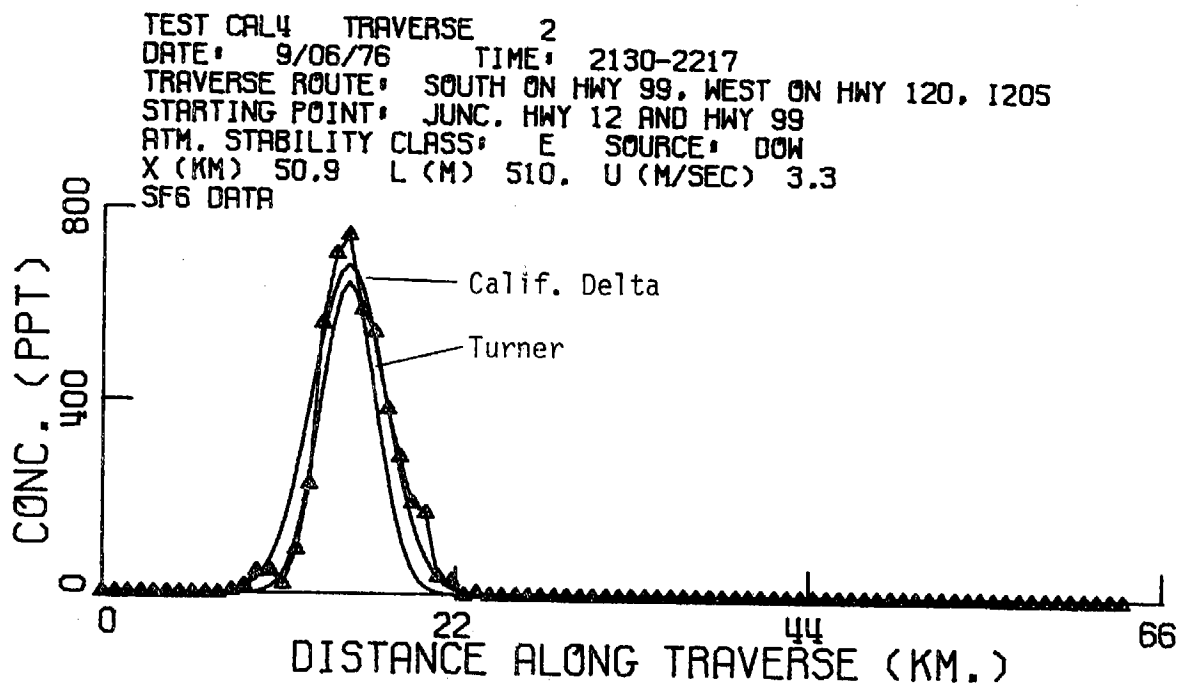


Figure 111. Crosswind tracer profiles compared with crosswind profiles predicted using the Gaussian plume model. The "Turner" curve is based upon Pasquill dispersion parameters given by Turner (1970); the "Calif. Delta" curve is based upon experimental dispersion parameters. Meteorological data represent the average values for the region during the test.

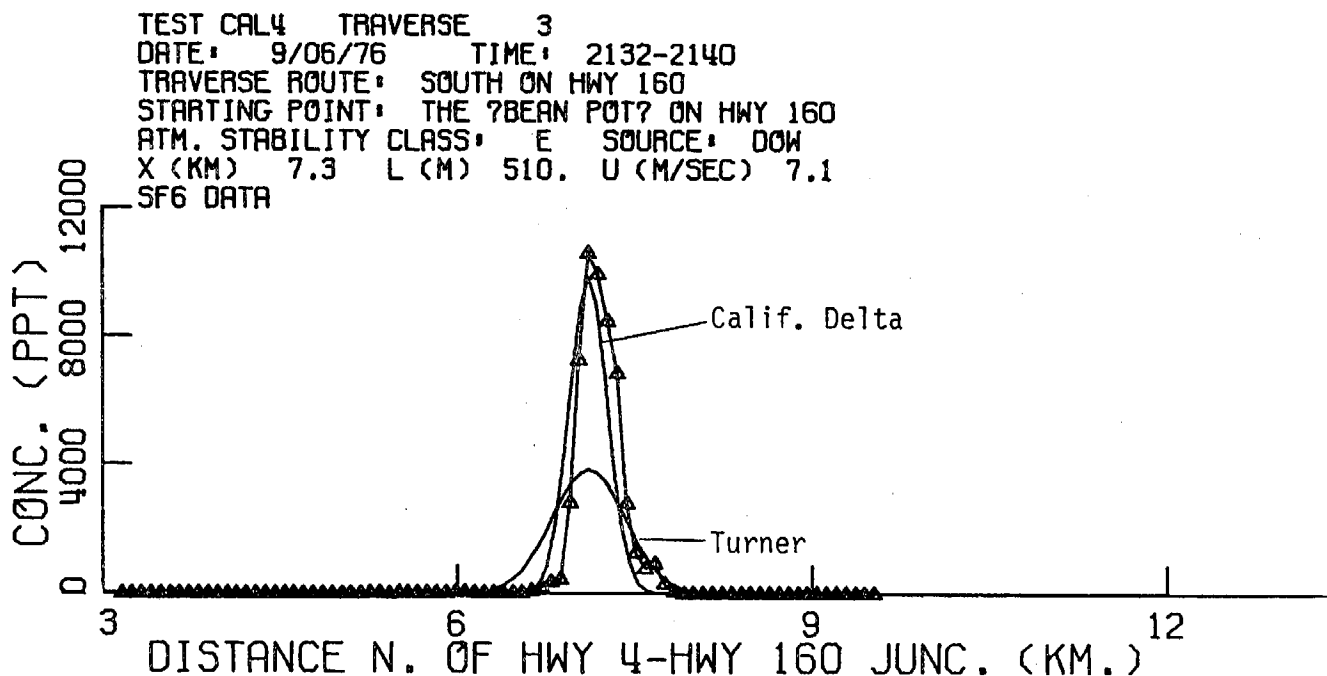
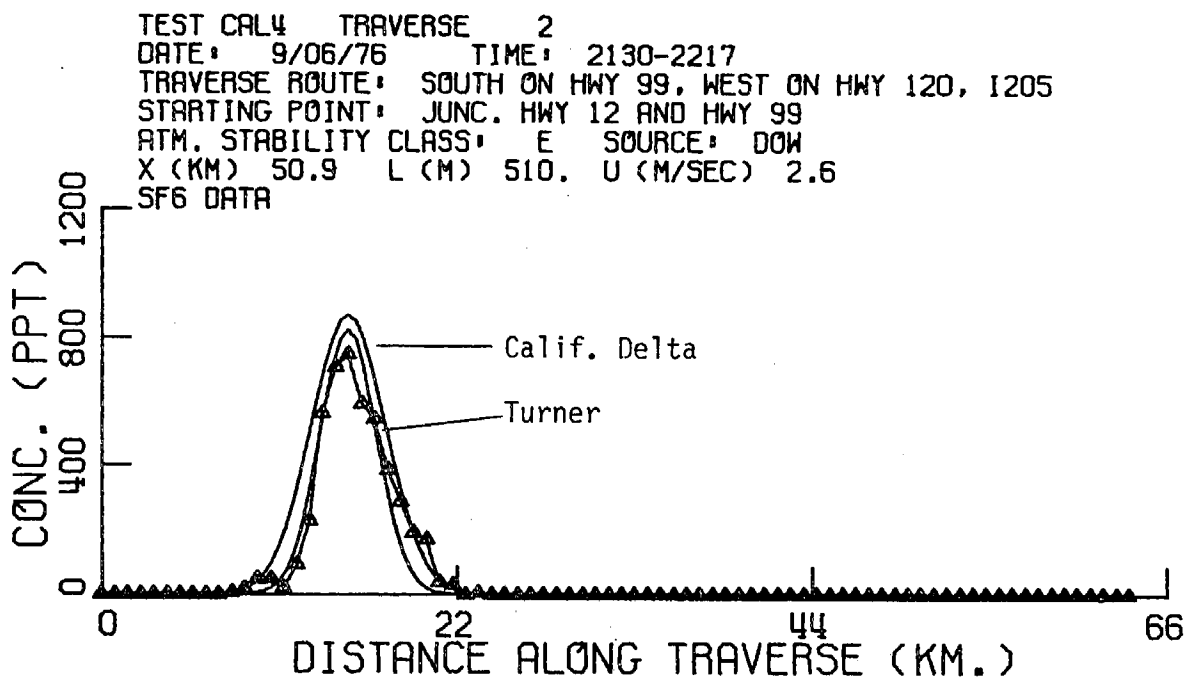


Figure 112. Crosswind tracer profiles compared with crosswind profiles predicted using the Gaussian plume model. The "Turner" curve is based upon Pasquill dispersion parameters given by Turner (1970); the "Calif. Delta" curve is based upon experimental dispersion parameters. Wind speeds for Traverse 2 and Traverse 3 were averaged from measurements taken at Venice Ferry and the Dow site, respectively.

3, just 7 km downwind, the Delta curve overestimates the peak concentration by a factor of two. In Figure 112 however, where average wind speed measured at the release point was used for Traverse 3, the Delta curve gives a very accurate description of the data. The average wind speed for Traverse 2 in Figure 112 was measured at Venice Ferry for the duration of the release. The use of this wind speed does not change the predicted results significantly.

This exercise in detailed Gaussian modeling indicates that under the test conditions, the Gaussian model provides a simple and accurate method for determining pollutant impact. Peak concentrations and plume widths were more than adequately predicted for these traverses. Calculations show that this is true for most of the data obtained during these tests.

Although tracers were released near the surface in every test, the results of the tracer tests can be extended to include effective stack heights which might be typical of industrial chemical facilities. We have seen that the Gaussian expression can be used to predict tracer concentrations given the average meteorological variables as input data. It is also possible to input stack characteristics into an appropriate plume rise model to determine effective stack heights under a variety of wind and stability conditions. The resulting value of H , the effective stack height, can then be used in the Gaussian expression in order to determine the sensitivity of the regional dispersion processes to stack height. Preliminary design data available for the Dow project include stack heights, stack diameters, stack gas temperatures, and exit velocities (Moyer, 1977). These are listed in Table 12. We have taken

TABLE 12

STACK CHARACTERISTICS FROM MONTEZUMA PLANT
(Moyer, 1977)

Source	Stack Height (m)	Stack Diameter (m)	Gas Exit Temperature ($^{\circ}$ K)	Exit Velocity (m/sec)
Stack 1 A	36.6	3.8	450	9.60
Stack 1 B	36.3	3.8	450	9.60
Stack 1 C	19.8	3.4	450	8.40
Stack 1 D	19.8	3.4	450	8.40
Stack 2	19.8	2.1	450	8.40
Stack 3 A	15	1.5	450	12.44
Stack 3 B	15	1.5	450	12.44
Stack 3 C	45	3.0	450	9.34
Stack 4	15	1.7	450	8.25
Stack 5	15	2.9	450	8.25
Stack 6	25	2.5	450	11.50

data for the tallest stack, 37 meters, for input into the Brigg's Plume Rise Model; for details concerning the model, see Briggs (1969) and (1972). The wind speed was taken as the average speed observed at the Dow site during each test, and the Pasquill stability conditions used in the previous modeling analysis were used. Effective stack heights calculated from this data base for each tracer test period ranged from 101 m during Test 3 under class E stability to 415 m during Test 5 under class C stability. The relatively high wind speeds normally observed in the Montezuma Hills cause the calculated plume rise to be smaller than might be expected. The value of H for each test period was used in the Gaussian expression to predict the tracer centerline concentrations. Typical results are given in Figures 113-115. The agreement between predicted and experimental tracer concentrations for Test 1 and Test 6 is representative of all the tests except Tests 3 and 4. In most cases, the concentrations at both close and far downwind distances were predicted reasonably accurately. In Test 4, Figure 114, where conditions were stable, the maximum concentrations observed at 8 km were sharply underestimated by the calculated curves. As could be expected, under some conditions, plume rise decreases the maximum impact at close distances. However, further downwind, the predicted and experimental values are in excellent agreement. Thus, we see that the field study results can, in most cases, be extended directly to characterization of dispersion from stacks typical of possible industrial developments in the area.

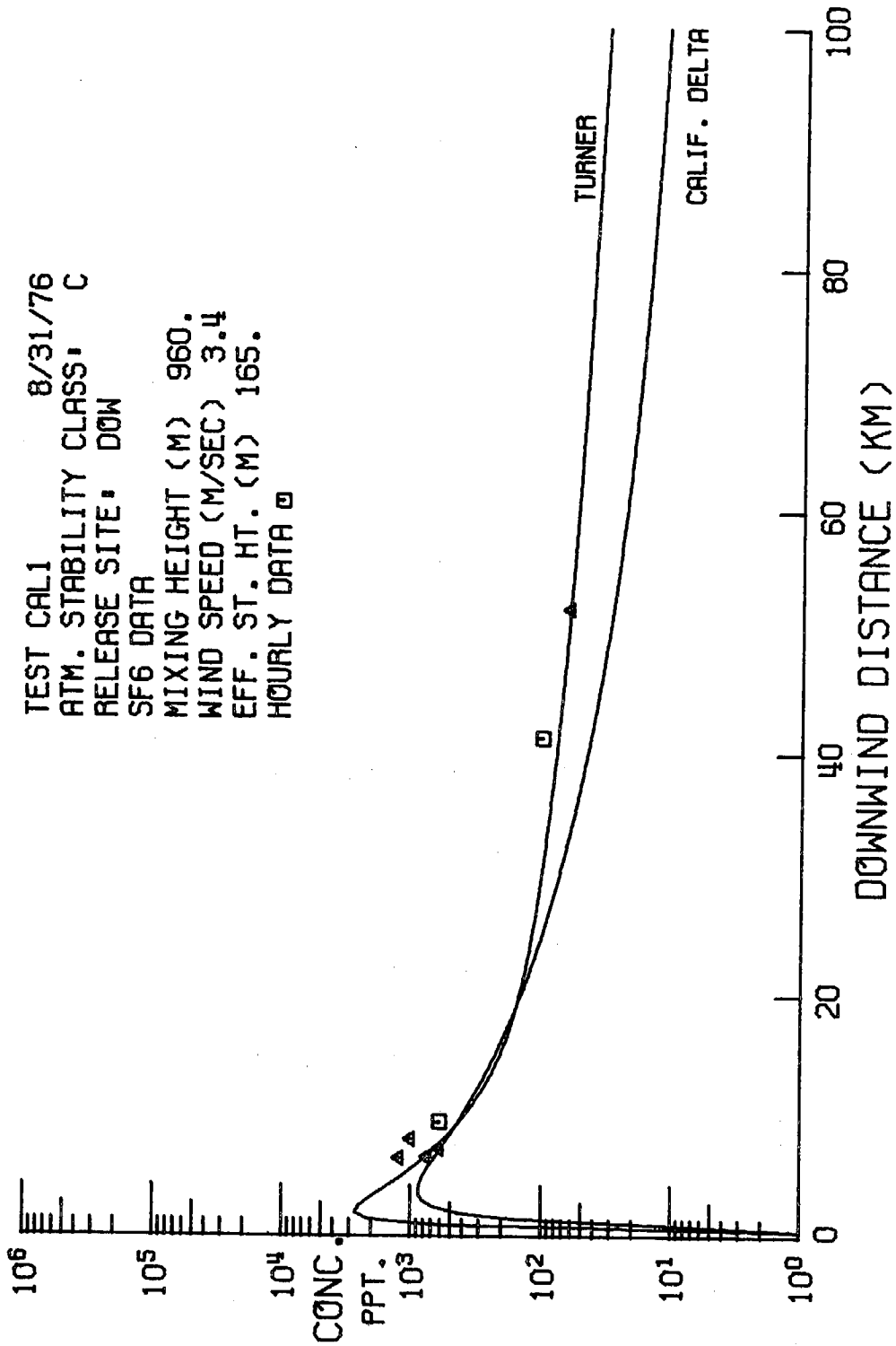


Figure 113. Centerline tracer concentrations compared with centerline concentrations predicted using the Briggs plume rise model and the Gaussian plume model. Stack characteristics were taken from design data for the Dow Montezuma Hills complex. The "Turner" curve is based upon Pasquill dispersion parameters given by Turner (1970); the "Calif. Delta" curve is based upon experimental dispersion parameters.

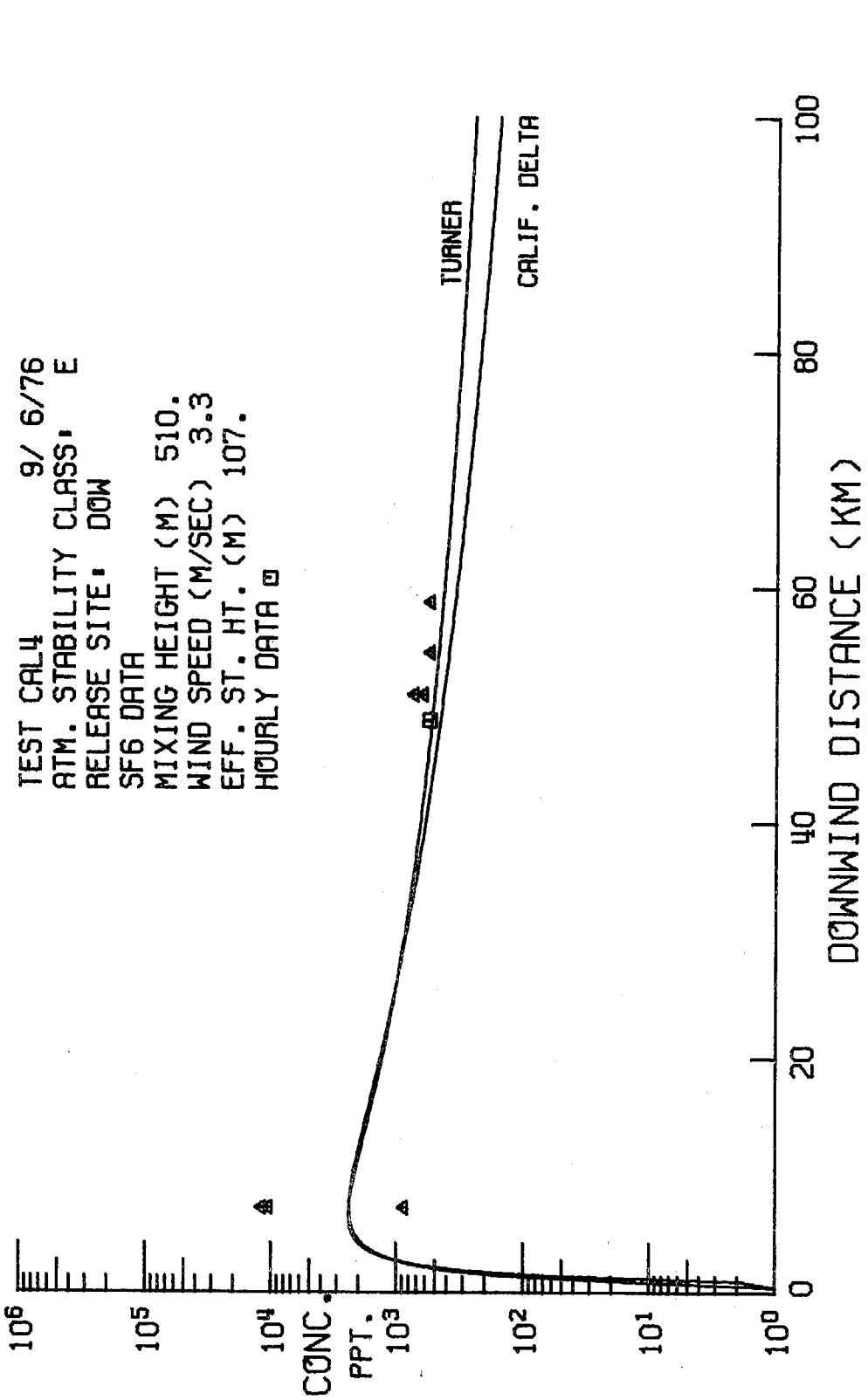


Figure 114. Centerline tracer concentrations compared with centerline concentrations predicted using the Briggs plume rise model and the Gaussian plume model. Stack characteristics were taken from design data for the Dow Montezuma Hills complex. The "Turner" curve is based upon Pasquill dispersion parameters given by Turner (1970); the "Calif. Delta" curve is based upon experimental dispersion parameters.

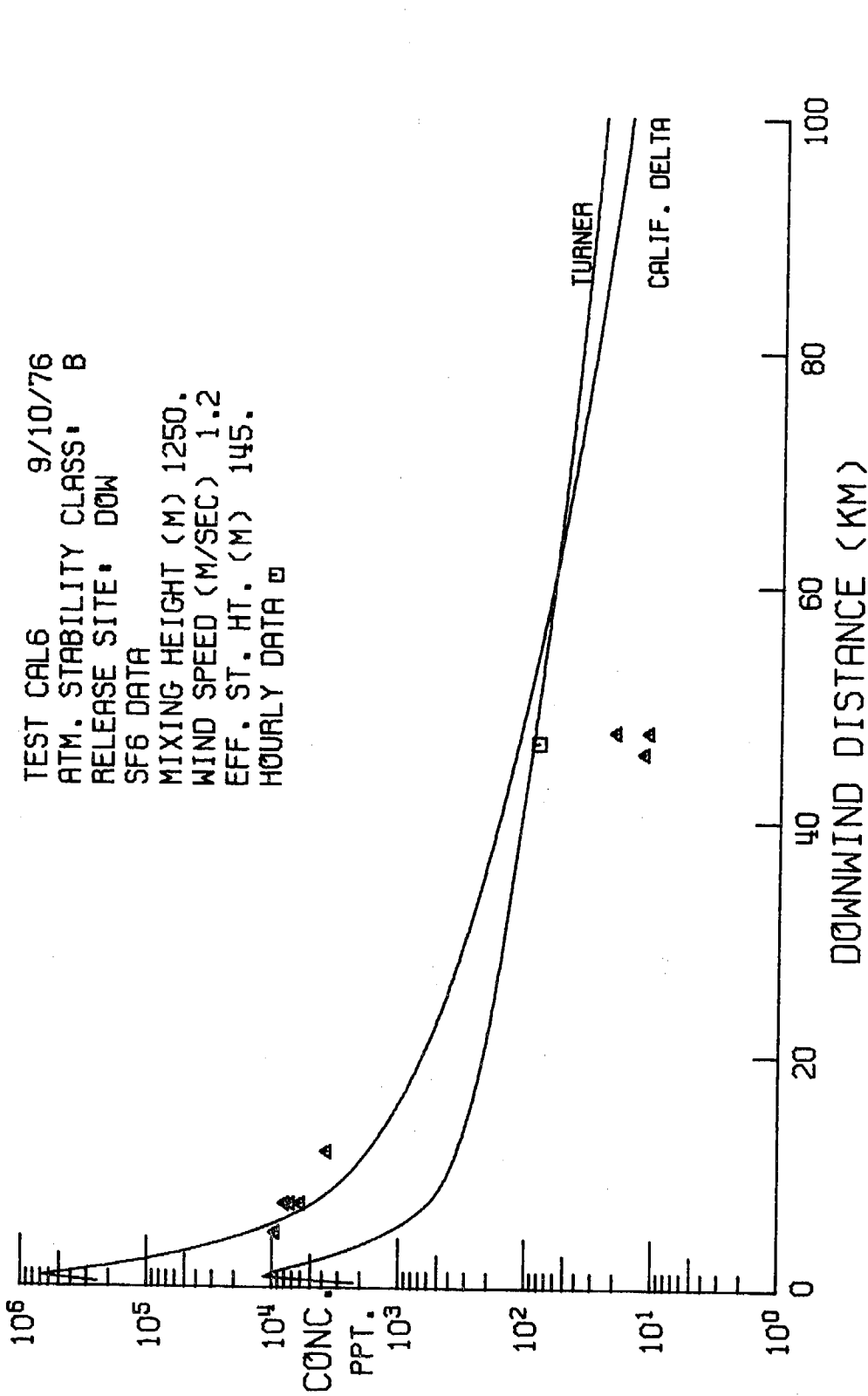


Figure 115. Centerline tracer concentrations compared with centerline concentrations predicted using the Briggs plume rise model and the Gaussian plume model. Stack characteristics were taken from design data for the Dow Montezuma Hills complex. The "Turner" curve is based upon Pasquill dispersion parameters given by Turner (1970); the "Calif. Delta" curve is based upon experimental dispersion parameters.

4.8 Relation of Dispersion Data to Fluctuations of the Wind

Wind data measured by Rockwell at two levels at the Dow site (10 meters and 56 meters) and at Brentwood (10 meters) and data obtained from MRI for the Rancho Seco Nuclear Plant site (61 meters) can be formulated in terms of the hourly horizontal standard deviation of the winds, σ_{θ} . Hourly values of σ_{θ} for Dow and Brentwood were calculated using 5-minute averaged wind directions. Values of σ_{θ} from the Rancho Seco tower were obtained in tabulated form; no information is available concerning the calculation procedure. All of the data are tabulated in Volume II, Part B, Table 17.

A summary of the wind fluctuation data is presented in Figures 116 and 117 for the four locations. The data are plotted for all eight tracer tests as σ_{θ} versus time of day. Gifford (1968) categorized the magnitude of σ_{θ} in terms of the Pasquill stability classes. The values of σ_{θ} corresponding to Pasquill classes are shown in each figure.

The steady nature of the horizontal winds passing over the Montezuma Hills is very apparent in Figure 116. The average values of σ_{θ} during the test period at the Dow site for the lower and upper heights were 10° and 9° , respectively. At distances 19 km downwind of the Montezuma Hills at Brentwood and 65 km at Rancho Seco, the respective averages during the eight tests were 34° and 17° .

The effects of the steadiness of the winds over the Montezuma Hills upon pollutant transport are readily apparent in Figure 118. The plume centerlines observed in traverses along Highway 160 during the releases from the Dow site, on the average, crossed Highway 160 7.6 km north of the

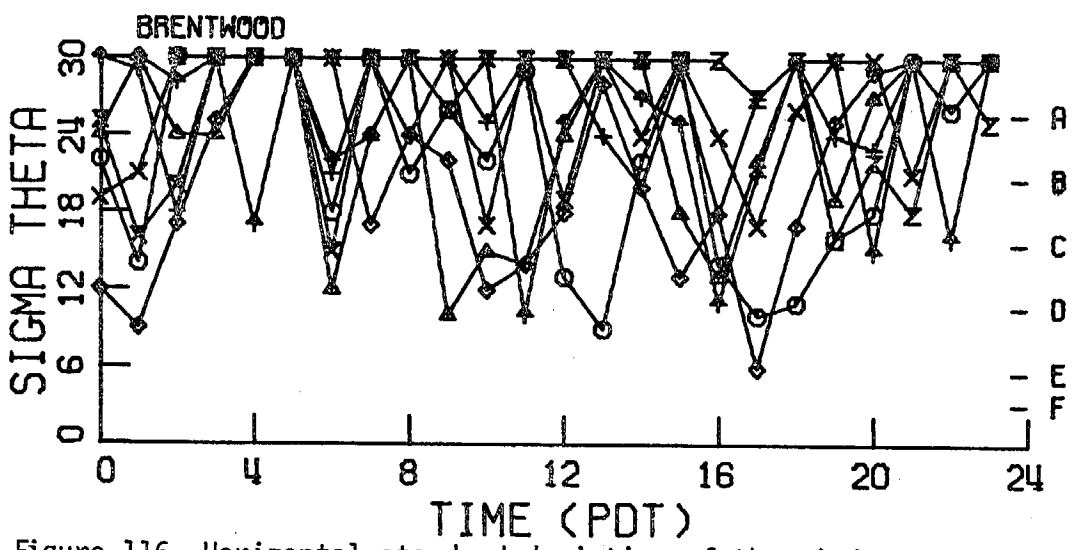
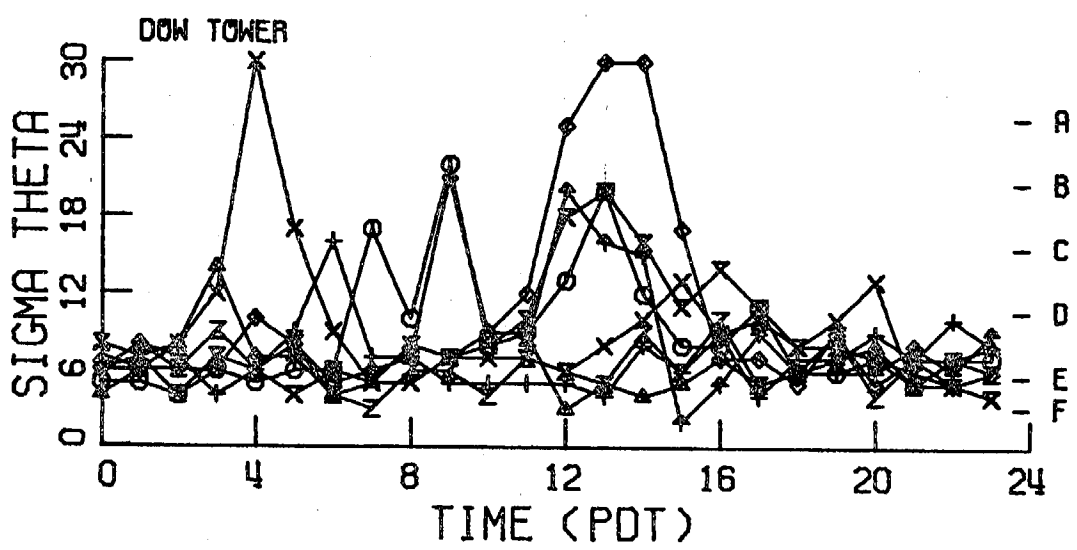
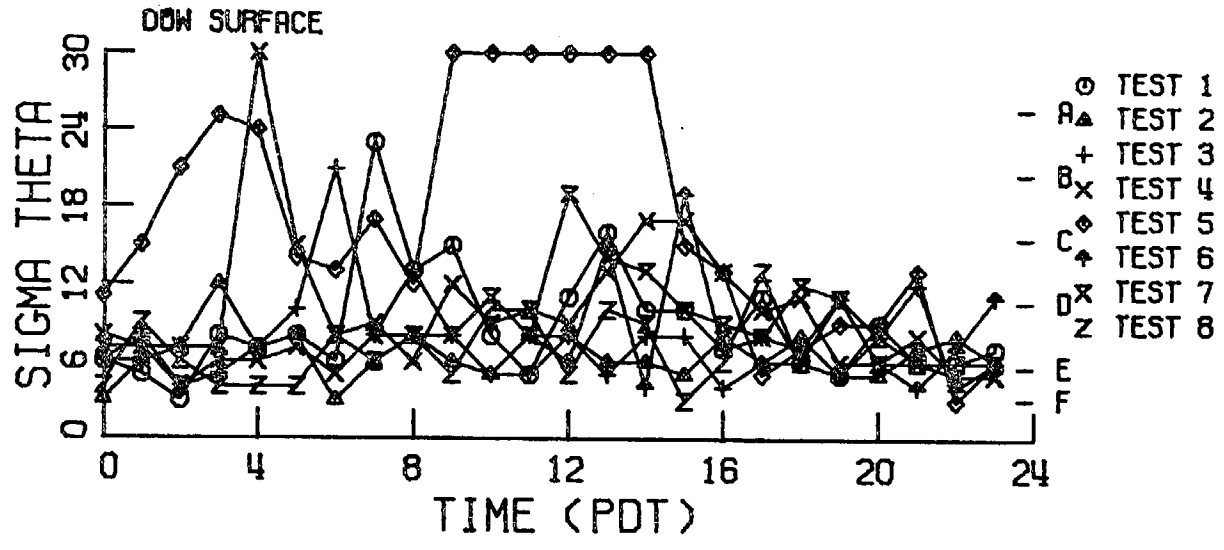


Figure 116. Horizontal standard deviation of the wind as a function of time of day.

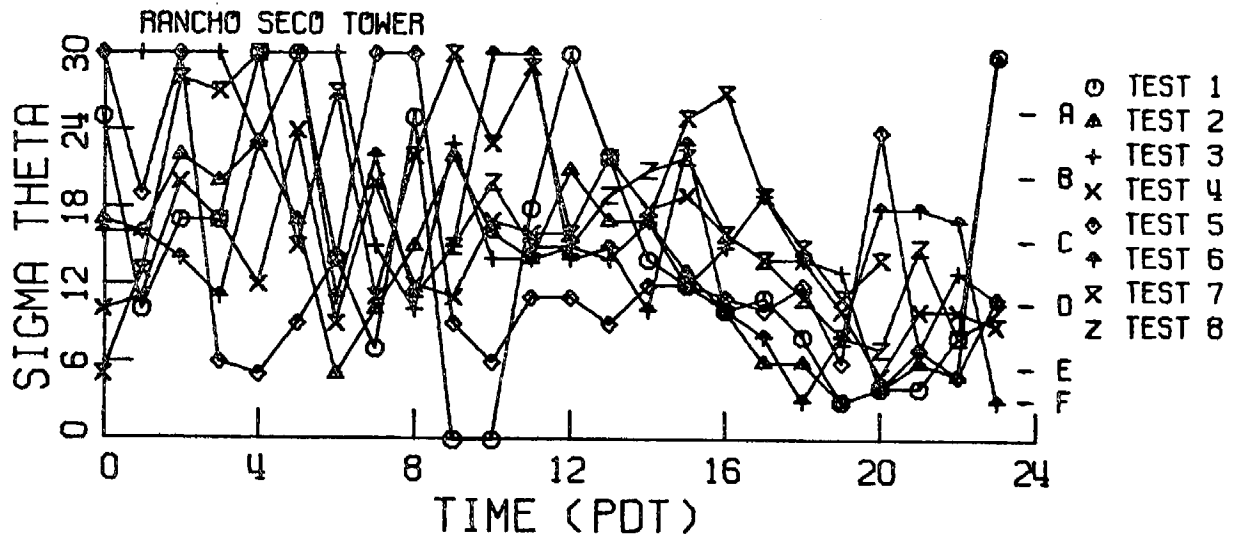


Figure 117. Horizontal standard deviation of the wind as a function of time of day.

Highway 160-Highway 4 junction. The standard deviation of the centerline locations was only ± 1.05 km. Thus, the plume centerlines of pollutants emitted from the Dow site under the test period meteorological conditions would have crossed Highway 160 within a 2.1 km zone, 8 km downwind.

Performing a similar analysis upon the traverse and hourly averaged data obtained along Highway 99 yields Figure 119. In this case, the average plume centerline crossed Highway 99 approximately 72 km south of Sacramento or 5 km south of Stockton. The transport zone across Highway 99 calculated from the standard deviation of the centerline locations extended 28 km along the highway. A straight line can be drawn from the release point in the Montezuma Hills to the average centerline position of the plume crossing Highway 160. The extension of this line intersects Highway 99 approximately 2 km north of the observed centerline position. On the average, plumes emitted from the Montezuma Hills during the test periods were transported southeast directly over Stockton. The average plume centerlines from the Dow site to Highway 160 and from Highway 160 to Highway 99 are shown in Figure 120; the standard deviations associated with the centerline positions are also shown. The area enclosed by the standard deviations of the plume centerline positions correspond to the area of major impact which was observed during the eight tracer tests. This area also appears to be closely related to the area swept out by the average value of σ_{θ} during the field study. The angle associated with the standard deviation

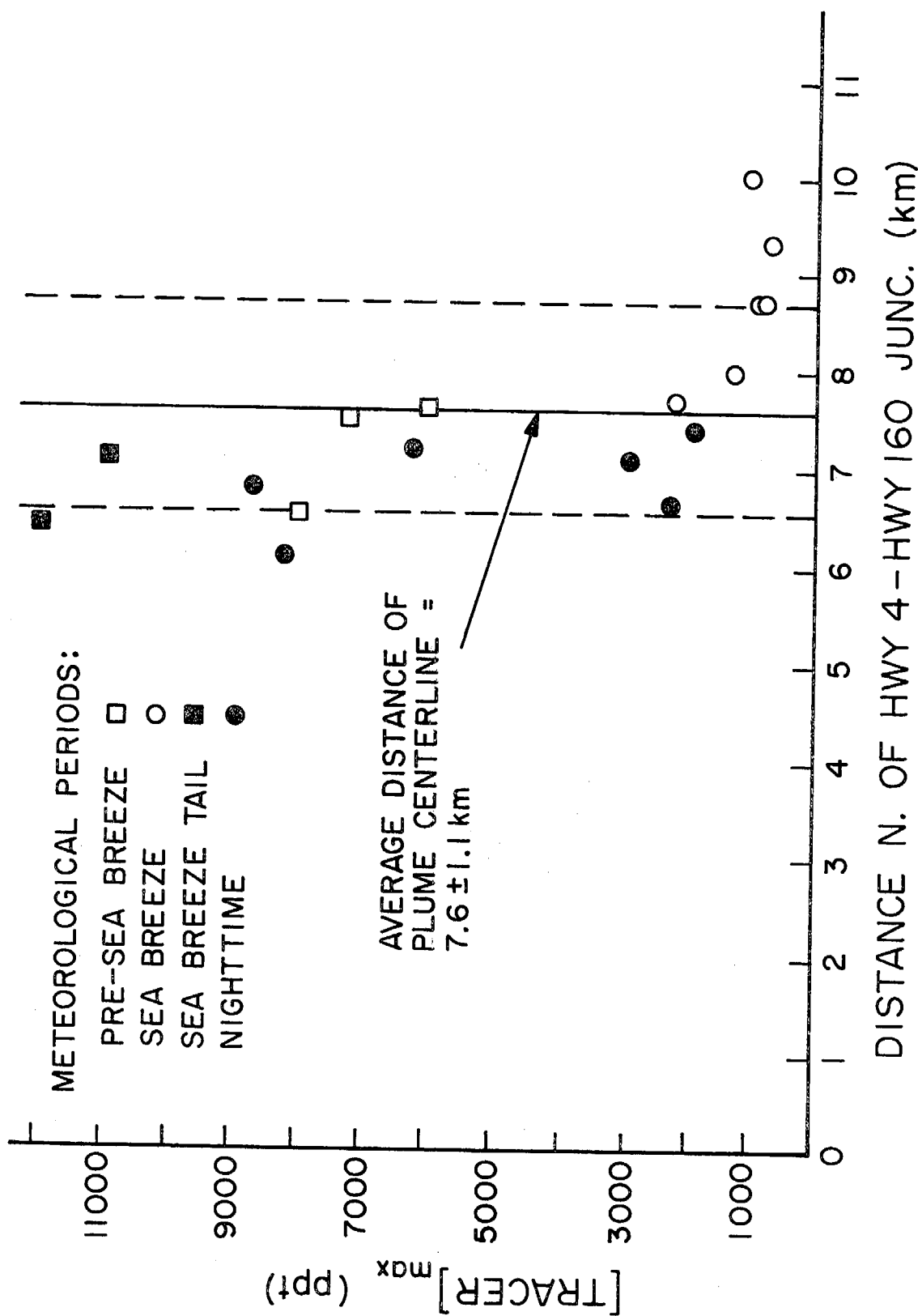


Figure 118. Plume centerline concentration as a function of distance north of the Highway 4 - Highway 160 junction taken from automobile traverse data for Dow tracer releases.

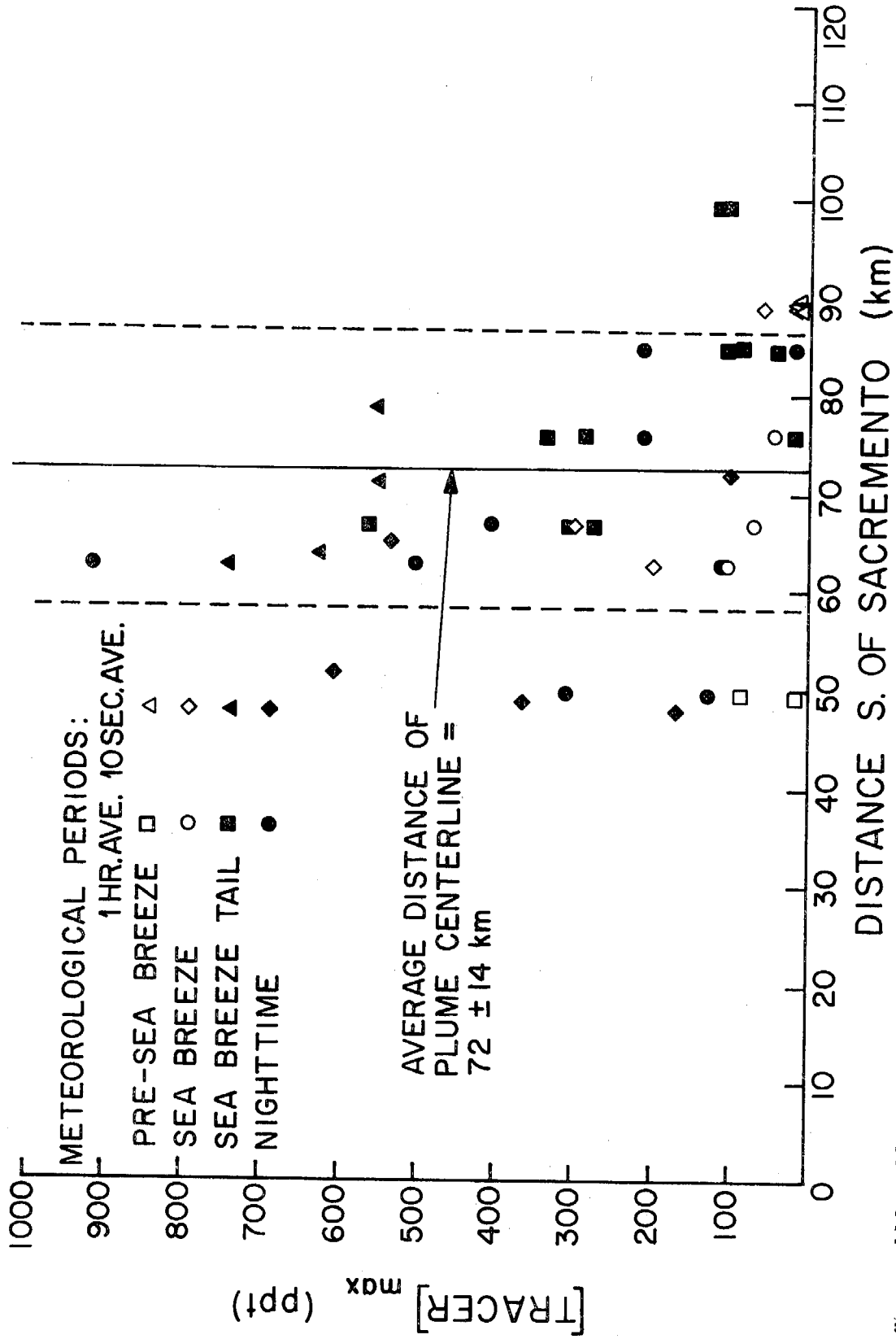


Figure 119. Plume centerline concentration as a function of the distance south of Sacramento along Highway 99 taken from automobile and hourly averaged crosswind tracer profiles.

of the centerline locations along Highway 160 is 8° ; the average value of σ_{θ} during the tests was 9° . Although the average value of σ_{θ} agrees very well with the angle determined from the traverse centerline fluctuations, the vector-averaged wind direction during the seven Dow releases does not coincide with the average centerline locations along Highway 160 and Highway 99. The average wind direction was 275° ; the angle associated with the location of the average centerline was approximately 285° . The location of maximum impact predicted from the average Dow wind direction is 11 Km north of the location of the average centerline along Highway 99. It appears that curvature of the winds immediately downwind of the Dow site causes the plumes emitted from the Montezuma Hills to turn slightly more to the southeast than expected. As we will see in Section 5, this curvature does appear when wind data from stations downwind of Dow are included in a plume trajectory analysis.

A further result of the nature of the winds over the Delta region is the relationship observed between maximum tracer concentrations in the 10-second and hourly averaged data. Hino (1968) states that the "maximum or axial time-mean concentration of effluent generally decreases with increasing sampling time because the lateral dispersion of effluent increases with time." Hino found in an analysis of a variety of diffusion data that the relationship between maximum concentrations and sampling times generally followed:

$$\frac{C_1}{C_2} = \left(\frac{t_1}{t_2} \right)^{-1/5} \quad \text{for sampling times less than 10 minutes} \quad (16)$$

and

$$\frac{C_1}{C_2} = \left(\frac{t_1}{t_2} \right)^{-1/2} \quad \text{for sampling times from 10 minutes to several (17) hours.}$$

Hino showed that the exponent of $-1/2$ in the second relationship was predicted from theoretical grounds as well as from experimental data. The value of $-1/5$ for short sampling times had been recommended by Nonhebel (1960) and was confirmed in the Hino analysis.

In view of these relationships, conversion of the 10-second averaged maximum concentrations to hourly averaged values should follow the combined relationship:

$$\frac{C_{HR}}{C_{10s}} = \left(\frac{t_{10m}}{t_{10s}} \right)^{-1/5} \left(\frac{t_{HR}}{t_{10m}} \right)^{-1/2} \quad (18)$$

where C_{HR} is the hourly value, C_{10s} is the 10-second value, t_{10m} equals 10 minutes, t_{10s} equals 10 seconds, and t_{HR} equals 3600 seconds. Equation (18) results from converting C_{10s} to a 10-minute value using Equation (16) and substituting the converted concentration into Equation (17). The final result may be written as

$$\frac{C_{HR}}{C_{10s}} = 0.18 \quad (19)$$

Thus, according to Hino, maximum hourly averaged concentrations should be approximately one-fifth of the 10-second averaged maximum concentrations. This relationship can be checked easily for the Delta region by comparing the traverse results along Highway 160 and Highway 99 with the hourly averaged data for the hours in which traverses were completed. The results of this comparison are tabulated in Table 13; the ratio of C_{HR}/C_{10s} for each case is also listed. No comparisons were made for the last three tracer tests because traverses were not taken during the hours where maximum hourly values were found.

In view of our previous discussion concerning the steadiness of the winds over the Delta region, the results are not at all surprising. Instead of changes in concentrations by the factor of 5 suggested by Hino, the hourly values are generally no more than a factor of 2 less than the 10-second maximum concentrations. The overall average of the experimental ratio is

$$\frac{C_{HR}}{C_{10s}} = 0.7 \quad (20)$$

These results indicate that the 10-second averaged maximum tracer data can be converted to hourly averaged values rather simply and with reasonable accuracy. This will allow us to estimate maximum hourly averaged pollutant concentrations using the traverse σ_y and σ_z data with the Gaussian plume model. Such estimations will be useful in determining where and when air quality standards might be violated due to emissions from an industrial facility. Presentation of this analysis follows in Section 4.9.

220
TABLE 13

COMPARISON OF 10-SECOND AND HOURLY AVERAGED MAXIMUM TRACER CONCENTRATIONS

Date	Time PDT	C _{10s} PPT	C _{HR} PPT	C _{HR} /C _{10s}
8/31/76	1347-1447	611	241	0.394
		1013	241	0.238
	1447-1547	756	470	0.622
	1547-1647	1223	602	0.492
	1700-1800	64	44	<u>0.688</u>
			Ave. =	0.487 ± 0.180
9/2/76	1336-1436	33	17	0.515
		CBrF ₃	2168	2427
	1436-1536	19	11	0.579
		28	11	0.393
	CBrF ₃	840	1905	2.27
		1600-1700	29	12
	1700-1800	91	13	0.143
	1800-1900	32	21	<u>0.656</u>
			Ave. =	0.761 ± 0.671
9/5/76	0200-0300	537	504	0.939
	0400-0500	370	309	0.835
		608	309	<u>0.508</u>
			Ave. =	0.761 ± 0.225
9/6/76	2100-2200	746	305	0.409
	2200-2300	628	566	0.901
		553	566	1.024
	2300-2400	553	333	<u>0.602</u>
			Ave. =	0.734 ± 0.280

Overall average = 0.687 ± 0.452

The preceding results suggest that it is possible to relate the magnitude of the wind fluctuations to the magnitude of the horizontal dispersion parameter in a straightforward manner. If one assumes that the centerline of a plume fluctuates within the angle of the standard deviation of the wind as we have seen, then an ideal crosswind dispersion distance can be defined as

$$A = X \tan(\sigma_{\theta}) \approx X \sigma_{\theta} \quad (21)$$

where σ_{θ} is measured in radians and A is simply half the crosswind distance through which the plume centerline moves in an hour, measured at the downwind distance, X. In other words, A represents an ideal dispersion parameter based only upon the crosswind fluctuation of the plume centerline. To see how the experimental dispersion parameter is related to values of σ_{θ} in the Delta region, σ_y for each traverse is plotted in Figure 121 as a function of σ_{θ} . Values of A were based upon the value of σ_{θ} measured at the surface on the Dow site for the hour in which the traverse was taken. The best-fit line through the data in Figure 121 indicates that σ_y can be written as a simple function of σ_{θ} :

$$\sigma_y \approx 0.6 X \sigma_{\theta} . \quad (22)$$

Values of σ_{θ} were calculated from 5-minute averaged wind directions.

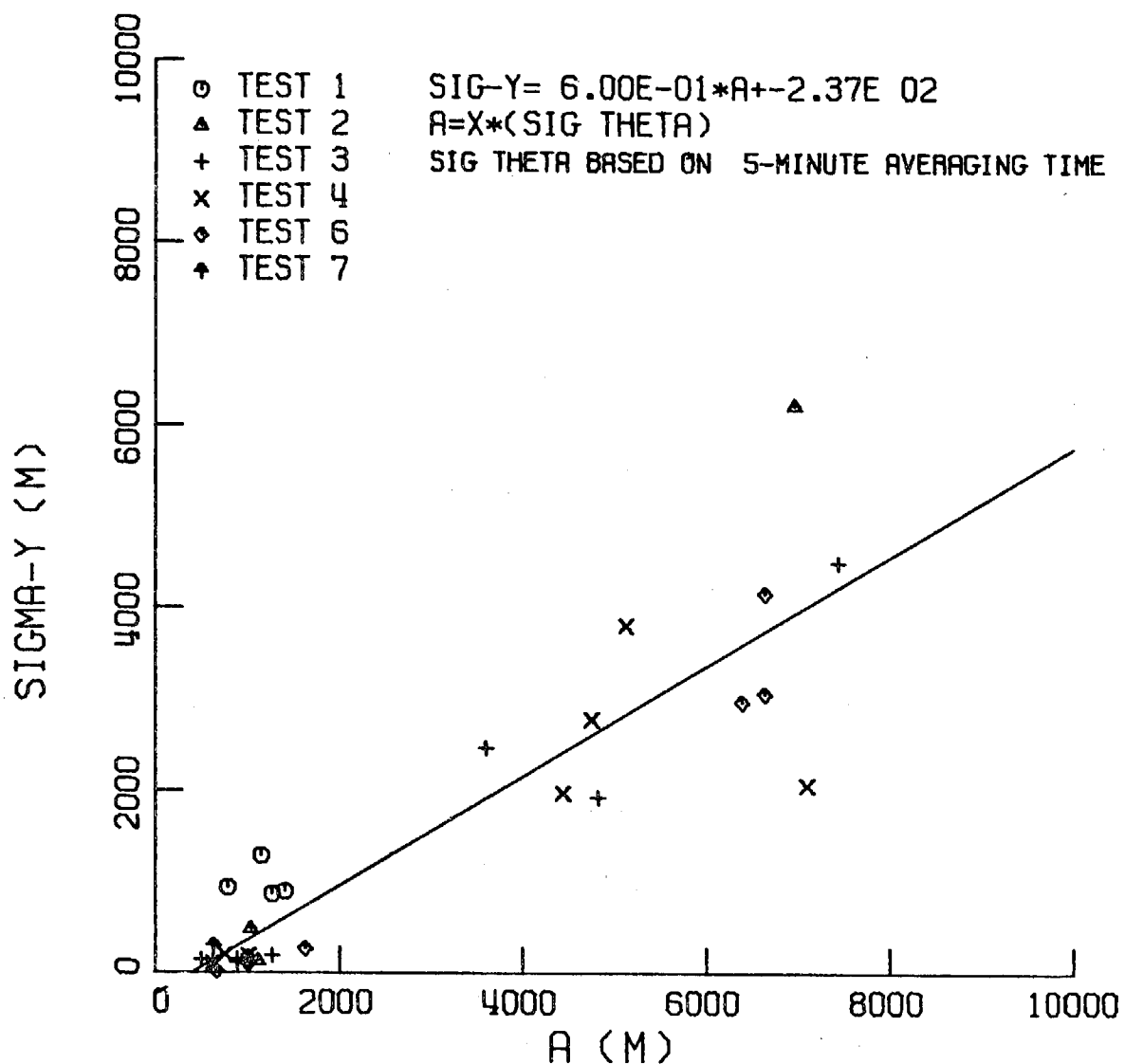


Figure 121. Horizontal Crosswind Standard Deviation (σ_y) as a function of the horizontal standard deviation of the wind (σ_θ) measured at the Dow site in the Montezuma Hills.

This relationship is very similar to an equation given by Islitzer (1961) for an unstable atmosphere:

$$\sigma_y = 0.81 \times \sigma_\theta \quad (23)$$

where σ_θ was based on 5-second averaged wind directions and σ_y was measured at downwind distances up to 3.2 km. In a later work, Islitzer and Dumbauld (1963) found that values of σ_y equaled $\times \sigma_\theta$ for unstable atmospheres if values of σ_θ were based on averaging times dependent upon the travel time from the source to the receptor. These times were determined to be a function of β , the ratio of the Lagrangian to Eulerian time scales.

The difference between the results of these earlier works and the relationship predicted from the field study can possibly be explained by noting that the wind direction averaging times were considerably different and the transport distances in the Delta study were considerably greater than in those cited above. Islitzer, recalling work by Hay and Pasquill (1959), states that the correct averaging time is determined from the proper part of the spectrum of turbulence by

$$s = T/\beta \quad (24)$$

where β is taken to equal 5 and T is the transport time, X/u . In the Delta field study values of s were of order 7 minutes at 8 km and 50 minutes at 50 km. The actual averaging time used was 5 minutes.

The 5-minute wind direction averages can be summed and averaged to give 10-minute and longer averaging times. These average directions can then be used to determine the hourly standard deviation of the winds based on a new averaging time. To investigate the effects of longer averaging times upon the relationship between σ_y and σ_θ , we have calculated hourly averaged values of σ_θ based on 10-minute, 15-minute, and 20-minute averaging times. The results for all eight tests are given in Figure 122. The general effect of longer averaging times is to decrease the standard deviation of the wind during an hour. The new relationships between σ_y and σ_θ for increasing averaging times are shown in Figures 123 - 125 .

The slopes of the best-fit lines for the three averaging times appear to go through a maximum for σ_θ (15-minutes). The respective relationships for the increasing values of s are:

$$\sigma_y = 0.60 \times \sigma_\theta \text{ (5-minutes)}, \quad (25)$$

$$\sigma_y = 0.65 \times \sigma_\theta \text{ (10-minutes)}, \quad (26)$$

$$\sigma_y = 0.76 \times \sigma_\theta \text{ (15-minutes)}, \quad (27)$$

and

$$\sigma_y = 0.75 \times \sigma_\theta \text{ (20-minutes)}. \quad (28)$$

These results indicate that the proportionality coefficient between σ_y and $\sigma_\theta(s)$ is very sensitive to the magnitude of s . If, indeed, $\sigma_y = X \sigma_\theta (s)$ for a specified value of s , then the results of this analysis suggest that s lies close to 15 minutes for the dispersion data under consideration. Of course, it is possible that the difference between $s = 15$ and $s = 20$ is insignificant, and the correct value of s is larger than 20 minutes. At any rate, it does appear that the initial

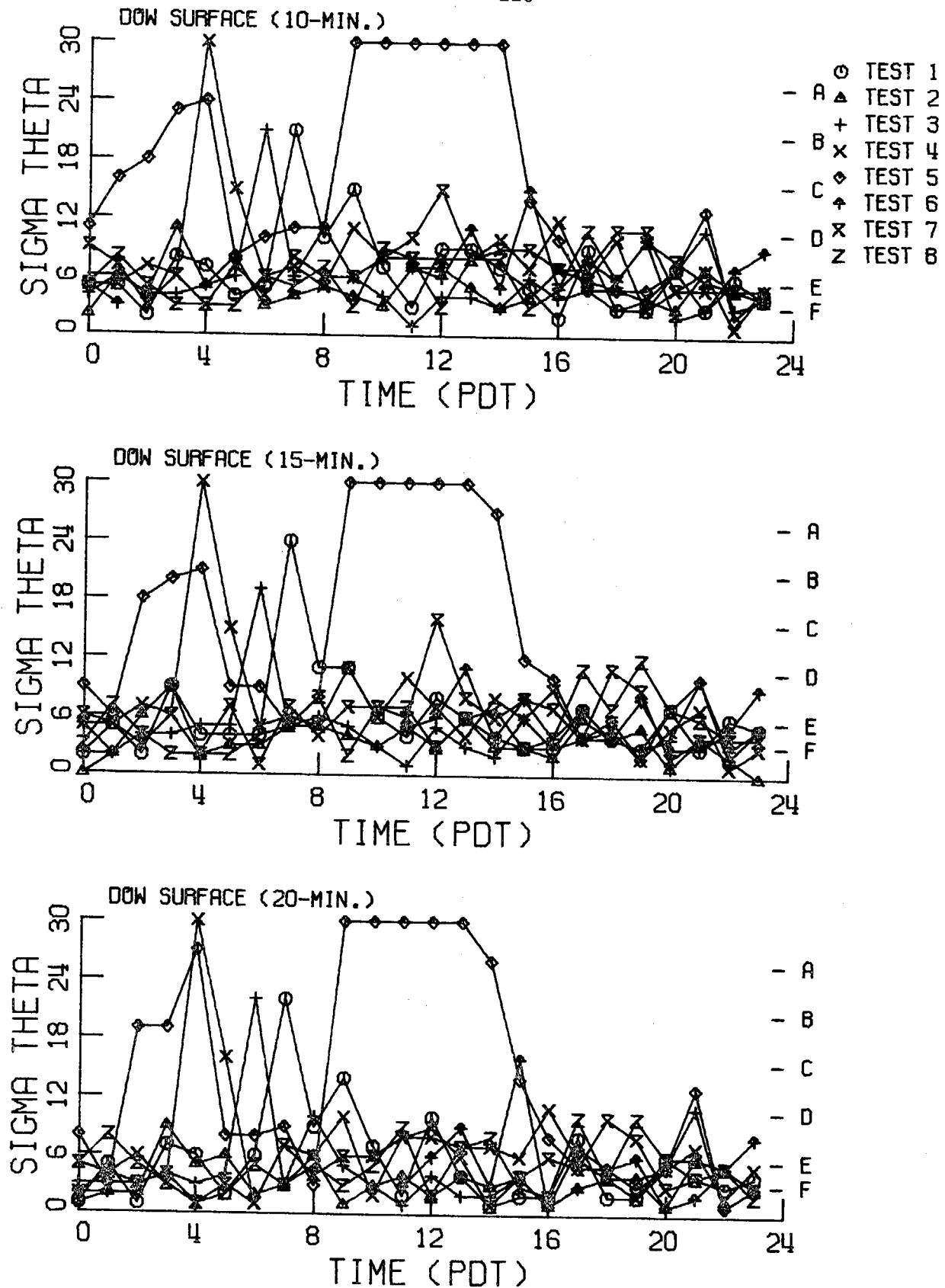


Figure 122. Horizontal standard deviation of the wind, σ_θ , as a function of time of day for different averaging periods.

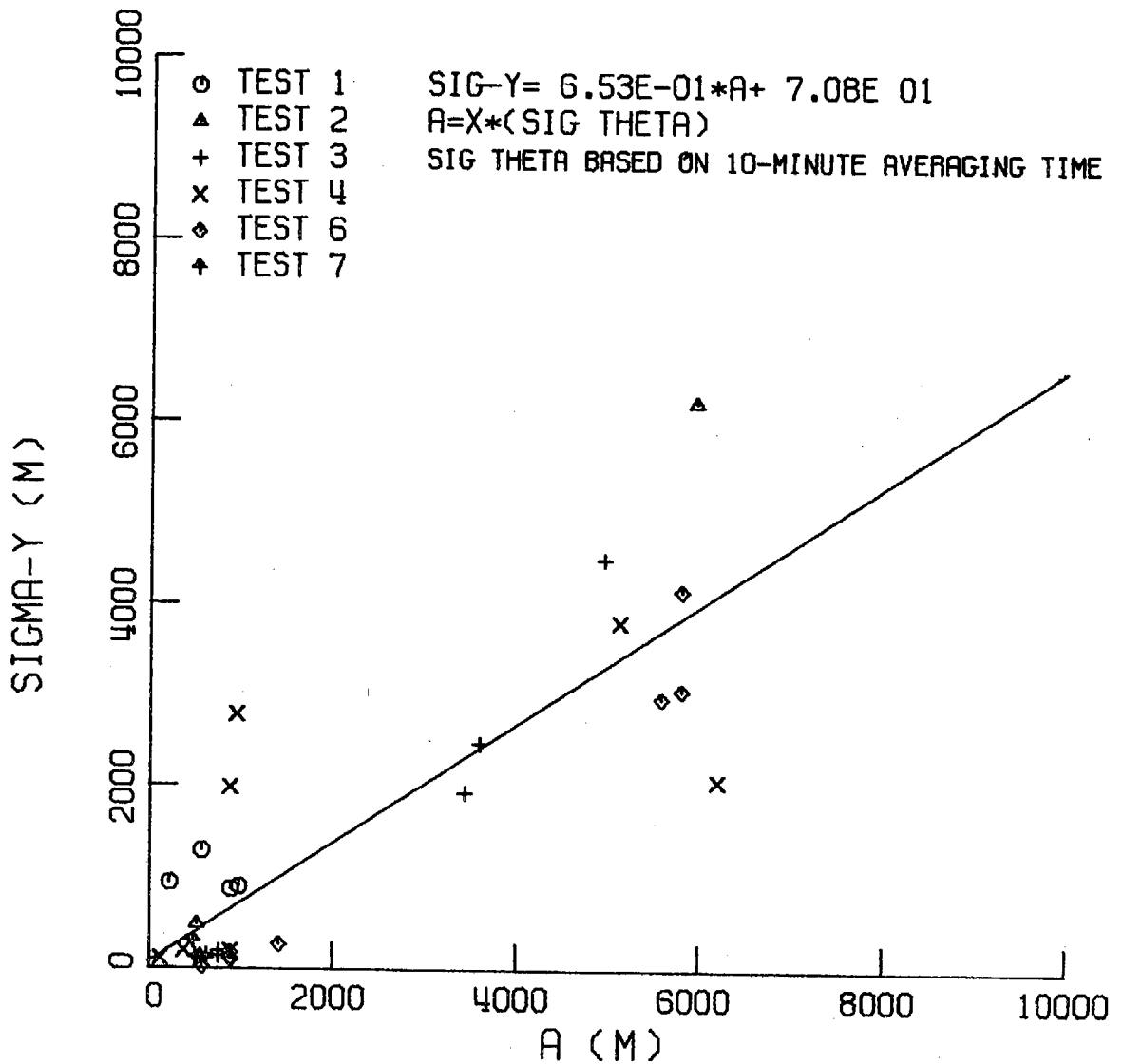


Figure 123. Horizontal crosswind standard deviation, σ_y , as a function of the horizontal standard deviation of the wind, σ_θ , measured at the Dow site in the Montezuma Hills.

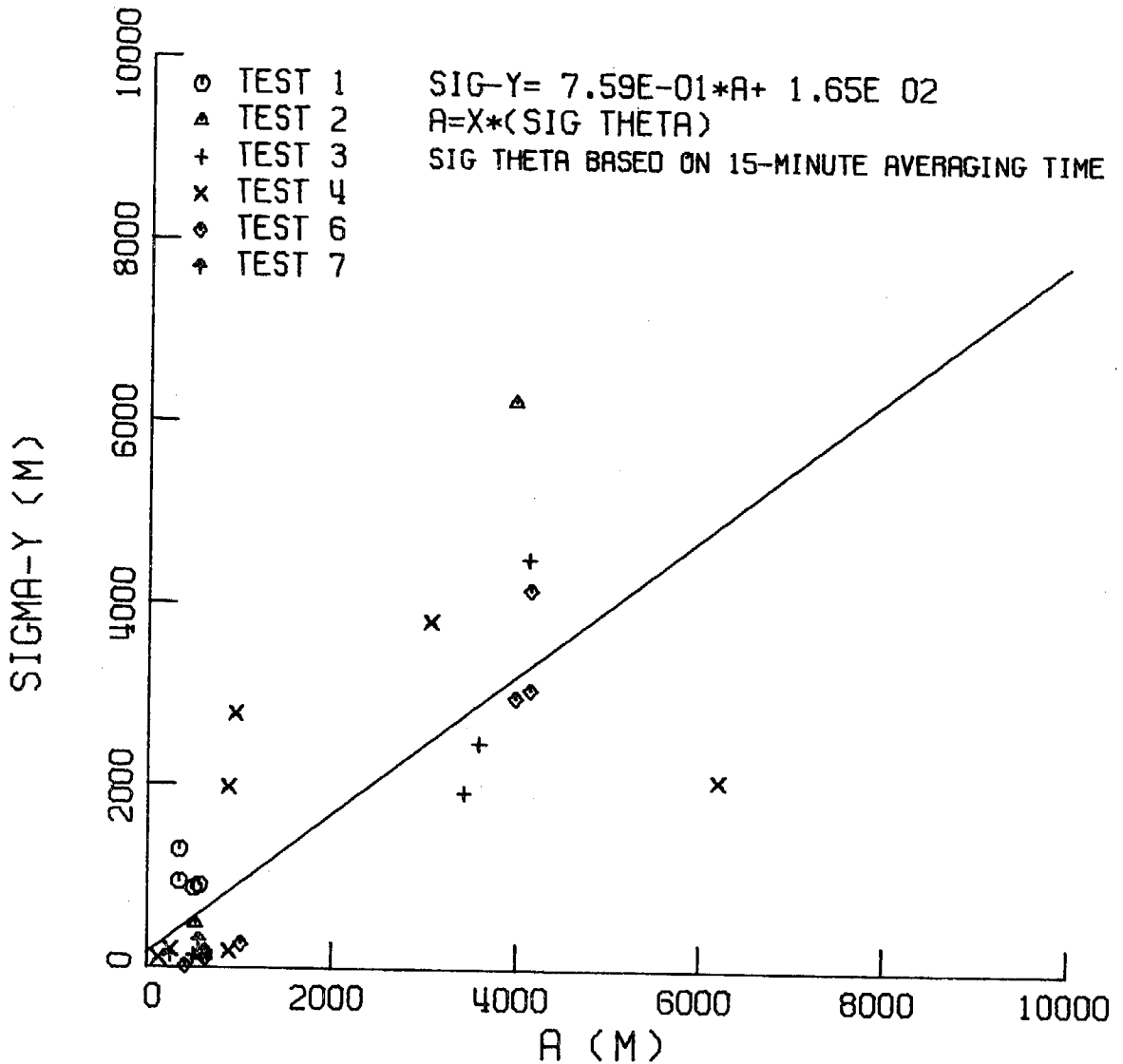


Figure 124. Horizontal crosswind standard deviation, σ_y , as a function of the horizontal standard deviation of the wind, σ_θ , measured at the Dow site in the Montezuma Hills.

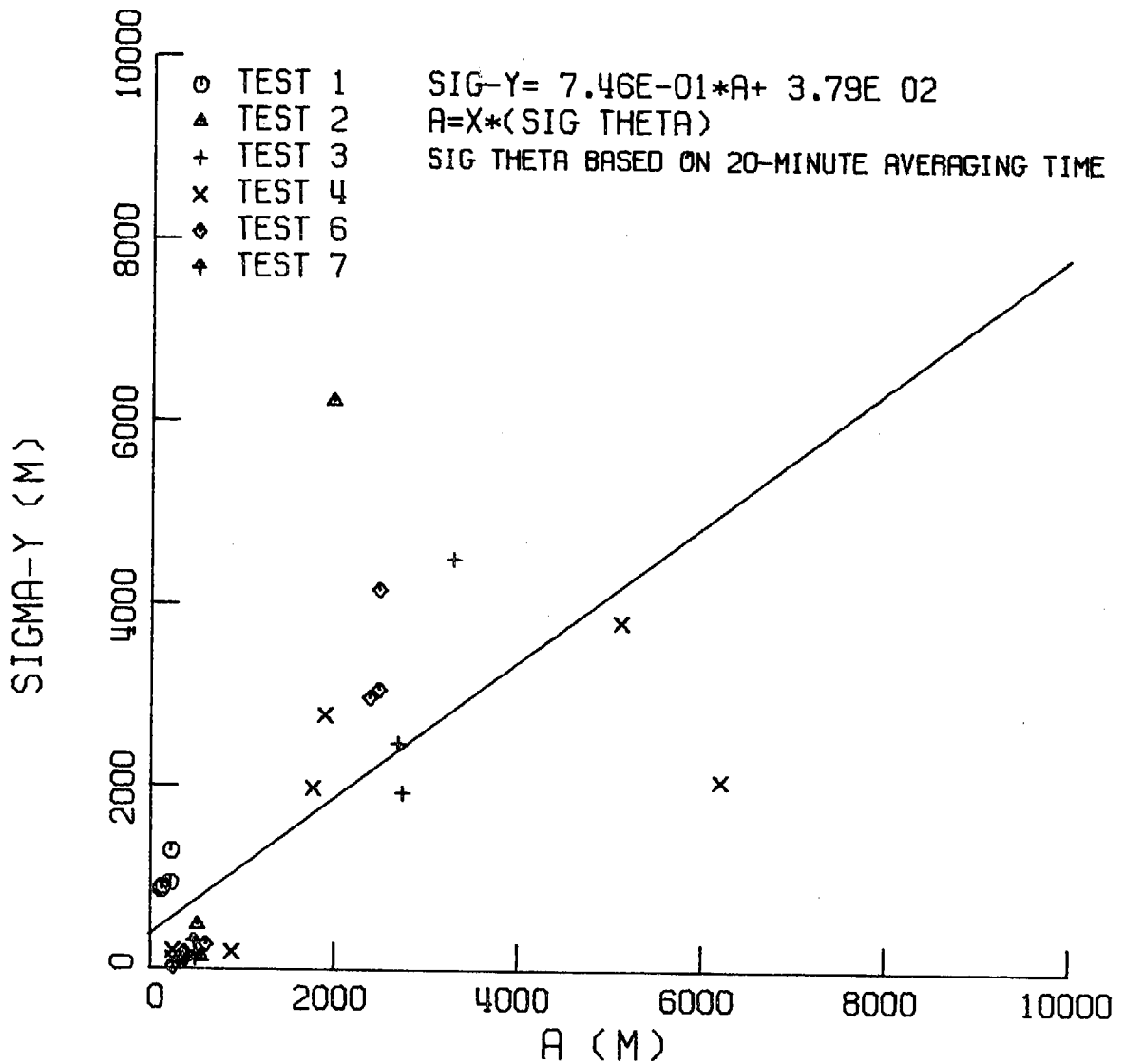


Figure 125. Horizontal crosswind standard deviation, σ_y , as a function of the horizontal standard deviation of the wind, σ_θ , measured at the Dow site in the Montezuma Hills.

relationship determined from a 5-minute average time can be improved by considering the proper range of averaging times. However, this improvement is limited since the wind data is available only in 5-minute increments. For the distances and transport times under consideration in the Delta region, a better averaging time for wind fluctuation measurements might be 1 minute. Summation of 1-minute intervals would provide a more flexible means of determining the proper averaging time.

Even though the available wind fluctuation data does not yield a one-to-one relationship between σ_y and $X \sigma_\theta$, it appears that the experimental extent of horizontal dispersion in the Delta region can be determined for other periods of the year by simply acquiring the appropriate wind fluctuation data. Although it may prove difficult to obtain a suitable amount of historical σ_θ data in the area, acquiring a data base in the future will only be a matter of operating a wind anemometer and strip-chart recorder at the appropriate times and places. The acquisition of a suitable data base and the application of the simple relationship between σ_y and σ_θ to the data provide a simple, but important method of extending the results of the California Delta tracer tests to other periods of the year.

4.9 Estimated Maximum Pollutant Concentrations

The tracer data can be used with the nomographs and projected Dow emissions in Section 4.1 to estimate the maximum pollutant concentrations which would have been measured during the test periods if the Dow facility were in operation. The maximum tracer concentrations which were measured during the study and the corresponding pollutant concentrations are given in Table 14. The values of the California air quality standards are also listed. Emissions of NO are assumed to be rapidly converted to NO₂. Results due to the Dow + turbine emissions are also given.

Comparison of the calculated pollutant concentrations and the air quality standards indicate that only the standard for NO₂ appears to be in danger of violation. Both SO₂ and CO levels are far below the respective standards. For NO₂, the observed hourly averaged data indicate that the standard would not have been violated during the test period. Except for the first two tests, the hourly data were all collected 50 km downwind along Highway 99. In 10-second data, much higher concentrations were measured approximately 10 km downwind. However, in no case based on the Dow emissions were tracer concentrations great enough to cause the NO₂ standard to be violated. The possibility of a standard violation appears more likely if the Dow facility were to include a gas turbine. If the sampling time correction from Section 4.8 is applied to the 10-second data for the Dow + turbine emissions, the data indicate that the NO₂ standard might have been violated during Tests 3, 4, 6, and 7 at downwind distances of approximately 10 km. Converted NO₂ 10-second concentrations greater than 357 ppb are in violation of the standard. Worst-case conditions, according to this data, occur during the evening Sea Breeze Tail period.

TABLE 14

MAXIMUM POLLUTANT CONCENTRATIONS DUE TO PROJECTED DOW EMISSIONS

Test	[Tracer] _{max}	[Pollutant] _{max} *					
	ppt	Dow Emissions			Dow + Turbine Emissions		
	<u>10-second</u>	[NO ₂]**	[SO ₂]	[CO]	[NO ₂]	[SO ₂]	[CO]
1	1,013	30	3	5	74	3	25
2	2,168	42	4	7	103	4	35
3	8,660	286	24	49	701	28	241
4	11,900	346	29	59	848	34	290
5	801	23	2	4	57	2	20
6	9,526	284	24	49	698	28	241
7	12,140	238	20	41	584	23	201
	<u>1-hour</u>						
1	602	18	2	3	43	2	15
2	2,427	46	4	8	112	4	38
3	918	30	3	5	74	3	26
4	566	16	1	3	40	2	14
5	-						
6	83	3	.2	.4	6	.2	2
7	-						

California Hourly Air

Quality Standards: 250 ppb (NO₂); 500 ppb (SO₂); and 40,000 ppb (CO).

$$* \text{Pollutant}_{\max} = \text{Tracer}_{\max} \cdot \frac{MW_T}{RR_T} \cdot \frac{RR_P}{MW_P}$$

MW_T and MW_P are the tracer and pollutant molecular weights, respectively;
 RR_T and RR_P are the tracer and pollutant emission rates, respectively.

** Emissions of NO have been assumed to react rapidly to form NO₂.

The Gaussian model predictions can be used to estimate the extent that the Dow project might influence existing air quality in the area. It appears that the air quality standard for NO_2 could possibly be violated at downwind distances of 10 km during stable evening and nighttime periods. It is of interest to determine how far downwind emissions of NO might produce levels of NO_2 greater than those that currently exist. During the two-week test period, maximum NO_2 concentrations in the area reached 0.06 ppm. By utilizing the nomograph in Section 4.1 and the predicted concentration curve for the evening test shown in Figure 126, we estimate that hourly averaged NO_2 concentrations due to Dow emissions were greater than 0.06 ppm up to 24 km downwind. This estimation assumes the conversion of NO to NO_2 is rapid and that hourly averaged values are related to the 10-second averaged data as given in Section 4.8. Similar use of the curves for the Sea Breeze period and for the Nighttime period indicate that NO_2 concentrations were greater than 0.06 ppm up to 4 km and 14 km, respectively. The emission rate of NO from the Dow site was taken to be 9.4 tons/day. These distances would increase if the projected Dow + turbine emission rate of 23 tons/day were used. The estimated impact of projected Dow emissions could double NO_2 concentrations over a significant distance downwind of Montezuma Hills.

The results of the analysis of maximum NO_2 concentrations due to projected Dow emissions are summarized in Table 15. The ambient NO_2 levels and the tracer-converted NO_2 data are compared with Gaussian model predictions presented by Dow and the predictions presented in this report. The Dow-predicted value of NO_2 at 10 km was taken from data presented by Dow officials as testimony during State of California

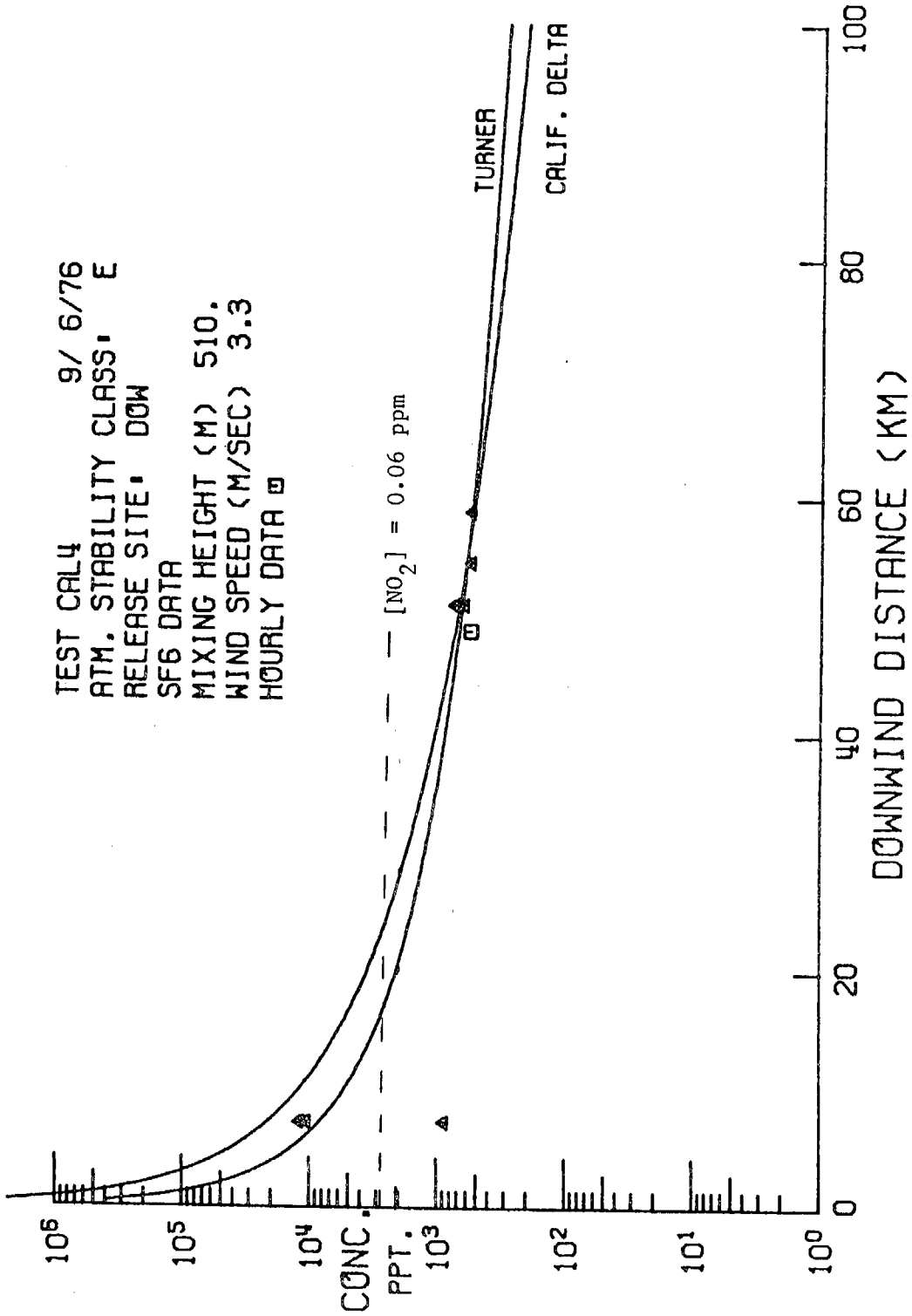


Figure 126. Estimation of distance downwind of the Montezuma Hills where the concentration of NO₂ (caused by projected Dow emissions) equals maximum ambient levels.

TABLE 15

COMPARISON OF NO₂ CONCENTRATION MEASUREMENTS AND PREDICTIONS

Test	Ambient Measurements ¹		[NO ₂] _{max} ppb		Predicted by ³ Dow	Predicted Using Tracer Dispersion Data ⁴	
	Montezuma Hills	Stockton	Estimated from Tracer Data ² (hourly average) 10 Km	50 Km		10 Km	50 Km
1	50	70	18	3.0	5.8 at 10 Km from tracer release	12	0.7
2	60	80	46	-		81	2
3	40	70	(200)	30		105	6
4	50	60	(242)	16		250	17
5	70	-	(16)	-		9	1
6	70	80	(199)	-		-	-
7	10	60	(167)	-		-	2
8	40	60	-	-		-	-

¹ Ambient hourly averaged concentrations collected by Rockwell at Montezuma Hills and the San Joaquin APCD at Stockton during the test period.

² NO₂ concentrations estimated using maximum observed hourly-averaged tracer concentrations and projected Dow emission rates. Values in parentheses are hourly values estimated from 10-second data, $C_{HR}/C_{10s} = 0.7$.

³ Predicted by Dow for worst-case conditions using the Gaussian plume model. Data presented as testimony during State of California multi-agency hearings, December, 1976.

⁴ NO₂ concentrations predicted using the experimental σ_y and σ_z values and projected Dow emissions in the Gaussian plume model. Although σ_y and σ_z were obtained from 10-second average tracer data, comparison of 10-second and hourly averaged tracer data indicate that $C_{HR}/C_{10s} = 0.7$. The values given above have been converted to hourly averaged levels.

(California air quality standard for NO₂ equals 250 ppb, hourly average)

multi-agency hearings, December, 1976 (State of California, 1976). No information is available concerning the calculation procedures employed by Dow.

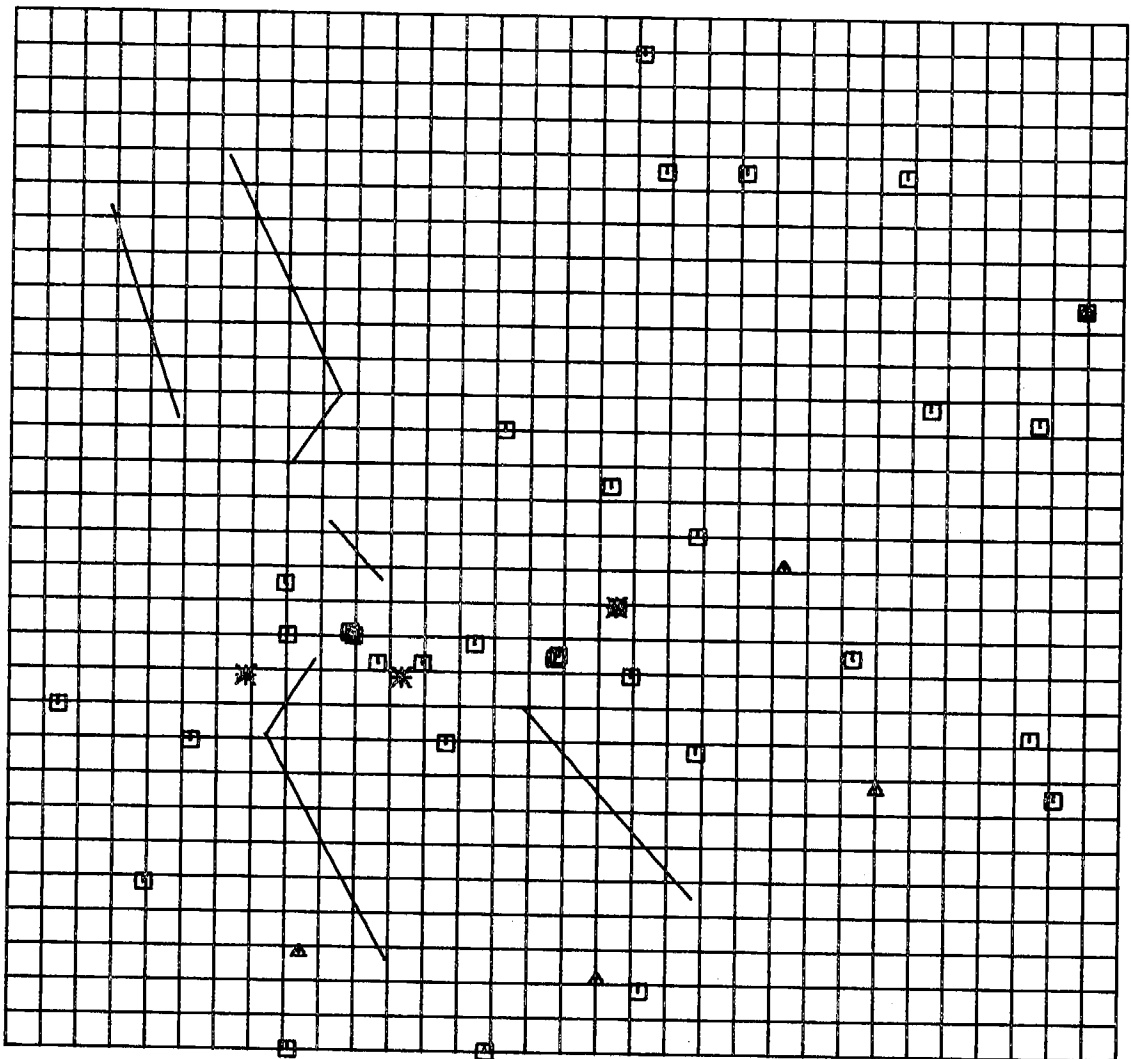
The summary indicates that maximum levels of NO_2 due to projected Dow emissions are generally within a factor of 4 of the ambient levels. Measured tracer data and predicted concentrations based on the dispersion data suggest that the air quality standard for NO_2 could be violated during the evening meteorological period at distances downwind of the Montezuma Hills of approximately 10 km. This analysis has not considered the impact of NO emissions upon ambient levels of ozone downwind of the proposed construction sites.

5. Calculation of the Surface Wind Field

The rather comprehensive set of surface wind data provides a data base for calculating hourly wind fields in terms of hourly wind vectors based upon a numerical solution of the mass balance equation. The determination of the hourly surface wind vectors, in turn, provide a basis for performing an air parcel trajectory analysis of the tracer tests. In this section, we present results of wind field and trajectory calculations covering the first tracer release. The computer programs used for these calculations were developed and kindly provided by William Goodin (1977).

The numerical solutions of the mass balance equation were determined for the 4 km square grid system shown in Figure 12Z. The surface and upper air wind stations and the tracer release sites are marked on the grid. The numerical procedure is designed to account for the presence of topographical barriers in the grid system. Barrier lines appropriate to the Bay and Delta topography are shown in Figure 12Z. The program is designed to accept digital topography data. The data for the Bay Area is available, but was not used in the results presented here.

The program accepts one hour of wind data and calculates a wind vector for each grid square. If several hours of data are processed, forward air parcel trajectories can be determined from the calculated vectors. A starting point and time must be specified. The program then determines how far and in what direction an air parcel would move in an hour according to the hourly wind vectors. The trajectory develops as the parcel is moved according to each succeeding hour of data. As an example of this procedure, the surface wind data for August 31, 1976,



- SURFACE WIND STATIONS
- ▲ UPPER AIR WIND STATIONS
- * TRACER RELEASE POINTS
- / TOPOGRAPHICAL BARRIERS

Figure 127. Grid system for calculation of wind fields over the California Delta Region. Grid squares are 4 Km x 4 Km.

from 1200 to 2300 PDT were used to calculate the wind fields given in Figures 128-139. Because no data were available for the northwestern corner of the grid, a dummy wind station using data from the Davis station was placed in the corner for calculation purposes. Although the wind vectors in the northwestern sector are meaningless, the effects of the dummy data upon the remainder of the grid are considered negligible.

The major features apparent in the complex flow patterns which occurred during the first tracer test include the turning of the marine air into the northern Bay Area and the subsequent channeling of air through the Carquinez Strait. From 1200 to 1500 PDT, flow over the Delta was directed to the southeast; after 1600 PDT, the winds at the Montezuma Hills straightened towards the east. Immediately downwind of the Montezuma Hills, the flow diverged to the northeast and southeast. From 1700 to 2000 PDT, an exceptionally strong flow to the south appeared in the Stockton-Tracy area.

Upper air data obtained for the first release day were used to determine the average wind fields in 3 layers extending from 300 to 900 feet, from 900 to 1500 feet, and from 1500 to 3000 feet above the surface. The surface wind field was assumed to extend to 300 feet above the surface. The resulting three-dimensional wind field is presented in Figures 140-142 for 1700 PDT. Comparison of these upper air wind fields with the surface wind field at 1700 PDT readily illustrates the effects of the complex topography upon the gradient westerly flow. Above the surface layer, flow is uniformly from the west throughout the region. Note that if the digital topography data were used to specify the boundary condition

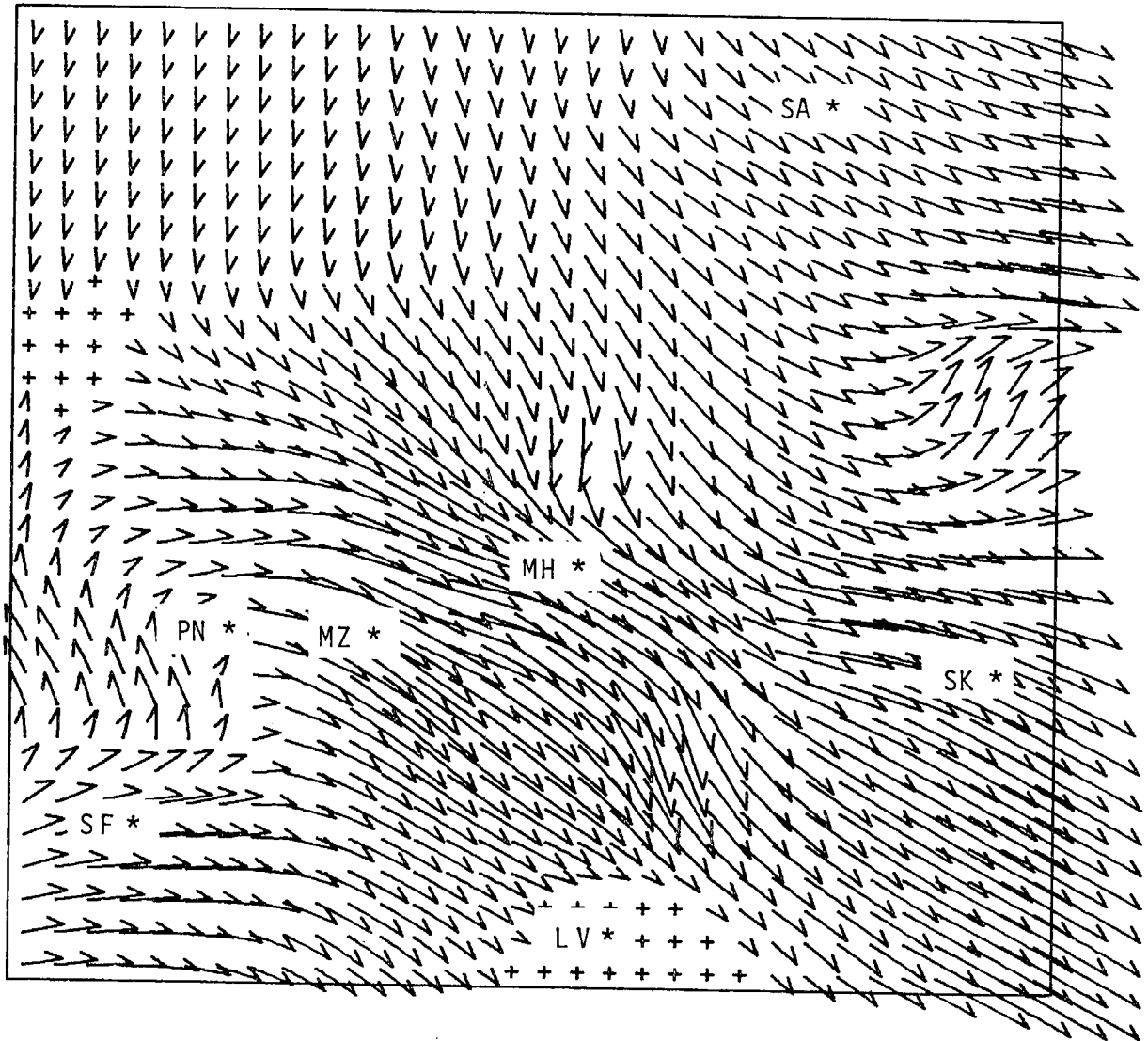


Figure 128. Hourly surface wind vectors, 1200 PDT, 8/31/76.
 Reference locations: Martinez (MZ), Montezuma Hills (MH),
 Pinole (PN), Sacramento (SA), San Francisco (SF),
 Stockton (SK), Livermore (LV).

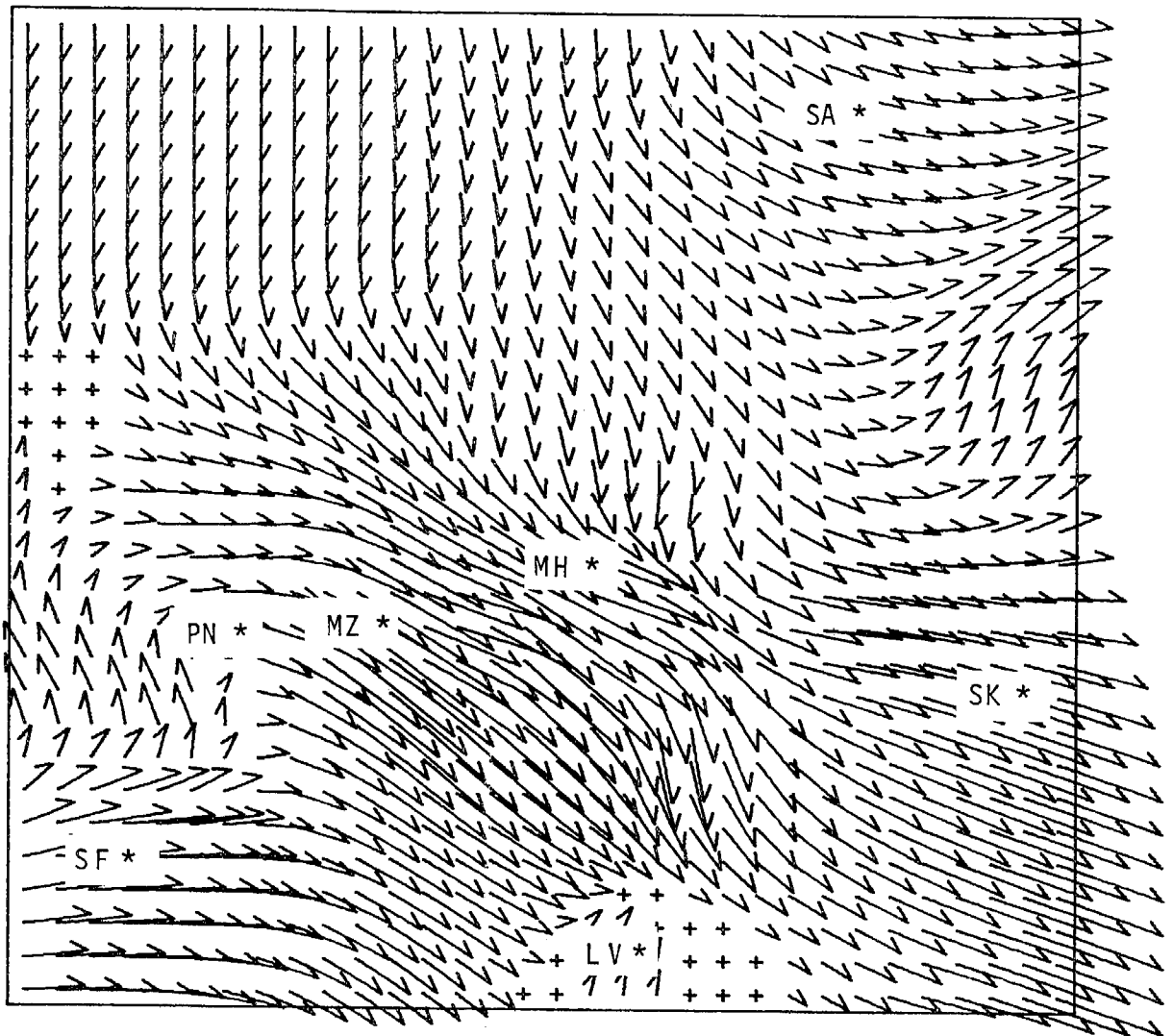


Figure 129. Hourly surface wind vectors, 1300 PDT, 8/31/76.
 Reference locations: Martinez (MZ), Montezuma Hills (MH),
 Pinole (PN), Sacramento (SA), San Francisco (SF),
 Stockton (SK), Livermore (LV).

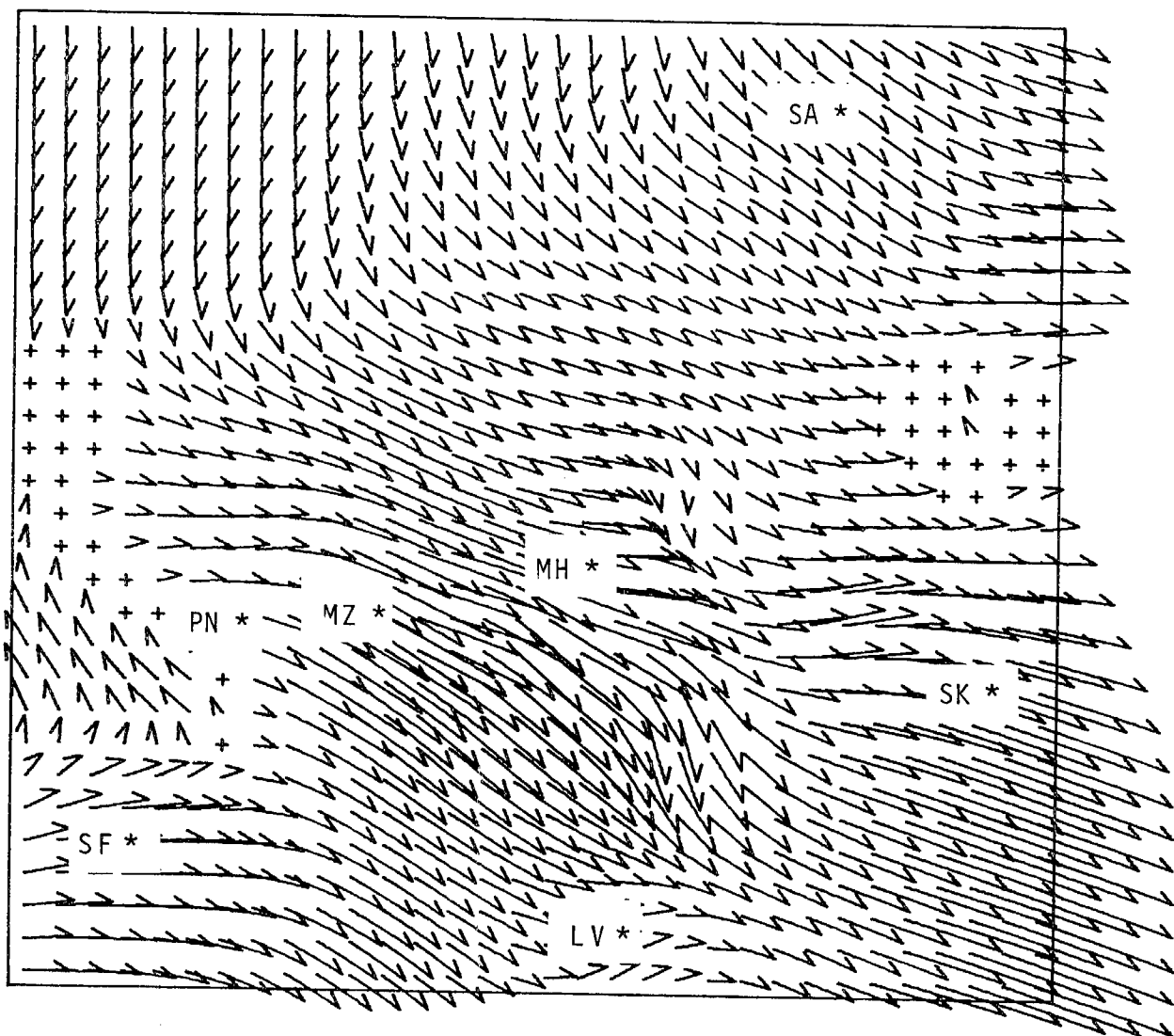


Figure 130. Hourly surface wind vectors, 1400 PDT, 8/31/76.
Reference locations: Martinez (MZ), Montezuma Hills (MH),
Pinole (PN), Sacramento (SA), San Francisco (SF),
Stockton (SK), Livermore (LV).

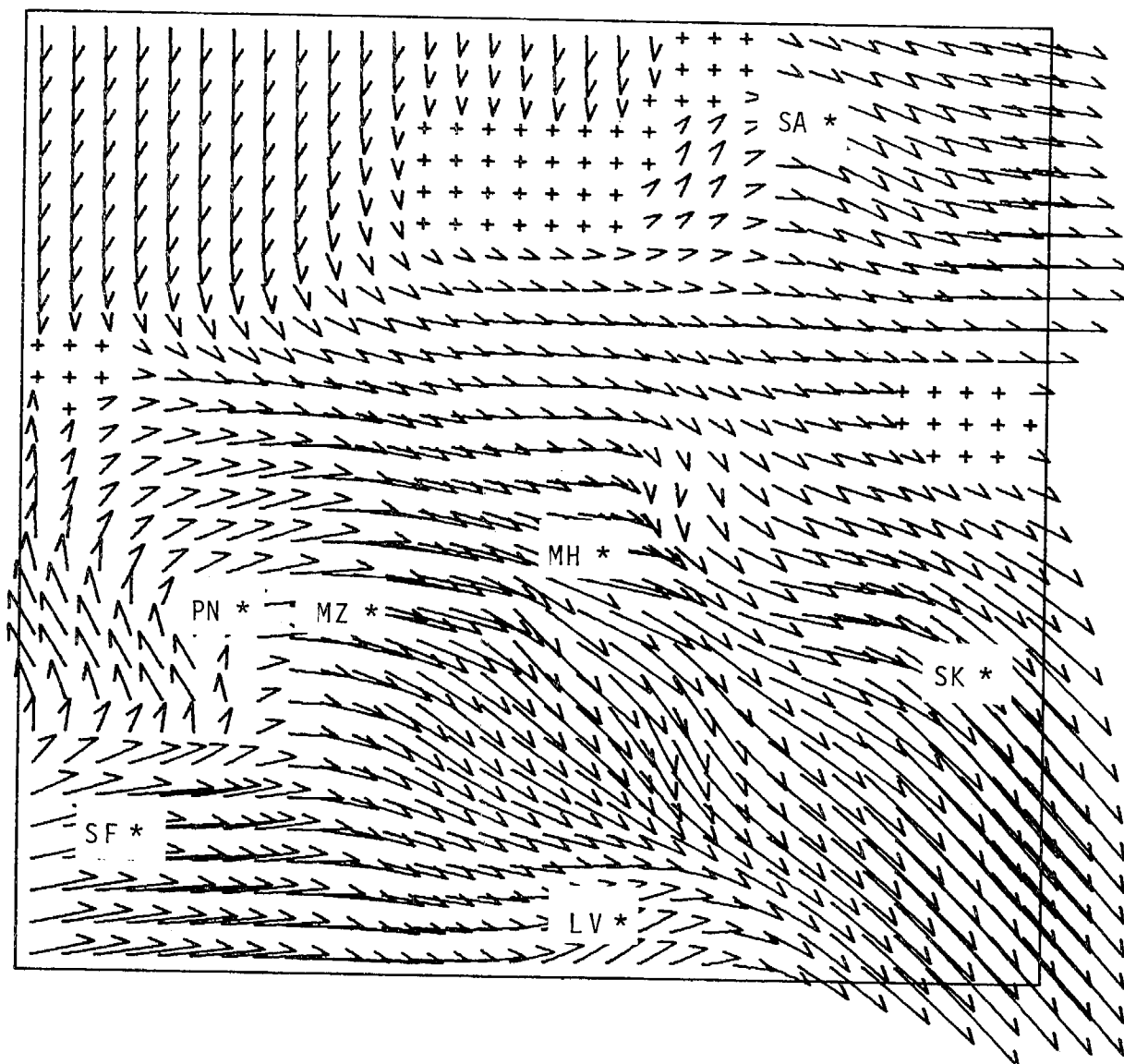


Figure 131. Hourly surface wind vectors, 1500 PDT, 8/31/76.
 Reference locations: Martinez (MZ), Montezuma Hills (MH),
 Pinole (PN), Sacramento (SA), San Francisco (SF),
 Stockton (SK), Livermore (LV).

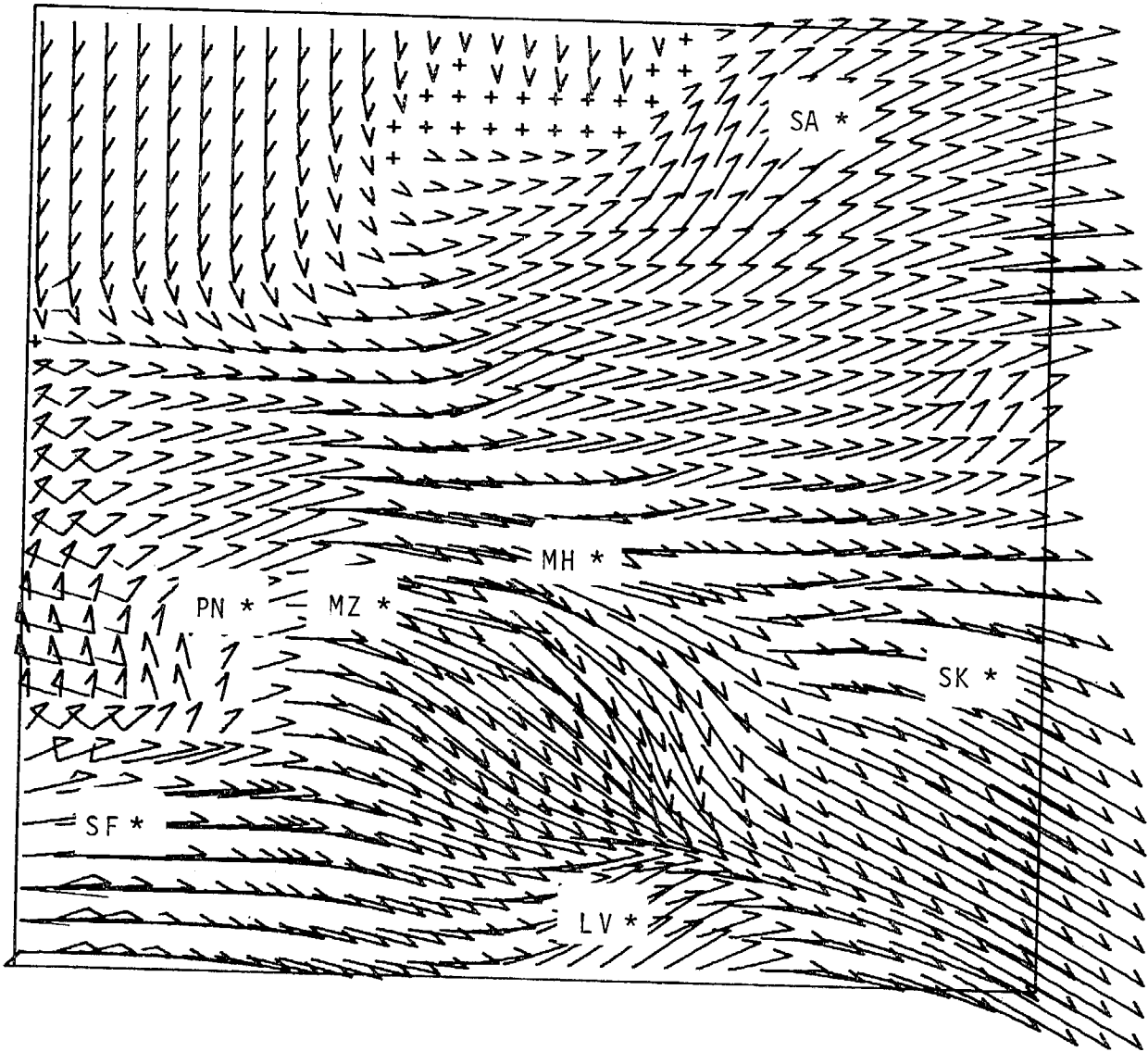


Figure 132. Hourly surface wind vectors, 1600 PDT, 8/31/76.
Reference locations: Martinez (MZ), Montezuma Hills (MH),
Pinole (PN), Sacramento (SA), San Francisco (SF),
Stockton (SK), Livermore (LV).

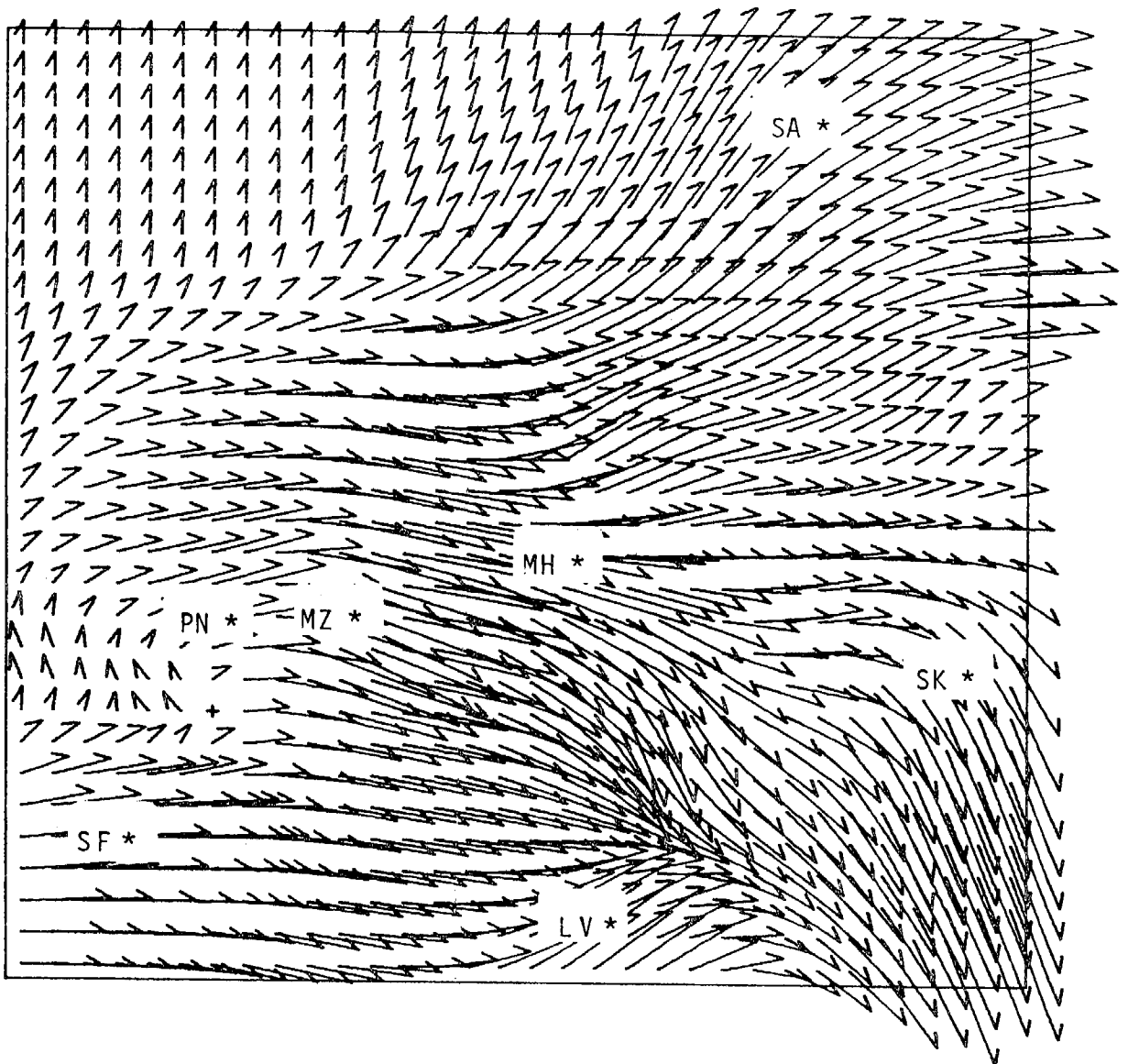


Figure 133. Hourly surface wind vectors, 1700 PDT, 8/31/76.
 Reference locations: Martinez (MZ), Montezuma Hills (MH),
 Pinole (PN), Sacramento (SA), San Francisco (SF),
 Stockton (SK), Livermore (LV).

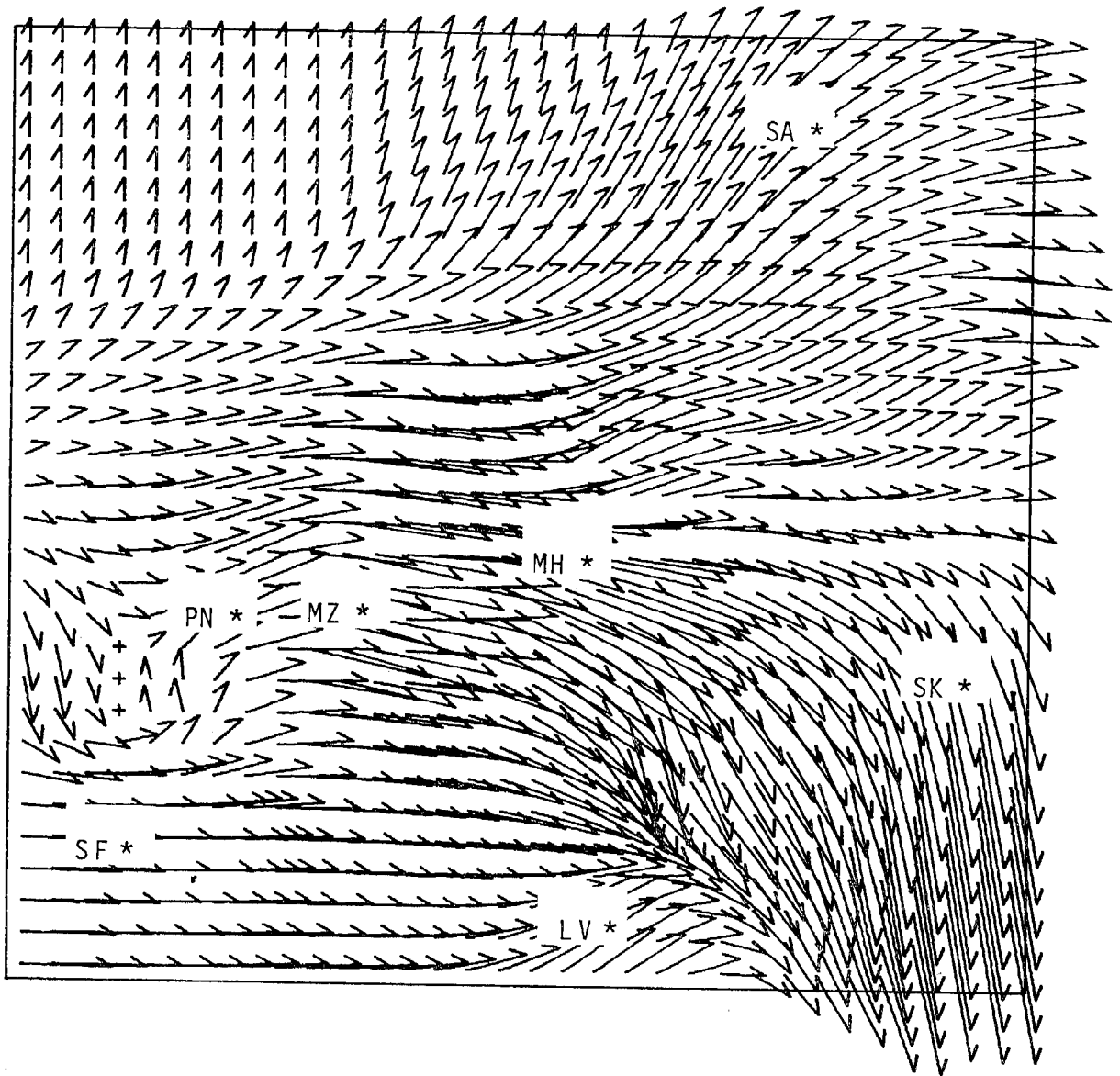


Figure 134. Hourly surface wind vectors, 1800 PDT, 3/31/76.
 Reference locations: Martinez (MZ), Montezuma Hills (MH),
 Pinole (PN), Sacramento (SA), San Francisco (SF),
 Stockton (SK), Livermore (LV).

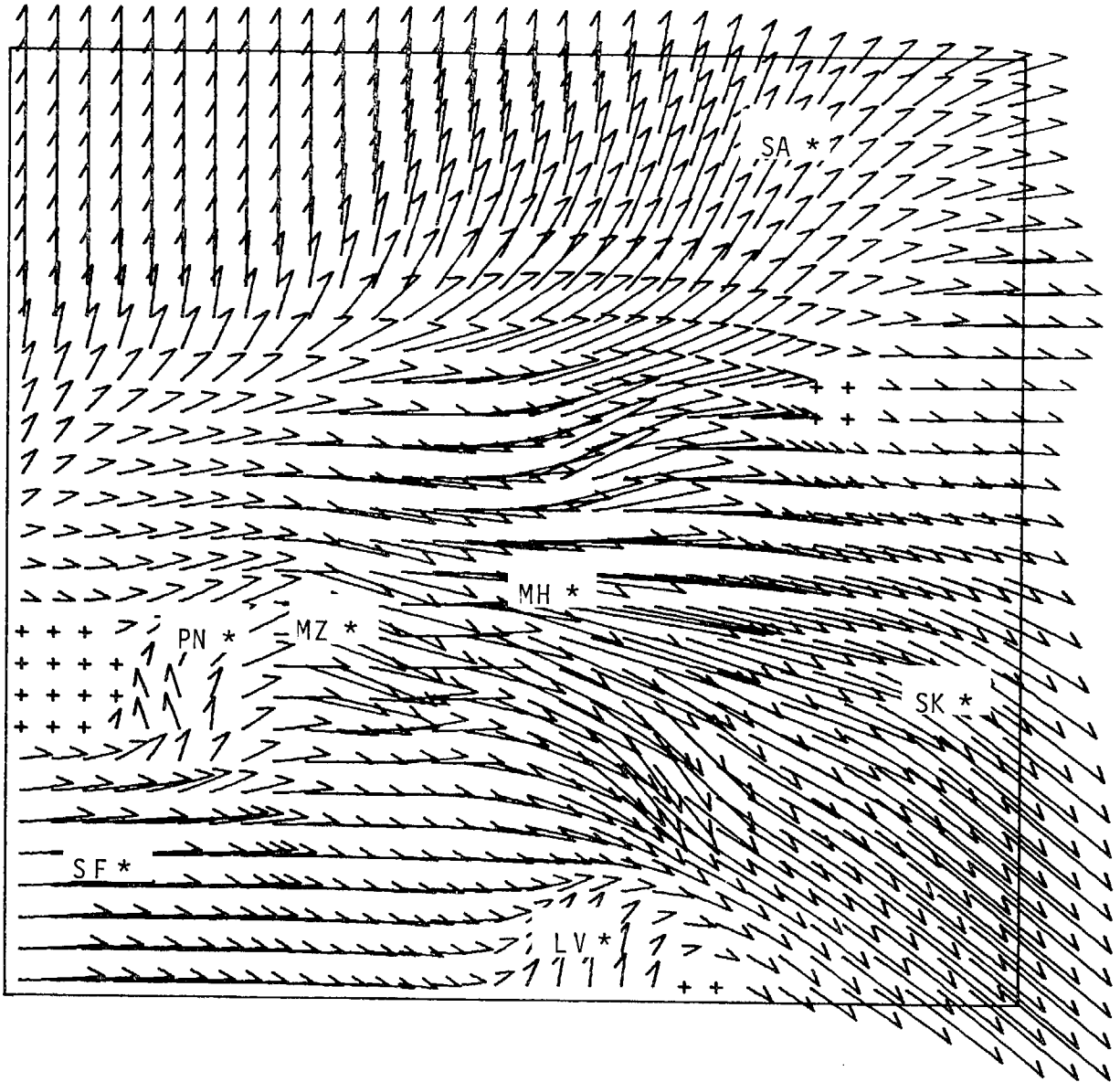


Figure 135. Hourly surface wind vectors, 1900 PDT, 8/31/76.
 Reference locations: Martinez (MZ), Montezuma Hills (MH),
 Pinole (PN), Sacramento (SA), San Francisco (SF),
 Stockton (SK), Livermore (LV).

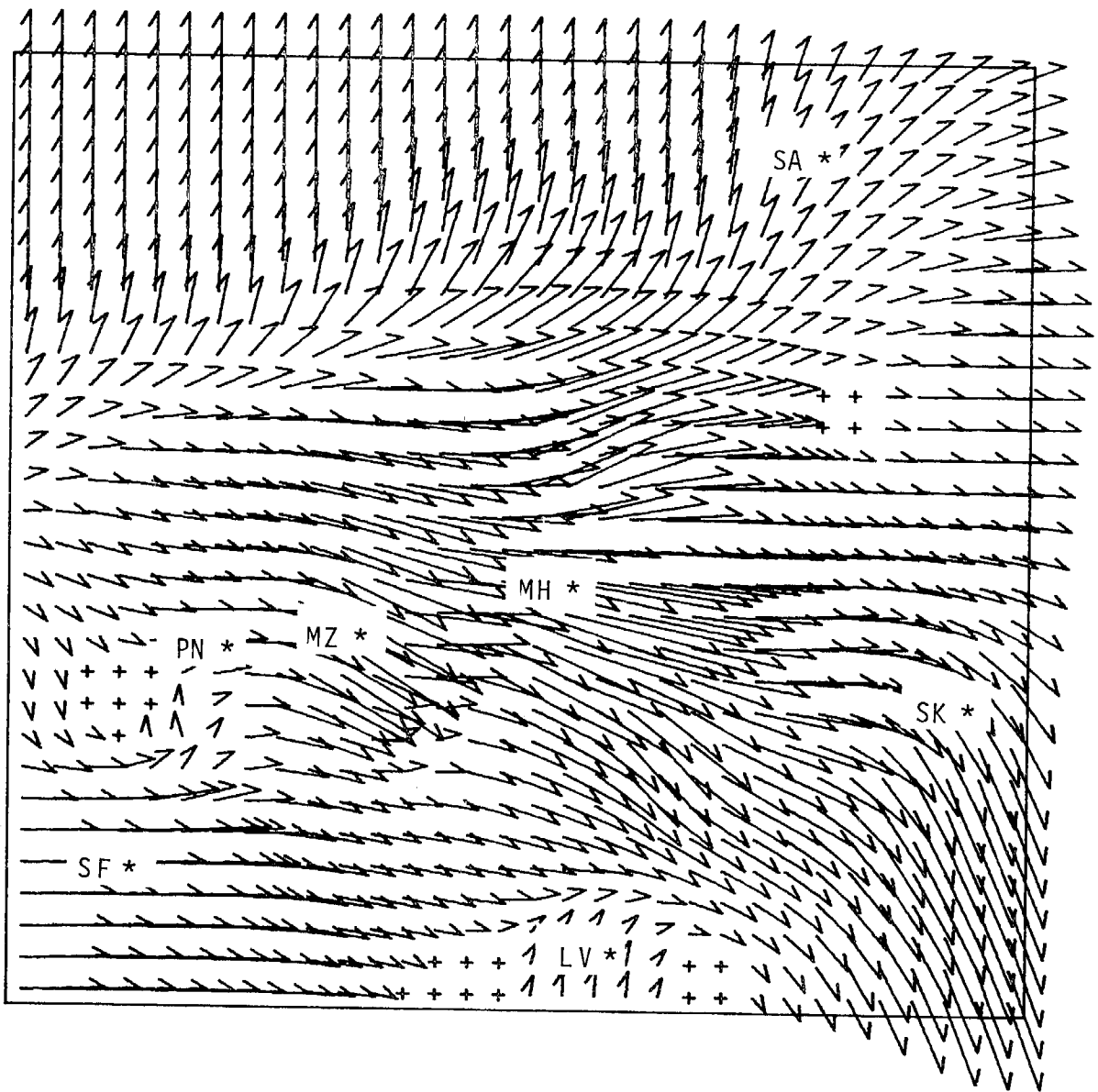


Figure 136. Hourly surface wind vectors, 2000 PDT, 8/31/76.
 Reference locations: Martinez (MZ), Montezuma Hills (MH),
 Pinole (PN), Sacramento (SA), San Francisco (SF),
 Stockton (SK), Livermore (LV).

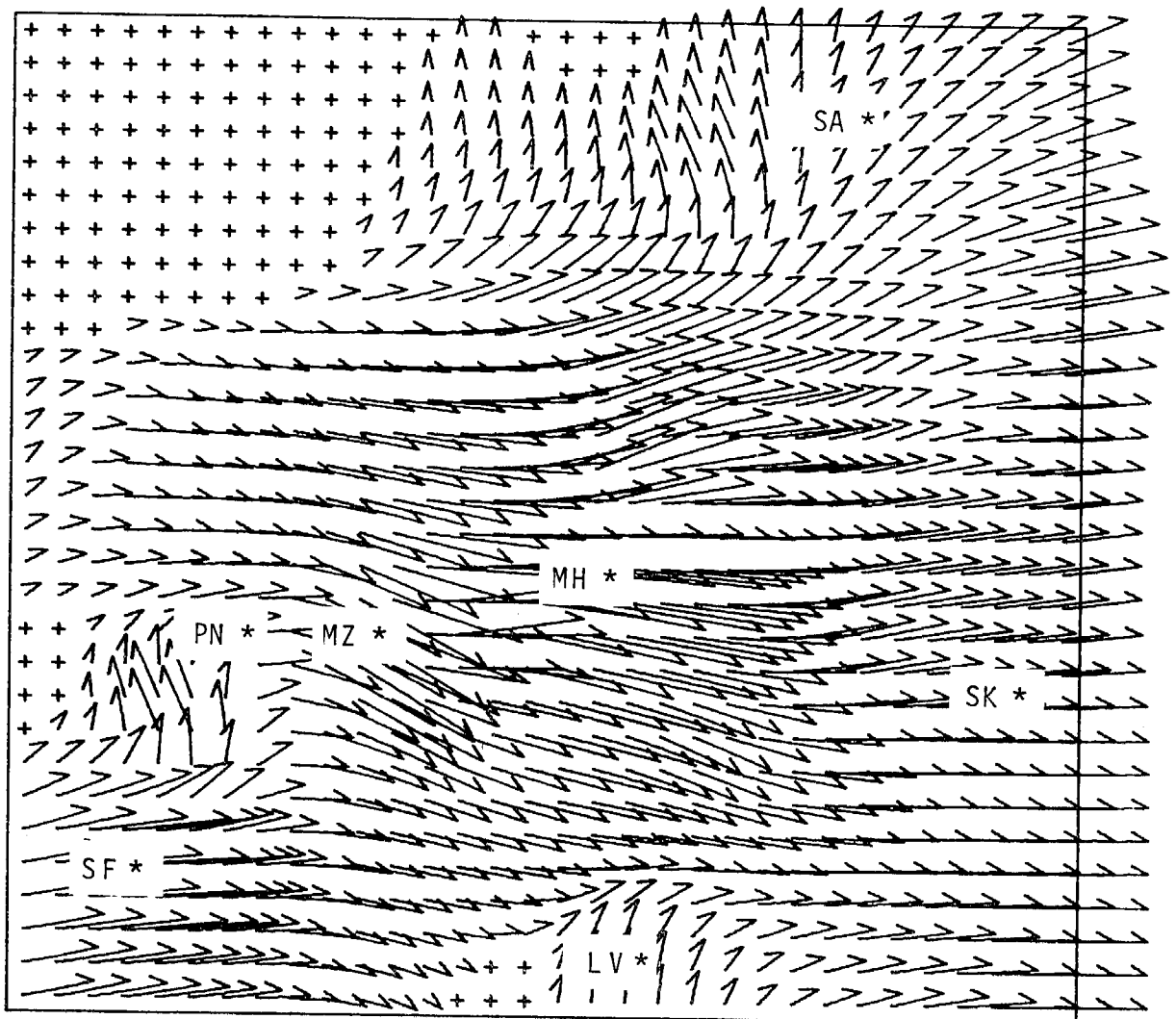


Figure 137. Hourly surface wind vectors, 2100 PDT, 8/31/76.
 Reference locations: Martinez (MZ), Montezuma Hills (MH),
 Pinole (PN), Sacramento (SA), San Francisco (SF),
 Stockton (SK), Livermore (LV).

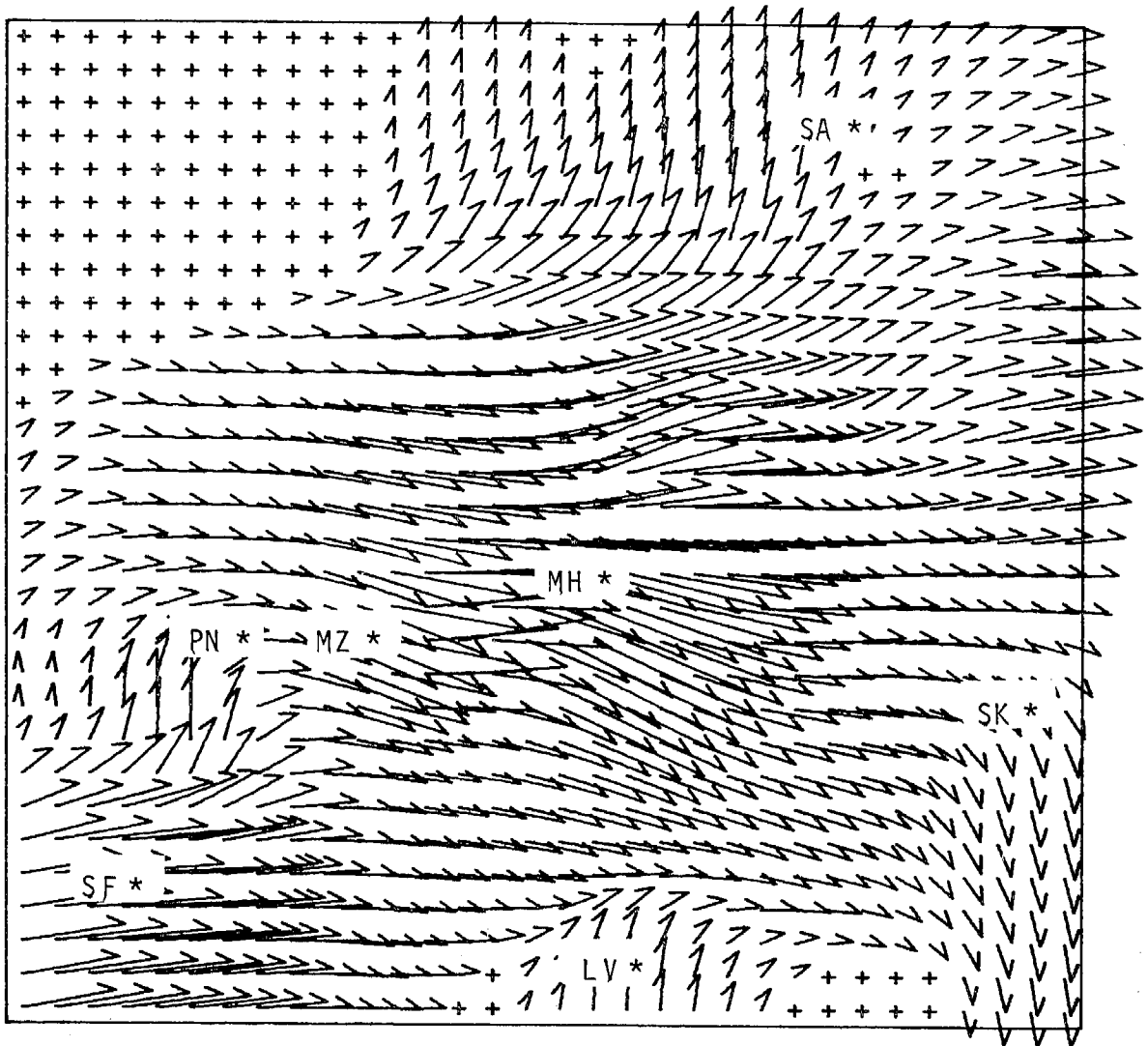


Figure 138. Hourly surface wind vectors, 2200 PDT, 8/31/76.
 Reference locations: Martinez (MZ), Montezuma Hills (MH),
 Pinole (PN), Sacramento (SA), San Francisco (SF),
 Stockton (SK), Livermore (LV).

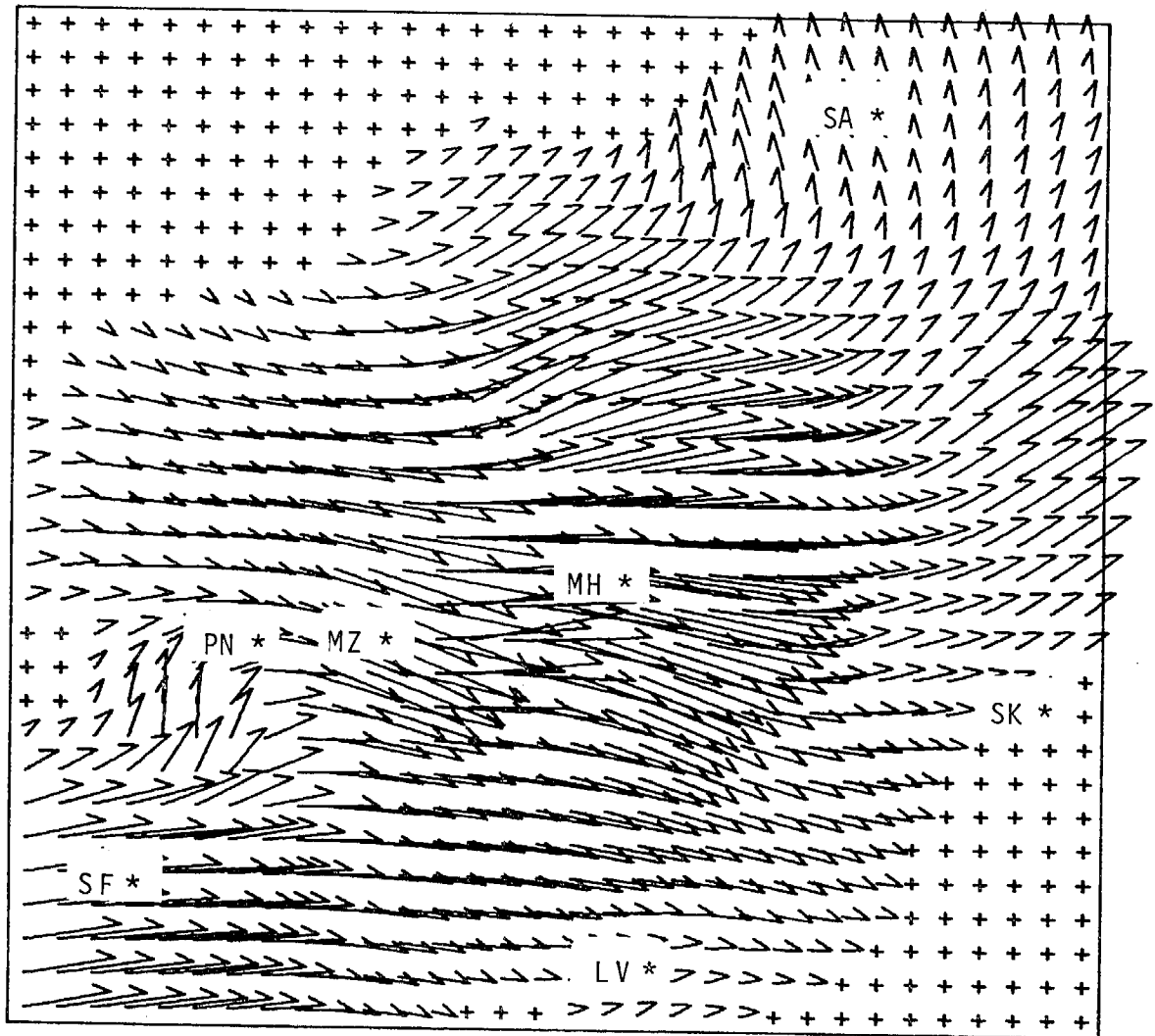


Figure 139. Hourly surface wind vectors, 2300 PDT, 8/31/76.
 Reference locations: Martinez (MZ), Montezuma Hills (MH),
 Pinole (PN), Sacramento (SA), San Francisco (SF),
 Stockton (SK), Livermore (LV).

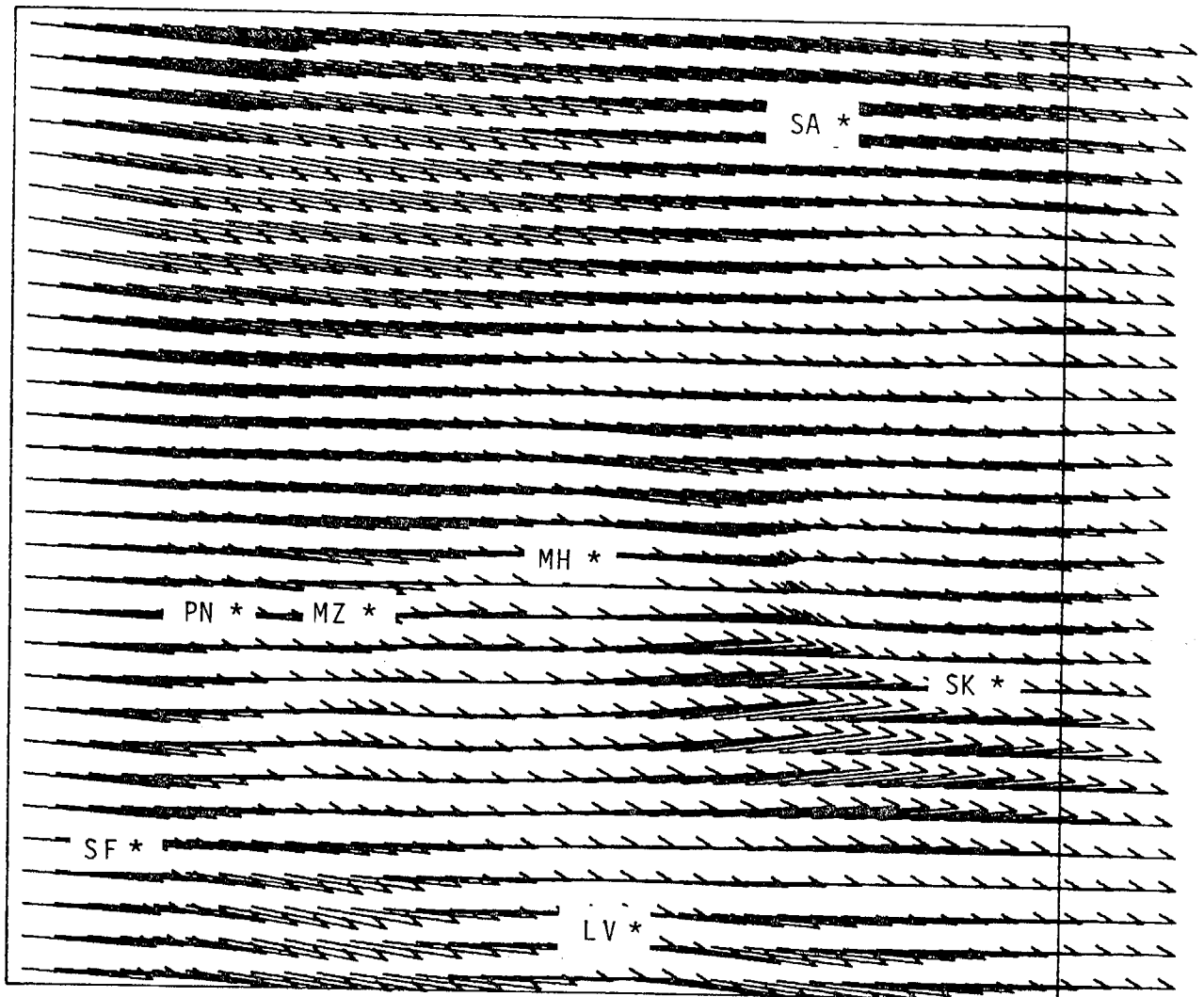


Figure 140. Hourly upper air wind vectors, average wind field from 300 to 900 feet, 1700 PDT, 8/31/76. Reference locations: Martinez (MZ), Montezuma Hills (MH), Pinole (PN), Sacramento (SA), San Francisco (SF), Stockton (SK), Livermore (LV).

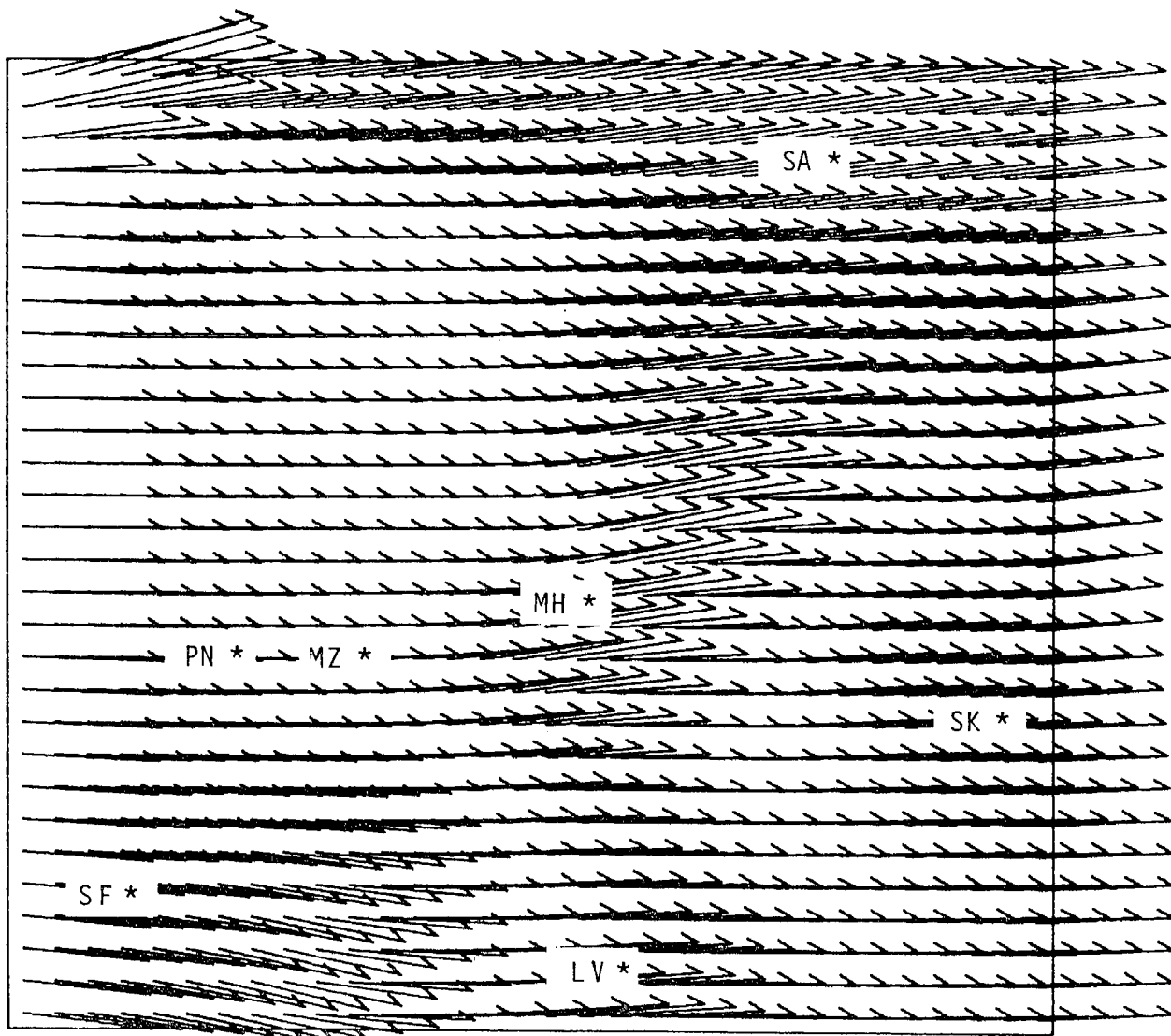


Figure 141. Hourly upper air wind vectors, average wind field from 900 to 1500 feet, 1700 PDT, 8/31/76. Reference locations: Martinez (MZ), Montezuma Hills (MH), Pinole (PN), Sacramento (SA), San Francisco (SF), Stockton (SK), Livermore (LV).

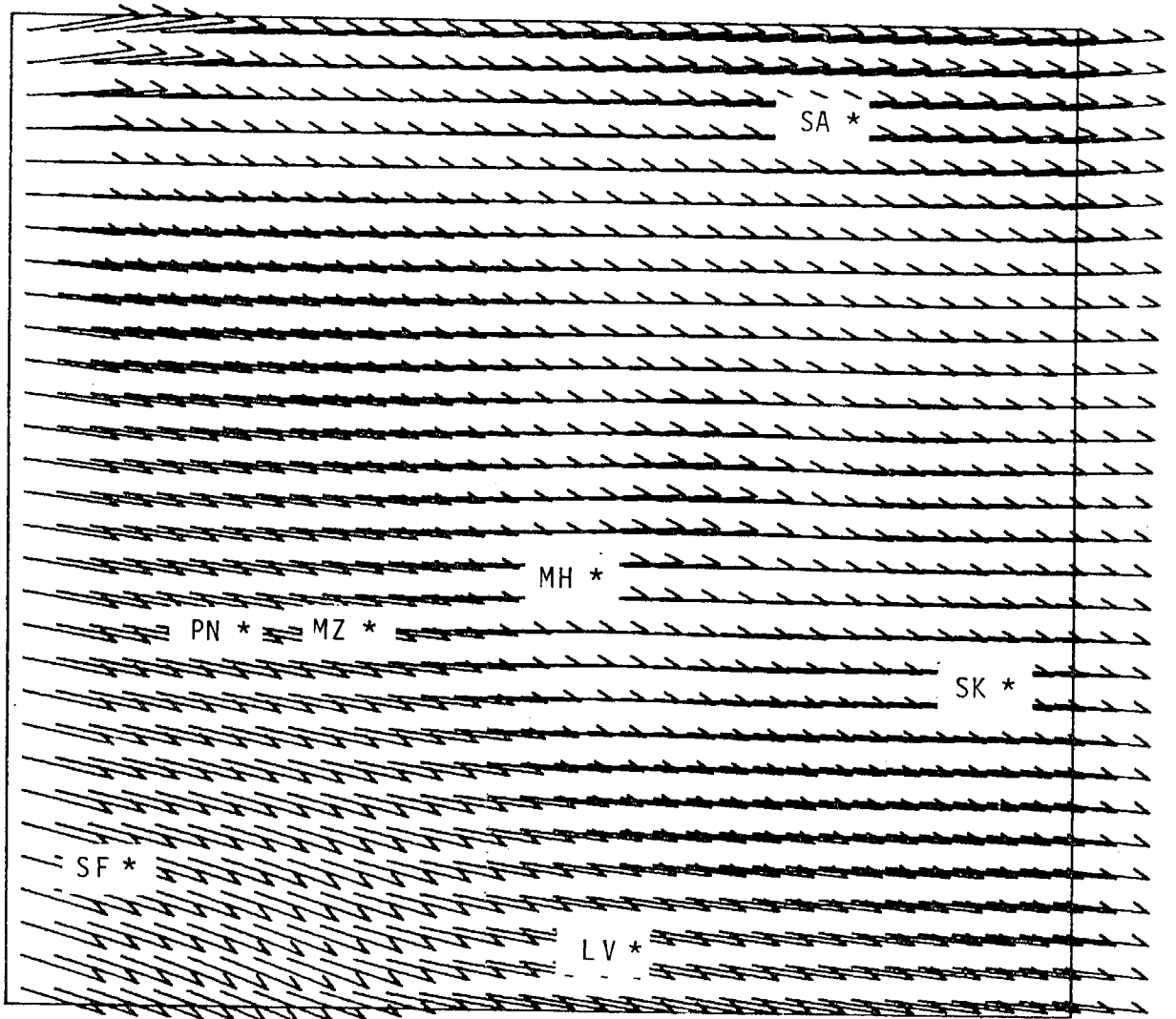


Figure 142. Hourly upper air wind vectors, average wind field from 1500 to 3000 feet, 1700 PDT, 8/31/76. Reference locations: Martinez (MZ), Montezuma Hills (MH), Pinole (PN), Sacramento (SA), San Francisco (SF), Stockton (SK), Livermore (LV).

at the surface, then more complex flow would probably appear in all of the upper air wind fields. The terrain surrounding the Bay Area reaches to over 1000 feet in places; Mt. Diablo rises to an elevation of 3849 feet (16 km south of Pittsburg).

Forward hourly air parcel surface trajectories beginning at the Dow site in the Montezuma Hills were calculated from the surface wind fields for starting times from 1200 to 1700 PDT. As indicated in Figure 143, all of the surface trajectories moved southeast to the Stockton-Tracy area. The effects of stagnant conditions in Stockton at 2300 PDT are apparent in the later trajectories. The paths and transport times of the surface trajectories are in excellent agreement with observations made from the traverse tracer data along Highway 99. Tracer and calculated trajectories both appeared to pass between Tracy and Stockton beginning at 1700 PDT. The maximum hourly averaged SF_6 concentration occurred between 1800 and 1900 PDT 4 km north of Stockton. Crosswind hourly profiles indicated that the SF_6 plume fluctuated through a zone extending from Lodi to Tracy between 1700 and 2000 PDT. Although the calculated surface trajectories are in agreement with the automobile traverse data at 1700 PDT, it appears that the impact zone was wider than that predicted from the trajectories. We have seen that the calculated air flow above 300 feet was directed almost due east throughout the Delta region. Airborne tracer data collected during the sixth tracer test indicated that the tracer can be mixed vertically at least as high as 600 feet after being transported from the Dow site to Highway 99. One may envision a tracer plume at the surface moving southeast towards Tracy. As tracer is mixed vertically due to the afternoon heating of the

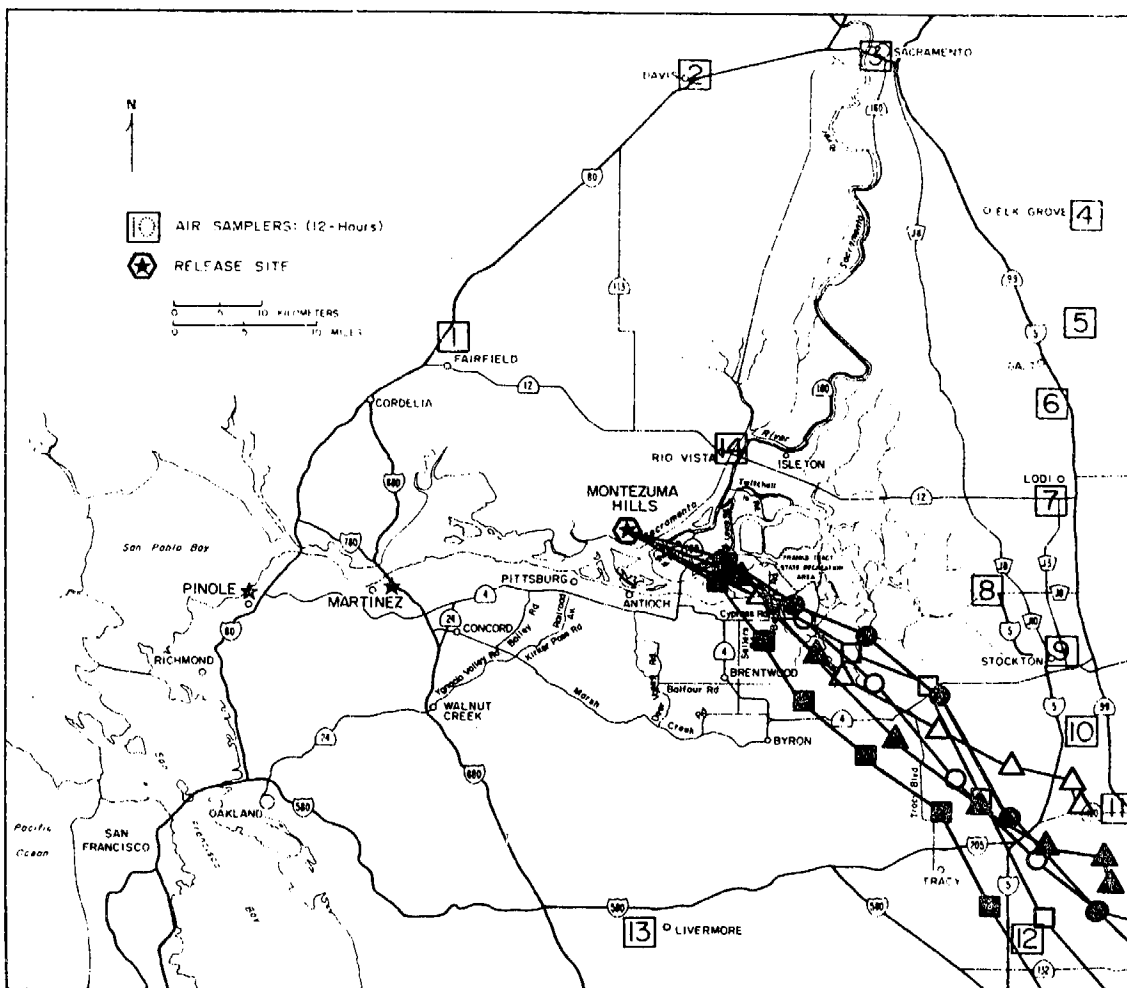


Figure 143. Forward air parcel surface trajectories; each point represents one hour of transport, 8/31/76. Trajectories were started from the Dow site in the Montezuma Hills at the following times:

- 1200 PDT ■
- 1300 PDT □
- 1400 PDT ●
- 1500 PDT ○
- 1600 PDT ▲
- 1700 PDT △

land, upper air flow from the west carries tracer east across Highway 99 in a zone from Lodi to Tracy. Although this explanation may explain the relationship between observed and calculated plume behavior, further work utilizing the digital topographical data and the three-dimensional aspects of the numerical procedure should be performed.

The surface wind fields were also used to construct air parcel trajectories beginning at Martinez and Pinole for two release times during the first tracer test. Even though we did not conduct tracer releases from these points during the first test, it is of interest to determine the transport paths of pollutants emitted in the northern Bay Area for the sake of comparison. The results for trajectories starting at 1200 and 1700 PDT from each point are shown in Figure 144. There appears to be a significant difference in paths initiated at 1200 and those started at 1700 PDT. The earlier releases from both Martinez and Pinole traveled south of Concord into the Tracy area. Winds at 1700 PDT forced the trajectories beginning at that time to move further east through Pittsburg before they turned southeast towards Tracy. Neither set of trajectories were carried over the Montezuma Hills. These patterns are very similar to those observed during Test 2 and Test 7. The trajectories which began at 1200 PDT reached Tracy at about the same time as those released from the Montezuma Hills at 1600 and 1700 PDT. Both the trajectories initiated from the Pinole-Martinez area and the trajectories started from the Montezuma Hills indicate that pollutants emitted from these points into the afternoon sea breeze can be transported into the mouth of the San Joaquin Valley.

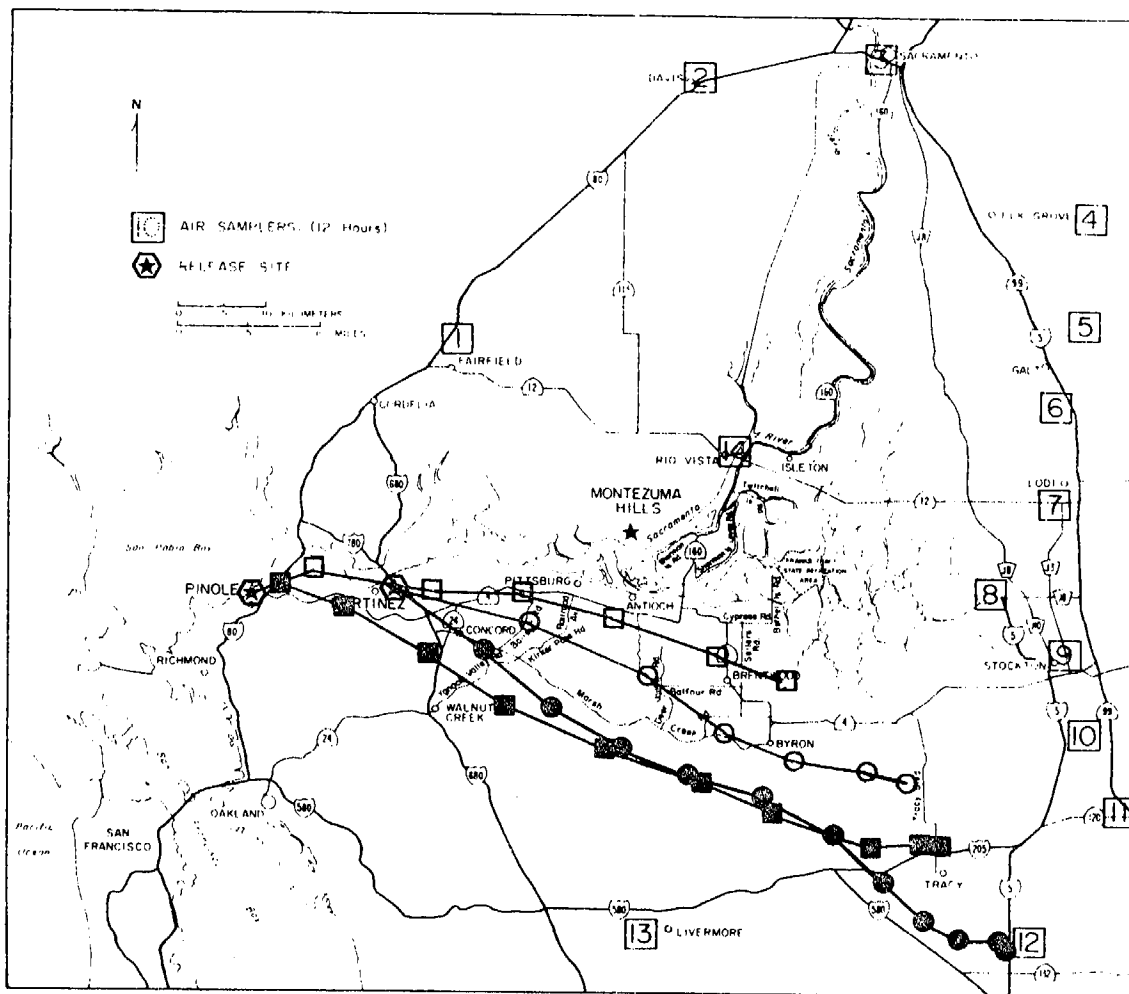


Figure 144. Forward air parcel surface trajectories; each point represents one hour of transport, 8/31/76. Trajectories were started from Pinole and Martinez at the following times:

Pinole	1200 PDT	■
	1700 PDT	□
Martinez	1200 PDT	●
	1700 PDT	○

258
Appendix A

Calibration of the twelve chromatographs (designated Z1-Z10, Y1 and Y2) was accomplished by means of a well-mixed exponential dilution system. Calibrations were completed prior to the field study on 8/21/76 and following the test on 9/28/76 and 9/29/76. The results of the calibrations are listed as KF values (integrator peak area in $\mu\text{V}\cdot\text{sec}/\text{ppt}$ tracer) in Table A-1. Several times during the field study, cross-check tests were performed among the gas chromatographs. A constant concentration sample was analyzed in several gas chromatographs in order to determine the standard deviation associated with the reproducibility of the analysis. The results of the cross-check tests are given in Table A-2.

TABLE A-1
GAS CHROMATOGRAPH CALIBRATION RESULTS

Chromatograph	SF_6			CBrF_3		
	KF Values		$\Delta\text{KF}(\%)$	KF Values		$\Delta\text{KF}(\%)$
	8/21/76	9/28/76		8/21/76	9/29/76	
Z5	102	102	0			
Z6	145	140	3			
Z7	101	87	$\frac{14}{9}$			
Z8	100	91	Average = $\frac{7}{9}\%$			
	8/21/76	9/29/76		8/21/76	9/29/76	
Z9	456	424	7	29	27	7
Z10	270	169	37	7	5	29
Y1	430	316	27	20	16	20
Y2	497	352	$\frac{29}{25}\%$	17	13	$\frac{24}{20}\%$

259
TABLE A-2

GAS CHROMATOGRAPH CROSS-CHECK RESULTS

Date	Test	Chromatographs	% Std. Deviation of measured Concentrations		Average Tracer Concentration (ppt)	
8-31-76	CC-1	Z8, Z9, Y1	20		24	(SF ₆)
	CC-2	Z5, Z6, Z7, Z10	20		24	(SF ₆)
9-2-76	CC-3	Y1, Y2, Z10	21		2693	(SF ₆)
	CC-4	Y1, Y2, Z10	3		2060	(SF ₆)
	CC-5	Y1, Z9, Z10	22		2253	(CBrF ₃)
	CC-6	Y1, Y2, Z9	14		932	(CBrF ₃)
	CC-7	Z5, Z6	6		294	(SF ₆)
	CC-8	Z5, Z7, Z8	13		273	(SF ₆)
	CC-9	Y1, Y2, Z9, Z10	11		332	(SF ₆)
				using 9-29-76 KF Values		
9-13-76	CC-10	Y1, Z5	17	(5%)	534	(SF ₆)
	CC-11	Y2, Z6	24	(1%)	430	(SF ₆)
	CC-12	Z8, Z9	23	(18%)	491	(SF ₆)
	CC-13	Z7, Z10	28	(5%)	513	(SF ₆)

Appendix BCalculation of Plume Parameters from Crosswind Traverses

Plumes are often modeled by assuming they have a gaussian shape; that is, the concentration along a crosswind traverse follows an equation:

$$C(y) = C_0 \exp \left[-\frac{1}{2} \left(\frac{y-Y_0}{\sigma} \right)^2 \right] \quad (B-1)$$

where Y_0 is the distance coordinate of the center of the plume, C_0 is the concentration at the center of the plume, and σ is the standard deviation of the plume. From standard data analysis techniques, equations relating σ and Y_0 to the data obtained ($C(y)$ and y) are:

$$Y_0 = \frac{\int_{-\infty}^{\infty} yC(y) dy}{\int_{-\infty}^{\infty} C(y) dy} \quad (B-2)$$

and

$$\sigma = \left[\frac{\int_{-\infty}^{\infty} y^2 C(y) dy}{\int_{-\infty}^{\infty} C(y) dy} - Y_0^2 \right]^{\frac{1}{2}} \quad (B-3)$$

A value for C_0 can also be calculated once Y_0 and σ have been calculated:

$$\int_{-\infty}^{\infty} C(y) dy = C_0 \sigma \sqrt{2\pi} \quad (B-4)$$

or, rearranging terms,

$$C_0 = \frac{\int_{-\infty}^{\infty} C(y) dy}{\sqrt{2\pi} \sigma} \quad (B-5)$$

These parameters (C_0 , Y_0 , σ) when used in Equation (B-1) represent a best-fit of the data ($C(y)$, y) to the equation.

Three major sources of error appear in the actual use of these equations: one is the error inherent in the data itself; another is due to the data being for discrete points rather than for all y ; and finally, due to limitation on the sampling locations, one or both edges of the plume might be chopped off (the integration cannot be carried out to the limits, $-\infty, \infty$). The errors in the data cannot be reduced once the data is taken, but errors in application of the above formulas can be estimated and reduced to some extent.

The error involved in calculating the integrals is dependent upon the method used, but the error involved in chopping off the edges of the plume can be treated generally and is considered first. By assuming a perfect gaussian plume and calculating the parameters from equations (B-2)-(B-5), but with limits of integration Y_a and Y_b instead of $-\infty$ and $+\infty$, the following expressions for error of the results can be found:

$$(5) Y_0' = Y_0 - \frac{\sigma e^{-\frac{1}{2}u^2} \Big|_{u_a}^{u_b}}{\sqrt{2\pi} P(u) \Big|_{u_a}^{u_b}} \quad (B-6)$$

$$(6) \sigma' = \sigma \left[1 - \frac{u e^{-\frac{1}{2}u^2} \Big|_{u_a}^{u_b}}{\sqrt{2\pi} P(u) \Big|_{u_a}^{u_b}} - \frac{1}{2\pi} \left(\frac{e^{-\frac{1}{2}u^2} \Big|_{u_a}^{u_b}}{P(u) \Big|_{u_a}^{u_b}} \right)^2 \right]^{\frac{1}{2}} \quad (B-7)$$

$$u = \left(\frac{Y - Y_0}{\sigma} \right)$$

$$P(u) = \frac{1}{\sqrt{2\pi}} \int_{-\infty}^u e^{-\frac{1}{2}v^2} dv \quad (\text{note } P(u) \text{ is the Normal Probability function.})$$

where σ and Y_0 are the actual parameters of the plume, and σ' and Y_0'

are the parameters calculated using formulas (B-2)-(B-5) with limits of integration Y_a and Y_b . No simple expressions for Y_0 and σ in terms of Y_0' and σ' could be found; however, equations (B-6) and (B-7) can be applied in an iterative manner so that successively better approximations of Y_0 and σ can be found.

$$Y_{0(n+1)} = Y_{0(o)} + \frac{\sigma(n) e^{-\frac{1}{2}u^2} \Big|_{ua(n)}^{ub(n)}}{\sqrt{2\pi} P(u) \Big|_{ua(n)}^{ub(n)}} \quad (B-8)$$

$$\sigma_{(n+1)} = \sigma_{(o)} \left[1 - \frac{u e^{-\frac{1}{2}u^2} \Big|_{ua(n)}^{ub(n)}}{\sqrt{2\pi} P(u) \Big|_{ua(n)}^{ub(n)}} - \frac{1}{2\pi} \left(\frac{e^{-\frac{1}{2}u^2} \Big|_{ua(n)}^{ub(n)}}{P(u) \Big|_{ua(n)}^{ub(n)}} \right)^2 \right]^{-\frac{1}{2}} \quad (B-9)$$

$$U_{n(n)} = \left(\frac{Y_y - Y_{o(n)}}{\sigma_n} \right) \quad (B-10)$$

where the small subscript in () refers to the number of times the iteration was performed to arrive at that approximation, (o) refers to initially calculated values.

Traverse data are usually taken at even intervals along the traverse which simplifies the integration considerably. The method we chose was Simpson's method; Simpson's Rule is written as follows:

$$\int_{Y_0}^{Y_{2n}} f(x) dx = \frac{h}{3} [f_0 + f_{2n} + 4 \sum_{i=1}^n (f_{2i-1}) + 2 \sum_{i=1}^{n-1} (f_{2i})] + \epsilon \quad (B-11)$$

where h is the difference between any two x_i , $f_i = f(x_i)$, and $2n+1$ is the number of data points. The error term ϵ is shown below:

$$\epsilon = \frac{nh^5}{90} \frac{d^4 f}{dx^4}(x) \quad \text{where } X_0 < \epsilon < X_{2n} \quad (\text{B-12})$$

Since ϵ is unknown only a minimum and maximum error can be found.

If $f(x)$ is of the form of a gaussian curve, the minimum and maximum errors are

$$\epsilon_{\min} = -.02061 \frac{C_0 nh^5}{\sigma^4} \quad \epsilon_{\max} = \frac{nh^5 C_0}{30\sigma^4} \quad (\text{B-13})$$

The curves we deal with are not exactly gaussian, so this error loses much of its significance; however, it is calculated as a check on the data (a grossly large error could mean that the data is bad).

Literature Cited

1. Angell, J. K., D. H. Pack, G. C. Holzworth, and C. R. Dickson (1966) "Tetroon Trajectories in an Urban Atmosphere," J. Appl. Meteor. 5, 565-572.
2. Angell, J. K., C. R. Dickson, and W. H. Hoecker, Jr. (1976) "Tetroon Trajectories in the Los Angeles Basin Defining the Source of Air Reaching the San Bernardino-Riverside Area in Late Afternoon," J. Appl. Meteor. 15, 197-204.
3. Briggs, G. A. (1969) Plume Rise USAEC Critical Review Series T1D-25075, National Technical Information Service, Springfield, Va. 22151.
4. Briggs, G. A. (1972) "Discussion on Chimney Plumes in Neutral and Stable Surroundings," Atmos. Environ. 6, 507-510.
5. California State (1976) Transcripts from State Consolidated Hearings concerning the Dow Petrochemical Project, December 8-9, 1976, State Lands Commission, 1807 13th Street, Sacramento, California 95814.
6. Drivas, P. J. (1974) "Investigation of Atmospheric Dispersion Problems by Means of a Tracer Technique," Ph.D. Thesis, California Institute of Technology, 16-26.
7. Drivas, P. J., and F. H. Shair (1974) "A Tracer Study of Pollutant Transport and Dispersion in the Los Angeles Area," Atmos. Environ. 8, 1155-1163.
8. Drivas, P. J. and F. H. Shair (1975) "The Chemistry, Dispersion, and Transport of Air Pollutants Emitted from Fossil Fuel Power Plants in California; Transport and Dispersion of Plumes Associated with Coastal Meteorology," Final Report for the California State Air Resources Board, Contract No. ARB 3-915, 1709 11th Street, Sacramento, California 95814.
9. Fosberg, M. A., D. G. Fox, E. A. Howard, and J. D. Cohen (1976) "Nonturbulent Dispersion Processes in Complex Terrain," Atmos. Environ. 10, 1053-1055.
10. Fosberg, M. A., and M. J. Schroeder (1966) "Marine Air Penetration in Central California," J. Appl. Meteor. 5, 573-589.
11. Frenzel, C. W. (1962) "Diurnal Wind Variations in Central California," J. Appl. Meteor. 1, 405-512.
12. Gifford, F. A., Jr. (1968) "An Outline of Theories of Diffusion in Lower Layers of the Atmosphere," in D. H. Slade (ed), "Meteorology and Atomic Energy, 1968," U. S. Atomic Energy Commission, Oak Ridge, Tenn. 101-103.

13. Giroux, H. D., L. E. Hausner, L. H. Teuscher, and P. Testerman (1974) "Power Plant Plume Tracing in the Southern California Marine Layer," from Proceedings of the Symposium on Atmospheric Diffusion and Air Pollution. Amer. Meteor. Soc., Boston, Mass. 02108 238-245.
14. Goodin, W. (1977), Environmental Quality Laboratory, California Institute of Technology, Pasadena, Calif. 91125, personal communication.
15. Hay, J. S., and F. Pasquill (1959) "Diffusion from a Continuous Source in Relation to the Spectrum and Scale of Turbulence," Advances in Geophys. 6, 345-364.
16. Hinds, W. T. (1970) "Diffusion Over Coastal Mountains of Southern California," Atmos. Environ. 4, 107-124.
17. Hino, M. (1968) "Maximum Ground-level Concentrations and Sampling Times," Atmos. Environ. 2, 149-165.
18. Islitzer, N. F. (1961) "Short-Range Atmospheric Dispersion Measurements from an Elevated Source," J. of Meteor. 18, 443-450.
19. Islitzer, N. F., and R. K. Dumbauld (1963) "Atmospheric Diffusion-deposition Studies Over Flat Terrain," Intern. J. Air Water Poll. 7, 999-1022.
20. Lamb, B. K., and F. H. Shair (1977) "Tracer Study of Power Plant Emission Transport and Dispersion from the Oxnard/Ventura Plain," California State Air Resources Board, Contract No. ARB-5-306, 1709 11th Street, Sacramento, Calif. 95814.
21. Liu, M., D. Durran, P. Mundkar, M. Yocke, and J. Ames (1976) "The Chemistry, Dispersion, and Transport of Air Pollutants Emitted from Fossil Fuel Power Plants in California: Data Analysis and Emission Impact Model," California State Air Resources Board, Contract No. ARB-4-258, 1709 11th Street, Sacramento, Calif. 95814.
22. MacReady, P. B., Jr., L. B. Baboolal, and P. B. S. Lissaman (1974) "Diffusion and Turbulence Aloft over Complex Terrain," from the Proceedings of the Symposium on Atmospheric Diffusion and Air Pollution, Amer. Meteor. Soc., Boston, Mass. 02108, 218-225.
23. Miller, A. (1968) "Wind Profiles in West Coast Temperature Inversions;" Report No. 4, San Jose State College, Dept. of Meteor., San Jose, Calif.
24. Moyer, N. (1977) California State Air Resources Board, personal communication.
25. Nonhebel, G. (1960) "Recommendations on Heights for New Industrial Chimneys," J. Inst. Fuel. 33, 479-511.
26. Pasquill, F. (1974) Atmospheric Diffusion. John Wiley and Sons, New York, 298-300.

27. Peters, L. K., and L. W. Richards (1977) "Extension of Atmospheric Dispersion Models to Incorporate Fast Reversible Reactions," Atmos. Environ. 11, 101-108.
28. Reynolds, S. D., P. M. Roth, and J. H. Seinfeld (1973) "Mathematical Modeling of Photochemical Air Pollution - I," Atmos. Environ. 7, 1033-1061.
29. Roberts, P. T. (1975) "Gas-To-Particle Conversion: Sulfur Dioxide in a Photochemically Reactive System," Ph.D. Thesis, California Institute of Technology, Pasadena, Calif. 91125.
30. Roffman, A., and R. Grimble (1974) "A Time-Dependent Air Quality Model With Terrain Corrections," from the Proceedings of the Symposium on Atmospheric Diffusion and Air Pollution, Amer. Meteor. Soc., Boston, Mass. 02108, 311-317.
31. Sandberg, J. S., W. J. Walker, and R. H. Thuiller (1970) "Fluorescent Tracer Studies of Pollutant Transport in the San Francisco Bay Area," J. Air Poll. Contr. Assoc. 20, 593-598.
32. Seinfeld, J. H. (1975) Air Pollution: Physical and Chemical Fundamentals McGraw-Hill, Inc., New York, 260-351.
33. Smalley, C. (1957) "A Study of Air Flow Patterns in the San Francisco Bay Area," Information Bulletin 6-15-70, Technical Services Division, Bay Area Air Pollution Control District, San Francisco, Calif.
34. Smith, T. B. (1977) Meteorology Research, Inc., Altadena, Calif. personal communication.
35. Start, G. E., C. R. Dickson, and N. R. Ricks (1974) "Effluent Dilutions Over Mountainous Terrain and Within Mountain Canyons," from the Proceedings of the Symposium on Atmospheric Diffusion and Air Pollution, Amer. Meteor. Soc., Boston, Mass. 02108 226-232.
36. Turner, D. B. (1961) "Relationships Between 24-Hour Mean Air Quality Measurements and Meteorological Factors in Nashville, Tennessee," J. Air Poll. Contr. Assoc. 11, 483-489.
37. Turner, D. B. (1970) "Workbook of Atmospheric Dispersion Estimates," Environmental Protection Agency, Research Triangle Park, North Carolina.